Aqueous SOA formation from the photo-oxidation of vanillin: Direct photosensitized reactions and nitrate-mediated reactions

Beatrix Rosette Go Mabato[1], Yan Lyu[1], Yan Ji[1], Yong Jie Li[2], Dan Dan Huang[3,2], Xue Li[4,3], Theodora Nah[1], Chun Ho Lam[1], and Chak K. Chan[1]*

[1]School of Energy and Environment, City University of Hong Kong, Hong Kong, China
[2]Department of Civil and Environmental Engineering, and Centre for Regional Ocean, Faculty of Science and Technology, University of Macau, Macau, China

[3,2]Shanghai Academy of Environmental Sciences, Shanghai 200233, China

[4,3]Institute of Mass Spectrometry and Atmospheric Environment, Jinan University No. 601 Huangpu Avenue West, Guangzhou 510632, China

Correspondence to: Chak K. Chan (Chak.K.Chan@cityu.edu.hk)

Abstract. Vanillin (VL), a phenolic aromatic carbonyl abundant in biomass burning emissions, forms triplet excited states (^{3}VL*) under simulated sunlight leading to aqueous secondary organic aerosol (aqSOA) formation. This direct photosensitized oxidation of VL was compared with nitrate-mediated VL photo-oxidation under atmospherically relevant cloud and fog conditions, through examining the VL decay kinetics, product compositions, and light absorbance changes. The majority of the most abundant products from both VL photo-oxidation pathways were potential Brown carbon (BrC) chromophores. In addition, both pathways generated oligomers, functionalized monomers, and oxygenated ring-opening products, but nitrate promoted functionalization and nitration, which can be ascribed to its photolysis products ($^{\bullet}$OH, $^{\bullet}NO_2$, and N(III), NO_2^- or HONO). Moreover, a potential imidazole derivative observed from nitrate-mediated VL photo-oxidation suggested that ammonium may be involved in the reactions. The effects of oxygen (O_2) ~~secondary oxidants from ^{3}VL*~~, pH, ~~the presence of volatile organic compounds (VOCs) and inorganic anions,~~ and reactants concentration and molar ratios on VL photo-oxidation were also explored. Our findings show that ~~the secondary oxidants ($^1O_2$, $O_2^{\bullet-}$/$^{\bullet}HO_2$, $^{\bullet}OH$) from the reactions of ^{3}VL* and~~ O_2 plays an essential role in VL photo-oxidation, and ~~. Enhanced~~ oligomer formation was enhanced ~~noted~~ at pH < 4 ~~and in the presence of VOCs and inorganic anions, probably due to additional generation of radicals ($^{\bullet}HO_2$ and $CO_3^{\bullet-}$)~~. Also, functionalization was dominant at low VL concentration, whereas oligomerization was favored at high VL concentration. Furthermore, comparisons of the apparent quantum efficiency of guaiacol photodegradation indicate that in this study, guaiacol oxidation by photosensitized reactions of VL ~~was observed to be more~~ is less efficient relative to nitrate-mediated photo-oxidation. Lastly, potential aqSOA formation ~~VL photo-oxidation~~ pathways via VL photo-oxidation ~~under different reaction conditions~~ were proposed. This study indicates that the direct photosensitized oxidation of VL and nitrate-mediated VL photo-

oxidation ~~, which nitrate photolysis products can further enhance,~~ may be ~~an~~ important aqSOA sources in areas influenced by biomass burning emissions.

1 Introduction

Aqueous reactions can be an important source of secondary organic aerosols (SOA) (Blando and Turpin, 2000; Volkamer et al., 2009; Lim et al., 2010; Ervens et al., 2011; Huang et al., 2011; Lee et al., 2011; Smith et al., 2014) such as highly-oxygenated and low-volatility organics (Hoffmann et al., 2018; Liu et al., 2019) which may affect aerosol optical properties due to contributions to Brown Carbon (BrC) (Gilardoni et al., 2016). BrC refers to organic aerosols that absorb radiation efficiently in the near-ultraviolet (UV) and visible regions (Laskin et al., 2015). The formation of aqueous SOA (aqSOA) via photochemical reactions involves oxidation, with hydroxyl radical ($^{\bullet}OH$) usually considered as the primary oxidant (Herrmann et al., 2010; Smith et al., 2014). The significance of photosensitized chemistry in atmospheric aerosols has recently been reviewed (George et al., 2015). For instance, triplet excited states of organic compounds ($^3C^*$) from the irradiation of light-absorbing organics such as non-phenolic aromatic carbonyls (Canonica et al., 1995; Anastasio et al., 1996; Vione et al., 2006; Smith et al., 2014) have been reported to oxidize phenols at faster rates and with higher aqSOA yields compared to $^{\bullet}OH$ (Sun et al., 2010; Smith et al., 2014; Yu et al., 2014; Smith et al., 2016). Aside from being an oxidant, $^3C^*$ can also be a precursor of singlet oxygen ($^1O_2$), superoxide ($O_2^{\bullet-}$) or hydroperoxyl ($^{\bullet}HO_2$) radical, and $^{\bullet}OH$ (via $HO_2^{\bullet}/O_2^{\bullet-}$ formation) upon reactions with O_2 and substrates (e.g., phenols)~~, respectively~~ (~~Tinel~~George et al., 2018). The $^3C^*$ concentration in typical fog water has been estimated to be > 25 times than that of $^{\bullet}OH$, making $^3C^*$ the primary photo-oxidant for biomass burning phenolic compounds (Kaur and Anastasio, 2018; Kaur et al., 2019). Recent works on triplet-driven oxidation of phenols have mainly focused on changes of physicochemical properties (e.g., light absorption) and aqSOA yield (e.g., Smith et al., 2014, 2015, 2016), with few reports on reaction mechanisms and characterization of reaction products (e.g., Yu et al., 2014; Chen et al., 2020; Jiang et al., 2021).

Inorganic nitrate is a major component of aerosols and cloud/fog water. In cloud and fog water, the concentrations of inorganic nitrate can vary from 50 μM to > 1000 μM, with higher levels typically noted under polluted conditions (Munger et al., 1983; Collett et al., 1998; Zhang and Anastasio, 2003; Li et al., 2011; Giulianelli et al., 2014; Bianco et al., 2020). Upon photolysis (Vione et al., 2006; Herrmann, 2007; Scharko et al., 2014), inorganic nitrate in cloud and fog water can contribute to BrC (Minero et al., 2007) and aqSOA formation (Huang et al., 2018; Klodt et al., 2019; Zhang et al., 2021) by generating $^{\bullet}OH$ and nitrating agents (e.g., $^{\bullet}NO_2$). For example, the aqSOA yields from the photo-oxidation of phenolic carbonyls in nitrate are twice as high as that in sulfate solution (Huang et al., 2018). Nitration is a significant process in the formation of light-absorbing organics or BrC in the atmosphere (Jacobson, 1999; Kahnt et al., 2013; Mohr et al., 2013; Laskin et al., 2015; Teich et al., 2017; Li et al., 2020). Furthermore, nitrate photolysis has been proposed to be a potentially important process for SO_2

oxidation via the generation of •OH, •NO_2, and N(III) within particles (Gen et al., 2019a, 2019b), and it can also potentially change the morphology of atmospheric viscous particles (Liang et al., 2021). Accordingly, both $^3C^*$ and inorganic nitrate can contribute to aqSOA and BrC formation.

~~———~~Biomass burning (BB) is a significant atmospheric source of both phenolic and non-phenolic aromatic carbonyls (Rogge et al., 1998; Nolte et al., 2001; Schauer et al., 2001; Bond et al., 2004). For ~~An~~ example~~,~~ ~~is~~ vanillin (VL) (Henry's law constant of 4.56×10^5 M atm^{-1}; Yaws, 1994), a model compound for methoxyphenols which are abundant in BB emissions (Pang et al., 2019a), ~~which~~ has been shown to yield low-volatility products (Li et al., 2014) via aqueous •OH oxidation and direct photodegradation. ~~–~~Photodegradation kinetics and aqSOA yields have been reported for direct VL photodegradation (Smith et al., 2016), with oxygenated aliphatic-like compounds (high H:C, ≥ 1.5 and low O:C, ≤ 0.5 ratios) reported as the most likely products (Loisel et al., 2021). Additionally, aqueous-phase reactions of phenols with reactive nitrogen species have been proposed to be a significant source of nitrophenols and SOA (Grosjean, 1985; Kitanovski et al., 2014; Kroflič et al., 2015; Pang et al., 2019a; Kroflič et al., 2021; Yang et al., 2021). For instance, nitrite-mediated VL photo-oxidation can generate nitrophenols, and the reactions are influenced by nitrite/VL molar ratios, pH, and the presence of •OH scavengers (Pang et al., 2019a). As BB aerosols are typically internally mixed with other aerosol components (Zielinski et al., 2020), VL may coexist with nitrate in BB aerosols. The aqueous-phase photo-oxidation of VL and nitrate may then reveal insights into the atmospheric processing of BB aerosols.

~~As BB aerosols are typically internally mixed with other aerosol components (Zielinski et al., 2020), VL may coexist with nitrate in BB aerosols. The aqueous-phase photo-oxidation of VL and nitrate may then reveal insights into the atmospheric processing of BB aerosols.~~ ~~In addition, pollution from large BB events in central Amazonia has been reported to interact with volatile organic compounds (VOCs) and soil dust (Rizzo et al., 2010). Moreover, the production, growth, and chemical complexity of SOA can be influenced by the uptake and aerosol phase reactions of VOCs (Pöschl, 2005; De Gouw and Jimenez, 2009; Ziemann and Atkinson, 2012). Accordingly, studies incorporating other atmospherically relevant species (e.g., VOCs and inorganic anions) in photo-oxidation experiments are warranted.~~

To evaluate the potential significance of VL and its reactions with nitrate in aqSOA formation in cloud/fog water, we studied the direct photosensitized oxidation of VL and nitrate-mediated VL photo-oxidation under atmospherically relevant conditions. In this work, reactions were characterized based on VL decay kinetics, light absorbance changes, and products. The influences of ~~-~~ O_2~~secondary oxidants from VL triplets~~, solution pH, ~~the presence of VOCs and inorganic anions,~~ and reactants concentration and molar ratios on these two photo-oxidation pathways were also assessed. The $^3C^*$ of non-phenolic aromatic carbonyls (e.g., 3-4-dimethoxybenzaldehyde, DMB; a non-phenolic aromatic carbonyl) (Smith et al., 2014; Yu et al., 2014; Jiang et al., 2021) and phenolic aromatic carbonyls (e.g., acetosyringone, vanillin) (Smith et al., 2016) have been shown to oxidize phenols, but the reaction products from the latter are unknown. We then examined the photo-oxidation of guaiacol, another non-carbonyl phenol, in the presence of VL and compared it with nitrate-mediated photo-oxidation. Finally, we proposed aqSOA formation pathways via VL photo-oxidation ~~pathways of VL under different reaction conditions~~. This work presents a comprehensive comparison of VL photo-oxidation by VL photosensitization and in the presence of inorganic nitrate.

2 Methods

2.1 Aqueous phase photo-oxidation experiments

Photo-oxidation experiments were performed in a ~~500 mL~~ custom-built quartz photoreactor. The solutions (initial volume of 500 mL) were continuously mixed throughout the experiments using ~~equipped with~~ a magnetic stirrer. The solutions were bubbled with synthetic air or nitrogen (N_2) (> 99.995%) (0.5 dm^3/min) for 30 min before irradiation to achieve air- and N_2-saturated conditions, respectively, and the bubbling was continued throughout the reactions (Du et al., 2011; Chen et al., 2020). The aim of the air-saturated experiments was to enable the generation of secondary oxidants ($^1O_2$, $O_2^{\bullet-}$/$^{\bullet}HO_2$, $^{\bullet}OH$) from ^{3}VL* as O_2 is present. Conversely, the N_2-saturated experiments would inhibit the formation of these secondary oxidants, which can lead~~ing~~ to ^{3}VL*-driven reactions (Chen et al., 2020). Solutions were irradiated through the quartz window of the reactor using a xenon lamp (model 6258, Ozone free xenon lamp, 300 W, Newport) equipped with a longpass filter (20CGA-305 nm cut-on filter, Newport) to eliminate light below 300 nm. Cooling fans positioned around the photoreactor and lamp housing maintained reaction temperatures at 27 ± 2 °C. The averaged initial photon flux in the reactor from 300 to 380 nm measured using a chemical actinometer (2-nitrobenzaldehyde) was 2.6×10^{15} photons cm^{-2} s^{-1} nm^{-1} (Fig. S1). Although the concentration of VL in cloud/fog water has been estimated to be < 0.01 mM (Anastasio et al., 1996), a higher VL concentration (0.1 mM) was used in this study to guarantee sufficient signals for product identification (Vione et al., 2019). The chosen ammonium nitrate (AN) concentration (1 mM) was based on values observed in cloud and fog water (Munger et al., 1983; Collett et al., 1998; Zhang and Anastasio, 2003; Li et al., 2011; Giulianelli et al., 2014; Bianco et al., 2020). It should be noted that this study is not intended to identify the concentrations of nitrate that would affect the kinetics. ~~We also examined the role of VOCs (2-propanol, IPA) (1 mM) and inorganic anions (sodium bicarbonate, NaBC) (1 mM) in these reactions. IPA can be classified as both a biogenic (from grass, Olofsson et al., 2003) and anthropogenic VOC (e.g., from solvents and industrial processes, Hippelein, 2004; Lewis et al., 2020), while bicarbonate is an inorganic anion observed in fog water from both urban and rural locations (Collett et al., 1999; Straub et al., 2012; Straub, 2017). IPA and NaBC are particularly interesting also because they can produce other radicals (e.g., $^{\bullet}HO_2$ and carbonate radical, $CO_3^{\bullet-}$) that may react with nitrate photolysis products (Vione et al., 2009; Wang et al., 2021) and they can act as $^{\bullet}OH$ scavengers (Warneck and Wurzinger, 1988; Vione et al., 2009; Gen et al., 2019b; Pang et al., 2019a), although it must be noted that these compounds were not added in excess for our experiments.~~ Moreover, comparisons were made between the photo-oxidation of guaiacol (0.1 mM), a non-carbonyl phenol, in the presence of VL (0.1 mM) or AN (1 mM). Samples (10 mL) were collected hourly for a total of 6 h for offline optical and chemical analyses. Absorbance measurements, VL (and GUA) decay kinetics (calibration curves for VL and GUA standard solutions; Fig. S2), small organic acids measurements, and product characterization were conducted using UV-Vis spectrophotometry, ultra-high-performance liquid chromatography with photodiode array detector (UHPLC-PDA), ion chromatography (IC), and UHPLC coupled with quadrupole time-of-flight mass spectrometry (UHPLC-qToF-MS) equipped with an electrospray

ionization (ESI) source and operated in the positive ion mode (the negative ion mode signals were too low for our analyses), respectively. Each experiment was repeated independently at least three times and measurements were done in triplicate. The reported decay rate constants and absorbance enhancement are the average of results from triplicate experiments, and the corresponding errors represent one standard deviation. The mass spectra are based on the average of results from duplicate experiments. ~~Details on the materials and analytical procedures are provided in the Supporting Information (Text S1 to S6)~~The Supporting Information (Text S1 to S7) provides details on the materials and analytical procedures. The pseudo-first-order rate constant (*k'*) for VL decay was determined using the following equation (Huang et al., 2018):

$$ln\,([\mathrm{VL}]_t/[\mathrm{VL}]_0) = -k't \quad \text{(Eq. 1)}$$

where $[\mathrm{VL}]_t$ and $[\mathrm{VL}]_0$ are the concentrations of VL at time t and 0, respectively. Replacing VL with GUA in Eq. 1 enabled the calculation of GUA decay rate constant. The decay rate constants were normalized to the photon flux measured for each experiment through dividing *k'* by the measured 2-nitrobenzaldehyde (2NB) decay rate constant, *j*(2NB) (see Text S6 for more details).

2.2 Calculation of normalized abundance of products

Comparisons of peak abundance in mass spectrometry have been used in many recent studies (e.g., Lee et al., 2014; Romonosky et al., 2017; Wang et al., 2017; Fleming et al., 2018; Song et al., 2018; Klodt et al., 2019; Ning et al., 2019) to show the relative importance of different types of compounds (Wang et al., 2021). However, ionization efficiency may greatly vary for different classes of compounds (Kebarle, 2000; Schmidt et al., 2006; Leito et al., 2008; Perry et al., 2008; Kruve et al., 2014). and so uncertainties may arise from comparisons of peak areas among compounds. In this work, we assumed equal ionization efficiency of different compounds, which is commonly used to estimate O:C ratios of SOA (Bateman et al., 2012; Lin et al., 2012; De Haan et al., 2019), to calculate their normalized abundance. The normalized abundance of a product, [P] (unitless), was calculated as follows:

$$[\mathrm{P}] = \frac{A_{P,t}}{A_{VL,t}} \cdot \frac{[\mathrm{VL}]_t}{[\mathrm{VL}]_0} \quad \text{(Eq. 2)}$$

where $A_{P,t}$ and $A_{VL,t}$ are the extracted ion chromatogram (EIC) ~~signal~~ peak areas of the product P and VL from UHPLC-qToF-MS analyses at time t, respectively; $[\mathrm{VL}]_t$ and $[\mathrm{VL}]_0$ are the VL concentrations (μM) determined using UHPLC at time t and 0, respectively. Here, we relied on the direct quantification ~~more accurate measurements~~ of [VL] using UHPLC ~~(see Fig. S2 for VL calibration curve)~~ ~~for semi-quantification~~. ~~It should be noted that the ionization efficiency may greatly vary for different classes of compounds (Kebarle, 2000). Hence, we assumed equal ionization efficiency of different compounds to calculate their normalized abundance, which is commonly used to estimate O:C ratios of SOA (Bateman et al., 2012; Lin et al., 2012; De Haan et al., 2019).~~ It should be noted that the normalized abundance of products in this study is a semi-quantitative analysis intended to provide an overview of how the signal intensities changed under different experimental conditions but not to

quantify the absolute concentration of products. Moreover, the major products detected in this study are probably those with high concentration or high ionization efficiency in the positive ESI mode. The use of relative abundance (product peaks are normalized to the highest peak) (e.g., Lee et al., 2014; Romonosky et al., 2017; Fleming et al., 2018; Klodt et al., 2019) would yield the same major products reported. Typical fragmentation behavior observed in MS/MS spectra for individual functional groups from Holčapek et al. (2010) are outlined in Table S1.

3 Results and Discussion

3.1 Kinetics, mass spectrometric, and absorbance changes analyses during aqueous phase photo-oxidation of vanillin

For clarity purposes, the reactions involving reactive species referred to in the following discussions are provided in Table 1. Table S2 summarizes the reaction conditions, initial VL (and GUA) decay rates constants, normalized abundance of products, and average carbon oxidation state ($\langle OS_c \rangle$ (of the 50 most abundant products). In general, the 50 most abundant products contributed more than half of the total normalized abundance of products. ~~For clarity purposes, the reactions involving reactive species referred to in the following discussions are provided in Table 1.~~

As shown in Figure S3, VL underwent oxidation both directly and in the presence of nitrate upon simulated sunlight illumination. VL absorbs light and is promoted to its excited singlet state ($^1VL^*$), then undergoes intersystem crossing (ISC) to the excited triplet state, $^3VL^*$. In principle, $^3VL^*$ can oxidize ground-state VL (Type I photosensitized reactions) via H-atom abstraction/electron transfer and form $O_2^{\bullet-}$ or $HO_2^\bullet$ in the presence of O_2 (~~Tinel~~George et al., 2018), or react with O_2 (Type II photosensitized reactions) to yield $^1O_2$ via energy transfer or $O_2^{\bullet-}$ via electron transfer (Lee et al., 1987; Foote et al., 1991). The disproportionation of $HO_2^\bullet/O_2^{\bullet-}$ (Anastasio et al., 1996) ~~and reaction of $HO_2^\bullet$ with $O_2^{\bullet-}$ (Du et al., 2011)~~ form hydrogen peroxide (H_2O_2), which is a photolytic source of $^\bullet OH$. Overall, air-saturated conditions, in which O_2 is present, enable the generation of secondary oxidants from $^3VL^*$ ($^1O_2$, $O_2^{\bullet-}/^\bullet HO_2$, $^\bullet OH$). Moreover, $^\bullet OH$, $^\bullet NO_2$, and NO_2^-/HNO_2, i.e., N(III), generated via nitrate photolysis (Reactions 1–3; Table 1), can also oxidize or nitrate VL. In this work, the direct photosensitized oxidation of VL ~~((by $^3VL^*$ or secondary oxidants from $^3VL^*$ and O_2~~VL only experiments) and nitrate-mediated VL photo-oxidation are referred to as VL* and VL+AN, respectively.

3.1.1 ~~Effect of secondary oxidants from VL triplets~~VL photo-oxidation under N_2 and air-saturated conditions

~~As mentioned earlier, secondary oxidants ($^1O_2$, $O_2^{\bullet-}/^\bullet HO_2$, $^\bullet OH$) can be generated from $^3VL^*$ when O_2 is present (e.g., under air-saturated conditions), while $^3VL^*$ is the only oxidant expected under N_2-saturated conditions.~~ The photo-oxidation of VL ~~To examine the contributions of $^3VL^*$-derived secondary oxidants and $^3VL^*$ only on VL photo-oxidation, experiments~~ under both N_2- ~~air~~ and air-~~N_2~~-saturated conditions (Fig. S3a) were carried out at pH 4, which is representative of moderately acidic aerosol and cloud pH values (Pye et al., 2020). No significant VL loss was observed for dark experiments. The oxidation of ground-state VL by $^3VL^*$ via H-atom abstraction or electron transfer can form phenoxy (which is in resonance with a carbon-

centered cyclohexadienyl radical that has a longer lifetime) and ketyl radicals (Neumann et al., 1986a, 1986b; Anastasio et al., 1996). The coupling of phenoxy radicals or phenoxy and cyclohexadienyl radicals can form oligomers as observed for both N_2- and air-saturated experiments (see discussions later). However, the little decay of VL under N_2-saturated condition indicates that these radicals probably predominantly decayed via back-hydrogen transfer to regenerate VL (Lathioor et al., 1999). A possible explanation for this is the involvement of O_2 in the secondary steps of VL decay. For instance, a major fate of the ketyl radical is reaction with O_2 (Anastasio et al., 1996). In the absence of O_2, radical formation occurs, but the forward reaction of ketyl radical and O_2 is blocked, leading to the regeneration of VL as suggested by the minimal VL decay. Aside from potential inhibition of secondary oxidants generation (Chen et al., 2020), N_2 purging may have also hindered the secondary steps for VL decay.

~~The low decay rate for VL* under N_2-saturated conditions suggests a minimal role for ^{3}VL* in VL photo-oxidation.~~ Contrastingly, the VL* decay rate constant under air-saturated conditions was 4 times higher~~, revealing the importance of ^{3}VL* derived secondary oxidants for photosensitized oxidation of VL~~. As mentioned earlier, secondary oxidants ($^1O_2$, $O_2^{\bullet-}$/$^{\bullet}HO_2$, $^{\bullet}$OH) can be generated from ^{3}VL* when O_2 is present (e.g., under air-saturated conditions). However, the photo-oxidation of VL in this study is likely mainly governed by ^{3}VL* and that these secondary oxidants have only minor participation. ~~Aside from $^{\bullet}$OH, $O_2^{\bullet-}$/$^{\bullet}HO_2$ and $^1O_2$ can also promote VL photo-oxidation (Kaur and Anastasio, 2018; Chen et al., 2020).~~ $^1O_2$ is also a potential oxidant for phenols (Herrmann et al., 2010; Minella et al., 2011; Smith et al., 2014), but $^1O_2$ reacts much faster (by ~60 times) with phenolate ions compared to neutral phenols (Tratnyek and Hoigne, 1991; Canonica et al., 1995; McNally et al., 2005). Under the pH values (pH 2.5 to 4) considered in this study, the amount of phenolate ion is negligible, so the reaction between VL and $^1O_2$ should be slow. Interestingly, however, $^1O_2$ has been shown to be important in the photo-oxidation of 4-ethylguaiacol (pK_a = 10.3) by ^{3}C* of 3,4-dimethoxybenzaldehyde (solution with pH of ~3) (Chen et al., 2020). Furthermore, while the irradiation of other phenolic compounds can produce H_2O_2, a precursor for $^{\bullet}$OH (Anastasio et al., 1996), the amount of H_2O_2 is small. Based on this, only trace amounts of H_2O_2 were likely generated from VL* (Li et al., 2014) under-air saturated conditions, suggesting that contribution from $^{\bullet}$OH was minor. Overall, these suggest that VL photo-oxidation in this study is driven by ^{3}VL*. Further study on the impact of O_2 on the reactive intermediates involved is required to understand the exact mechanisms occurring under air-saturated conditions. Nonetheless, the VL* decay trends clearly indicate that O_2 is important for efficient VL photo-oxidation~~an efficient oxidant for unsaturated organic compounds and has a lifetime that is much longer than ^{3}C* (Chen et al., 2020). Similar to VL*, t~~The decay rate constant for VL+AN under air-saturated conditions was also higher ~~faster~~ (6.6 times) than N_2-saturated conditions, which may ~~can~~ be due to ~~several~~ reactions facilitated by nitrate photolysis products ~~and the enhancement of N(III) mediated photo-oxidation~~ that may have been enhanced in the presence of O_2 ~~as reported in early works~~ (Vione et al., 2005; Kim et al., 2014; Pang et al., 2019a). As shown later, more nitrogen-containing species were observed under air-saturated conditions. An example is enhanced VL nitration likely from increased $^{\bullet}NO_2$ formation such as from the reaction of $^{\bullet}$OH and $O_2^{\bullet-}$ with NO_2^- (Reactions 4 and 5, respectively; Table 1) or the autoxidation of $^{\bullet}$NO from NO_2^- photolysis (Reactions 6~~-~~9; Table 1) in aqueous solutions (Pang

et al., 2019a). ~~Reactions involving $^{\bullet}HO_2/O_2^{\bullet-}$ which may originate from the photolysis of nitrate alone, likely from the production and subsequent photolysis of peroxynitrous acid (HOONO) (Reaction 10; Table 1) (Jung et al., 2017; Wang et al., 2021), or the reactions of ^{3}VL* in the presence of O_2, may have contributed as well. For instance, Wang et al. (2021) recently demonstrated that nitrate photolysis generates $^{\bullet}HO_2/O_2^{\bullet-}{}_{(aq)}$ and $HONO_{(g)}$ in the presence of dissolved aliphatic organic matter (e.g., nonanoic acid, ethanol), with the enhanced $HONO_{(g)}$ production caused by secondary photochemistry between $^{\bullet}HO_2/O_2^{\bullet-}{}_{(aq)}$ and photoproduced $NO_{x(aq)}$ (Reactions 11 and 12; Table 1), in agreement with Scharko et al. (2014). The significance of this increased HONO production is enhanced $^{\bullet}OH$ formation (Reaction 13; Table 1). In addition, $^{\bullet}HO_2$ can react with $^{\bullet}NO$ (Reaction 10; Table 1) from NO_2^- photolysis (Reaction 6; Table 1) to form HOONO, and eventually $^{\bullet}NO_2$ and $^{\bullet}OH$ (Reaction 14; Table 1) (Pang et al., 2019a).~~ Nevertheless, the comparable decay rate~~s~~ constants for VL* and VL+AN imply that ^{3}VL* chemistry still dominates even at 1:10 molar ratio of VL/nitrate, probably due to the much higher molar absorptivity of VL compared to that of nitrate (Fig. S1) and the high VL concentration (0.1 mM) used in this study. Although we have no quantification of the oxidants in our reaction systems as it is outside the scope of this study, these observations clearly substantiate that ~~secondary oxidants from ^{3}VL*, which are formed when O_2 is present, are required for efficient~~ photosensitized oxidation of VL and nitrate-mediated VL photo-oxidation are more efficient in the presence of O_2.

The products from VL* under N_2-saturated conditions were mainly oligomers (e.g., $C_{16}H_{14}O_4$) (Fig. 1a), consistent with triplet-mediated oxidation forming higher molecular weight products, probably with less fragmentation relative to oxidation by $^{\bullet}$OH (Yu et al., 2014; Chen et al., 2020). A threefold increase in the normalized abundance of products was noted upon addition of nitrate (VL+AN under N_2-saturated conditions; Fig. 1b), and in addition to oligomers, functionalized monomers (e.g., $C_8H_6O_5$) and nitrogen-containing compounds (e.g., $C_8H_9NO_3$; No. 2, Table S2~~3~~) were also observed, in agreement with $^{\bullet}$OH-initiated oxidation yielding more functionalized/oxygenated products compared to triplet-mediated oxidation (Yu et al., 2014; Chen et al., 2020). ~~Compared to N_2-saturated conditions, the normalized abundance of products such as o~~Oligomers, ~~and~~ functionalized monomers (e.g., demethylated VL; Fig. S4), and ~~The~~ nitrogen-containing compounds (e.g., $C_{16}H_{10}N_2O_9$; No. 3~~3, Table S3~~, Table S2) (for VL+AN) had higher normalized abundance~~were also more relatively abundant~~ under air-saturated conditions ~~were significantly higher under air-saturated conditions~~ (Figs. 1c-d), likely due to efficient ~~the secondary oxidants from~~ ^{3}VL*~~-~~initiated oxidation and enhanced VL nitration in the presence of ~~and~~ O_2 ~~and their interactions with nitrate photolysis products~~. ~~The nitrogen-containing compounds (e.g., $C_{16}H_{10}N_2O_9$; No. 3, Table S3) were also more relatively abundant under air-saturated conditions.~~ For both VL* and VL+AN under air-saturated conditions, the most abundant product was $C_{10}H_{10}O_5$ (No. 4, Table S2~~3~~), a substituted VL. Irradiation of VL by 254-nm lamp has also been reported to lead to VL dimerization and functionalization via ring-retaining pathways, as well as small oxygenates but only when $^{\bullet}$OH from H_2O_2 were involved (Li et al., 2014). In this work, small organic acids (e.g., formic acid) were observed from both VL* and VL+AN under air-saturated conditions (Fig. S5) due to simulated sunlight that could access the 308-nm VL band (Smith et al., 2016). Interestingly, we observed a potential imidazole derivative ($C_5H_5N_3O_2$; ~~Fig. 1d~~No. 5, Table S2) from VL+AN under air-saturated conditions (Fig. 1d), which may have formed from reactions induced by ammonium. This compound was not observed in a parallel experiment in which AN was replaced with sodium nitrate (SN) (Fig. S6a; see Sect.

3.3 for discussion). The potential aqSOA formation ~~most probable~~ pathways via ~~of direct photosensitized and nitrate-mediated photo-oxidation of~~ VL photo-oxidation in this study are summarized in Fig. 2~~were proposed (Fig. 4). In Scheme 1 (pH 4 and pH <4 under air-saturated conditions), ^{3}VL* and $^{\bullet}$OH (from ^{3}VL* or nitrate photolysis) can initiate H atom abstraction to generate phenoxy or ketyl radicals (Huang et al., 2018; Vione et al., 2019).~~ At pH 4, ring-opening products (Fig. S5) from fragmentation in both VL* and VL+AN may have reacted with VL or dissolved ammonia to generate $C_{10}H_{10}O_5$ (No. 4, Table S2) (Pang et al., 2019b) or~~and~~ a potential imidazole derivative ($C_5H_5N_3O_2$; No. 5, Table S2), respectively. Moreover, nitrate photolysis products promoted functionalization and nitration (e.g., $C_{16}H_{10}N_2O_9$; No. 3, Table S2). ~~At pH <4, the reactivity of ^{3}VL* increased as suggested by the abundance of oligomers (e.g., $C_{16}H_{14}O_8$) and increased normalized abundance of N-containing compounds.~~

The molecular transformation of VL upon photo-oxidation was examined using the van Krevelen diagrams (Fig. S7). For all experiments (A1-15~~9~~; Table ~~S~~2) in this study, the O:C and H:C ratios of the products were mainly similar to those observed from the aging of other phenolics (Yu et al., 2014) and BB aerosols (Qi et al., 2019). U~~u~~nder N_2-saturated conditions, o~~O~~ligomers with O:C ratios ≤ 0.6 were dominant in VL*. ~~under N_2-saturated conditions.~~ while smaller molecules (n_c ≤ 8) with higher O:C ratios (up to 0.8) were also observed f~~F~~or VL+AN. ~~For VL+AN under N_2-saturated conditions, smaller molecules (n_c ≤8) with higher O:C ratios (up to 0.8) were also observed.~~ In contrast, ~~M~~more products with higher O:C ratios (≥ 0.6) were noted under air-saturated conditions for both VL* and VL+AN. F~~f~~or experiments A5 to A8, ~~The~~ H:C ratios were mostly around 1.0 and double bond equivalent (DBE) values were typically (58% of the 50 most abundant products) ≥ 7, indicating that the products ~~for experiments A5 to A8 (Table S2)~~ were mainly oxidized aromatic ~~aromatic species~~ compounds (Xie et al., 2020). Compounds with H:C ≤ 1.0 and O:C ≤ 0.5 are common for aromatic species, while compounds with H:C ≥ 1.5 and O:C ≤ 0.5 are typical for more aliphatic species (Mazzoleni et al., 2012; Kourtchev et al., 2014; Jiang et al., 2021). ~~Moreover, majority of the products for experiments A5 to A8 have double bond equivalent (DBE) values >7, which corresponds to oxidized aromatic compounds (Xie et al., 2020).~~ In contrast, Loisel et al. (2021) reported mainly oxygenated aliphatic-like compounds ~~(H:C, ≥1.5 and O:C, ≤0.5 ratios)~~ from the direct irradiation of VL (0.1 mM), ~~which may be~~probably due to their use of ESI in the negative ion mode, which has higher sensitivity for detecting compounds such as carboxylic acids (Holčapek et al., 2010; Liigand et al., 2017), and solid-phase extraction (SPE) procedure causing the loss of some oligomers (LeClair et al., 2012; Zhao et al., 2013; Bianco et al., 2018). Among experiments A5 to A8 ~~(Table S2)~~, VL+AN under air-saturated conditions (A7) had the highest normalized abundance of products and $\langle OS_c \rangle$, ~~most~~ probably due to the combined influence of ~~the secondary oxidants from~~ ^{3}VL* and enhanced VL nitration in the presence of O_2~~, and nitrate photolysis products~~. ~~In our calculations, the increase in $\langle OS_c \rangle$ (except for VOCs and inorganic anions experiments; A9 to A12; Table S2) was lower than those in $^{\bullet}$OH or triplet mediated oxidation of phenolics (e.g., phenol, guaiacol) measured using an aerosol mass spectrometer (Sun et al., 2010; Yu et al., 2014),~~Our measured $\langle OS_c \rangle$ for all experiments range from -0.28 to +0.12, while other studies on phenolic aqSOA formation reported $\langle OS_c \rangle$ ranging from -0.14 to +0.47 (Sun et al., 2010) and 0.04 to 0.74 (Yu et al., 2014). This is likely because we excluded contributions from ring-opening products, which may have higher OS_c values as these products

are not detectable in the positive ion mode. Thus, the <OS_c> in this study likely were lower estimates. In brief, the presence of ~~secondary oxidants from ^{3}VL* and~~ O_2 increased the normalized abundance of products and promoted the formation of more oxidized aqSOA. ~~These trends were reinforced in the presence of nitrate, indicating synergistic effects between secondary oxidants from VL triplets and nitrate photolysis products.~~Compared to N_2-saturated condition, the higher normalized abundance of nitrogen-containing products under air-saturated condition for VL+AN (at pH 4) suggests a potential enhancement of VL nitration in the presence of O_2.

Illumination of phenolic aromatic carbonyls with high molar absorptivities ($\varepsilon_{\lambda max}$) (~8 to 22 × 10^3 M^{-1} cm^{-1}) leads to an overall loss of light absorption but increased absorbance at longer wavelengths (> 350 nm), where the carbonyls did not initially absorb light (Smith et al., 2016). Fig. ~~3~~2a illustrates the changes in total absorbance from 350 to 550 nm of VL* and VL+AN under N_2- ~~air~~ and ~~N_2~~ air-saturated conditions. The absorption spectra of VL* under air- and N_2- saturated conditions (pH 4) at different time intervals are shown in Fig. S8. For both VL* and VL+AN, evident absorbance enhancement was observed under air-saturated conditions, while the absorbance changes under N_2-saturated conditions were minimal, consistent with the VL decay trends. This absorbance enhancement can be explained by the formation of oligomers with large, conjugated π-electron systems (Chang and Thompson, 2010) and hydroxylated products (Li et al., 2014; Zhao et al., 2015), in agreement with the observed reaction products. In this work, phenoxy radicals (in resonance with a carbon-centered cyclohexadienyl radical) can be generated from several processes such as the oxidation ~~(Vione et al., 2019)~~ of ground-state VL by ^{3}VL* via H-atom abstraction ~~(Huang et al., 2018)~~or electron transfer coupled with proton transfer from the phenoxyl radical cation or from solvent water (Neumann et al., 1986a, 1986b; Anastasio et al., 1996) and photoinduced O-H bond-breaking (Berto et al., 2016). ~~Moreover, ^{3}VL* can initiate H atom abstraction from the CHO group of VL, generating ketyl radicals via Norrish type reactions (Vione et al., 2019).~~ Also, similar reactions can be initiated by ˙OH (Gelencsér et al., 2003; Hoffer et al., 2004; Chang and Thompson, 2010; Sun et al., 2010), which in this study can be generated from the reaction between ^{3}VL* and O_2, as well as nitrate photolysis. Trace amounts of H_2O_2 were likely formed during VL photodegradation (Li et al., 2014), similar to the case of other phenolic compounds (Anastasio et al., 1996). Oligomers can then form via the coupling of phenoxy radicals or phenoxy and cyclohexadienyl ~~ketyl~~ radicals (Sun et al., 2010; Yu et al., 2014~~Berto et al., 2016~~; Vione et al., 2019). Absorbance increase at > 350 nm has also been reported for photosensitized oxidation of phenol and 4-phenoxyphenol (De Laurentiis et al., 2013a, 2013b) and direct photolysis of tyrosine and 4-phenoxyphenol (Bianco et al., 2014) in which dimers have been identified as initial substrates. The continuous absorbance enhancement throughout 6 h of irradiation correlated with the observation of oligomers and nitrated compounds after irradiation. However, the increasing concentration of small organic acids (Fig. S5) throughout the experiments suggests that fragmentation, which results in the decomposition of initially formed oligomers and formation of smaller oxygenated products (Huang et al., 2018), is important at longer irradiation times. Overall, these trends establish that ~~secondary oxidants from ^{3}VL*and~~ O_2 ~~are~~ is necessary for the efficient formation of light-absorbing compounds from both VL* and VL+AN.

3.1.2 Effect of pH

The reactivity of $^3C^*$ (Smith et al., 2014, 2015, 2016), aromatic photonitration by nitrate (Machado and Boule, 1995; Dzengel et al., 1999; Vione et al., 2005; Minero et al., 2007), and N(III)-mediated VL photo-oxidation (Pang et al., 2019a) have been demonstrated to be pH-dependent. In this study, the effect of pH on VL photo-oxidation was investigated within the range of 2.5 to 4~~5~~, corresponding to typical cloud ~~(2-7)~~ pH values (2-7) (Pye et al., 2020). The decay rate~~s~~ constants for both VL* and VL+AN increased as pH decreased (VL* and VL+AN at pH 2.5: 1.6~~5~~ and 1.4~~3~~ times faster than at pH 4, respectively) (Fig. S3b). These differences in decay rate constants are small but statistically significant ($p < 0.05$). The pK_a for the VL triplet has been reported to be 4.0 (Smith et al., 2016). As there are a greater fraction of VL triplets that are protonated at pH 2.5 (0.96) than at pH 4 (0.5), it is possible that the pH dependence of the decay rate constants observed in this study is due to ^{3}VL* being more reactive in its protonated form. Smith et al. (2016) also observed a pH dependence for the direct photodegradation of VL (0.005 mM) (rate constants at pH ≤ 3 are ~two times lower than at pH ≥ 5) which they attributed to the sensitivity of the excimer of VL (i.e., the charge-transfer complex formed between an excited state VL molecule and a separate ground state VL molecule; Birks, 1973, Turro et al., 2010) to acid-base chemistry. The opposite trend observed in this study for 0.1 mM VL may be due to the reactivities of the protonated and neutral forms of the ^{3}VL* being dependent on the VL concentration (Smith et al., 2016). ~~For VL*, this pH trend indicates that ^{3}VL* are more reactive in their protonated form, which is opposite to that reported for 0.005 mM VL (Smith et al., 2016), likely due to the concentration dependence of the relative reactivities of protonated and neutral forms of ^{3}VL*.~~ It has been reported that the quantum yield for direct VL photodegradation is higher at pH 5 than at pH 2 for 0.005 mM VL, but they are not statistically different for 0.03 mM VL (Smith et al., 2016). ~~Also, increases in hydrogen ion concentration can enhance the formation of $HO_2^•$ and H_2O_2 and in turn, $^•OH$ formation (Du et al., 2011). In addition to these pH influences on VL* the dependence of N(III) (NO_2^- + HONO) speciation on solution acidity (Pang et al., 2019a) also contributed to the observed pH effects for VL+AN. At pH 3.3, half of N(III) exists as HONO (Fischer and Warneck, 1996; Pang et al., 2019a), which has a higher quantum yield for $^•OH$ formation than that of NO_2^- in the near-UV region (Arakaki et al., 1999; Kim et al., 2014). The increased $^•OH$ formation rates as pH decreases can lead to faster VL decay (Pang et al., 2019a). Also, NO_2^-/HONO can generate $^•NO_2$ via oxidation by $^•OH$ (Reactions 4 and 15; Table 1) (Pang et al., 2019a).~~ As pH decreases, the higher reactivity of ^{3}VL* and sensitivity of the excimer of VL to acid-base chemistry ~~HONO being the dominant N(III) species can lead~~ may have led to faster VL photo-oxidation. Similar to pH 4 experiments, comparable decay rate constants between VL* and VL+AN were also noted at pH < 4, again suggesting the predominant role of ^{3}VL* chemistry compared to nitrate, likely due to the high VL concentration (0.1 mM) used in this study.

As pH decreased, the normalized abundance of products, particularly oligomers and functionalized monomers, was higher for both VL* and VL+AN, further indicating that ^{3}VL* ~~are~~ may be more reactive in their protonated form. The most abundant products observed were a substituted VL ($C_{10}H_{10}O_5$; No. 4, Table S2) and VL dimer ($C_{16}H_{14}O_6$; No. 6~~5~~, ~~Table S3~~Table S2) at pH 4 and pH < 4, respectively (Figs. 1c-h). Furthermore, a tetramer ($C_{31}H_{24}O_{11}$) was observed only in VL* at pH 2.5. For VL+AN, the normalized abundance of nitrogen-containing compounds was also higher ~~increased~~ at lower pH

(Table S2), likely due to increased •OH and •NO_2 formation, which may be caused by the dependence of N(III) (NO_2^- + HONO) speciation on solution acidity (Pang et al., 2019a). At pH 3.3, half of N(III) exists as HONO (Fischer and Warneck, 1996; Pang et al., 2019a), which has a higher quantum yield for •OH formation than that of NO_2^- in the near-UV region (Arakaki et al., 1999; Kim et al., 2014). Also, NO_2^-/HONO can generate •NO_2 via oxidation by •OH (Reactions 4 and 105; Table 1) (Pang et al., 2019a). At pH < 4, ^{3}VL* likely have higher reactivity as suggested by the increased normalized abundance of oligomers (e.g., $C_{16}H_{14}O_6$; No. 6, Table S2 and $C_{31}H_{24}O_{11}$) and N-containing compounds (e.g., $C_{16}H_{10}N_2O_9$; No. 3, Table S2 and $C_{13}H_{14}N_2O_{10}$) (Fig. 2). The potential imidazole derivative ($C_5H_5N_3O_2$; No. 5, Table S2) was observed only at pH 4, possibly due to the pH dependence of ammonium speciation (pK_a = 9.25). Imidazole formation requires the nucleophilic attack of ammonia on the carbonyl group (Yu et al., 2011), and at pH 4, the concentration of dissolved ammonia in VL+AN was about 10 or 30 times higher than that at pH 3 or pH 2.5, respectively. At different pH, the O:C and H:C ratios in VL* and VL+AN had no significant differences (Figs. S7c–d and S9), but molecules with higher O:C ratios (> 0.6) were more abundant at pH < 4. Accordingly, the <OS_c> at pH < 4 for both VL* and VL+AN were higher than that at pH 4, consistent with higher <OS_c> observed at pH 5 compared to pH 7 for the •OH-mediated photo-oxidation of syringol (Sun et al., 2010). Essentially, the higher reactivity of ^{3}VL* and predominance of HONO over nitrite at lower pH may have resulted in increased formation of products mainly composed of oligomers and functionalized monomers.

The hHigher absorbance enhancement for both VL* and VL+AN (Fig. 32b) was observed as pH increased may be attributed to redshifts and increased visible light absorption of reaction products (Pang et al., 2019a). To determine whether the pH dependence is due to the acid-base chemistry of the products or of the reactions, we measured the pH dependence of the aqSOA formed from VL* at pH 4 and 2.5 over a range of pH conditions from 1.5 to 10.5 (Fig. S10). For both cases, the intensity of absorption at longer wavelengths significantly increased as the pH of the solutions was raised. Moreover, the comparable pH dependence of the two solutions suggests that the observed pH dependence may be attributed to the acid-base chemistry of the reactions, which may involve ^{3}VL* or the excimer of VL (Smith et al., 2016), as discussed earlier. When a phenolic molecule deprotonates at higher pH, an ortho- or para- electron-withdrawing group, such as a nitro or aldehyde group, can attract a portion of the negative charge towards its oxygen atoms through induced and conjugated effects, leading to the extension of chromophore from the electron-donating group (e.g., O^-) to the electron-withdrawing group via the aromatic ring (Carey, 2000; Williams and Fleming, 2008; Pang et al., 2019a). Hence, the delocalization of the negative charge in phenolates leads to significant redshifts (Mohr et al., 2013).

3.1.3 Effect of VOCs and inorganic anions

Aerosols are a complex mix of organic and inorganic compounds (Kanakidou et al., 2005). We explored the photo-oxidation behavior of VL, with and without nitrate, in the presence of VOCs (2-propanol, IPA) and inorganic anions (sodium bicarbonate, NaBC). For both VL* and VL+AN, there was no significant change in VL decay (Figs. S3c-d), and comparable absorbance enhancements (Figs. 2c-d) were observed upon the addition of IPA and NaBC. However, the characterization of reaction products revealed the distinct effects of these compounds on the photo-oxidation of VL. Both IPA and NaBC increased the

normalized abundance of products from VL* (by a factor of 2.4 and 1.4, respectively) and VL+AN (by a factor of ~4) (Table S2). The major product observed in VL*+IPA (Fig. S10a) was a dimer ($C_{16}H_{14}O_6$). Also, higher oligomers up to tetramers (e.g., $C_{31}H_{22}O_{12}$) not observed in VL* were noted. A possible explanation may be the additional generation of $^{\bullet}HO_2^-$ from the reaction of IPA with $^{\bullet}OH$ (Warneck and Wurzinger, 1988) (Reactions 16 and 17; Table 1), which can originate from ^{3}VL* or nitrate photolysis, inducing reactions such as oxidation and nitration. As discussed earlier, $^{\bullet}HO_2$ can form H_2O_2, a photolytic source of $^{\bullet}OH$ (Anastasio et al., 1996; Du et al., 2011). In the presence of IPA, the increase in normalized abundance of products (VL+AN+IPA: 3.8 times vs. VL*+IPA: 2.4 times; Table S2) and $\langle OS_c \rangle$ (VL+AN+IPA: 0.13 to 0.08 vs. VL*+IPA: 0.16 to 0.10; Table S2) being more evident for VL+AN compared to VL* also supports the potential importance of reactions involving $^{\bullet}HO_2$ and nitrate photolysis products such as the secondary photochemistry between $^{\bullet}HO_2/O_2^{\bullet-}{}_{(aq)}$ and photoproduced $NO_{x(aq)}$ enhancing $HONO_{(g)}$ production from nitrate photolysis in the presence of dissolved aliphatic organic matter (Wang et al., 2021) as discussed in Sect. 3.1.1. This chemistry may have operated in VL+AN+IPA considering that $^{\bullet}HO_2/O_2^{\bullet-}$ may originate from multiple sources in this experiment: nitrate photolysis (Reaction 10; Table 1) (Jung et al., 2017; Wang et al., 2021), the reactions of ^{3}VL* in the presence of O_2 (see Sect. 3.1), or reaction of IPA with $^{\bullet}OH$ (Warneck and Wurzinger, 1988) (Reactions 16 and 17; Table 1). In other words, the role of nitrate in VL photo-oxidation is enhanced in the presence of IPA, likely due to additional $^{\bullet}HO_2/O_2^{\bullet-}$ formation. In VL+AN+IPA, nitrate photolysis likely converted $C_{16}H_{14}O_6$ (from VL*+IPA) to $C_{15}H_{12}O_8$ (Figs. S10a-b) via demethylation and then multiple hydroxylations. Nitrate photolysis generates $^{\bullet}OH$, and demethylation has been reported to be enhanced at high $^{\bullet}OH$ exposure (Gold et al., 1983). Moreover, alcohols can affect the structure of water, causing a localized patterning or organization that changes the solvation environment, which can account for reactivity enhancement in the presence of alcohol containing solvents (Berke et al., 2019). Berke et al. (2019) has demonstrated that IPA and other alcohols (e.g., ethanol) can promote the production of light absorbing compounds, i.e., imidazoles, from the reactions between glyoxal and ammonium sulfate. This phenomenon has been attributed to the formation of micro-heterogeneities of hydrated alcohol molecules in a complex solution environment composed of solvated sulfate ions and a mixture of reactants and products upon the addition of alcohols. As proposed by an earlier study (Onori and Santucci, 1996), if the water in the SOA-mimicking solutions exists in two forms, bulk and hydrating, the micro-heterogeneities may interact with water/nitrate matrix to sequester the reactants and products, concentrating them within a smaller effective solvent volume and consequently resulting in increased normalized abundance of products (Berke et al., 2019).

For NaBC which does not produce $^{\bullet}HO_2$ upon reactions with $^{\bullet}OH$ under air-saturated conditions (Gen et al., 2019b), the increased normalized abundance of products may be due to other reactions promoted by the carbonate radical ($CO_3^{\bullet-}$), which can be generated from the reactions of bicarbonate/carbonate with $^{\bullet}OH$ (Reactions 18 and 19; Table 1) (Neta et al., 1988; Wojnárovits et al., 2020) or ^{3}VL* (Reactions 20 and 21; Table 1) (Canonica et al., 2005). $CO_3^{\bullet-}$ is a selective oxidant that reacts with organic molecules at a lower rate than $^{\bullet}OH$ and readily reacts with electron rich parts of phenols, aromatic amines, and sulfur containing compounds (e.g., glutathione) through both electron transfer and H abstraction (Huang and Mabury, 2000; Wojnárovits et al., 2020). Similar to IPA, the enhancement of normalized abundance of products (VL+AN+NaBC: 4.3 times vs. VL*+NaBC: 1.4 times; Table S2) and $\langle OS_c \rangle$ (VL+AN+NaBC: 0.13 to 0.08 vs. VL*+NaBC:

~~-0.16 to -0.11; Table S2) was more obvious for VL+AN+NaBC than VL*+NaBC, further underlining the contributions of nitrate photolysis products. For example, it has been reported that carbonate and bicarbonate can substantially increase the photodegradation of electron rich compounds (e.g., catechol) by nitrate (Vione et al., 2009). Bicarbonate can enhance the photolysis of nitrate via a solvent cage effect, reacting with photolysis-derived $^{\bullet}OH$ before it escapes the surrounding cage of the water molecules. This prevents the recombination of $^{\bullet}OH$ and $^{\bullet}NO_2$ inside the solvent cage that otherwise would yield back $NO_3^- + H^+$, which reduces the quantum yield of $^{\bullet}OH$ photoproduction (Bouillon and Miller, 2005). This scavenging of in-cage $^{\bullet}OH$ by bicarbonate would then hinder recombination, resulting in a higher generation rate of $CO_3^{\bullet-}$ + $^{\bullet}OH$ with bicarbonate compared to $^{\bullet}OH$ alone without bicarbonate. However, in our experiments, NaBC did not cause any substantial change in the decay of VL for both VL* and VL+AN, although it promoted higher normalized abundance of products. The major product in VL*+NaBC was a functionalized monomer ($C_7H_4O_4$; No. 6, Table S3; Fig. S10c). Unlike VL*+IPA, no tetramers were observed in VL*+NaBC. Similar to VL+AN+IPA, the addition of NaBC to VL+AN resulted in trimers and a high-abundance dimer ($C_{15}H_{12}O_8$; No. 7, Table S3) (Figs. S10b and S10d). Overall, VL+AN+IPA had more oligomers while VL+AN+NaBC had more functionalized monomers (e.g., $C_8H_6O_4$, No. 8, Table S3). These findings suggest that aside from low pH (<4), the formation of oligomers from VL photo-oxidation can also be promoted by presence of VOCs and inorganic anions likely via the generation of radicals such as $^{\bullet}HO_2$ and $CO_3^{\bullet-}$ which can also interact with nitrate photolysis products.~~

~~The addition of IPA or NaBC to VL* resulted in products with higher O:C and H:C ratios (Figs. S11a and S11c). Although the products were more abundant in VL*+IPA than with NaBC, the distribution of their products in van Krevelen diagrams was rather similar. The increased in $\langle OS_c \rangle$ in the presence of IPA or NaBC was more significant for VL+AN than VL*, likely due to the interactions of nitrate photolysis products with $^{\bullet}HO_2$ and $CO_3^{\bullet-}$. For VL+AN, IPA and NaBC also increased the O:C and H:C ratios (Figs. S11b and S11d), and most products had OS_c >0, similar to less volatile and semi-volatile oxygenated organic aerosols (LV-OOA and SV-OOA) (Kroll et al., 2011).~~

3.1.34 Distribution of potential BrC compounds

Figure S112 plots the DBE values vs. number of carbons (n_c) (Lin et al., 2018) for the 50 most abundant products from pH 4 experiments under air-saturated conditions, along with reference to DBE values corresponding to fullerene-like hydrocarbons (Lobodin et al., 2012), cata-condensed polycyclic aromatic hydrocarbons (PAHs) (Siegmann and Sattler, 2000), and linear conjugated polyenes with a general formula C_xH_{x+2}. As light absorption by BrC requires uninterrupted conjugation across a significant part of the molecular structure, compounds with DBE/n_C ratios (shaded area in Fig. S112) greater than that of linear conjugated polyenes are potential BrC compounds (Lin et al., 2018). Based on this criterion and the observed absorbance enhancement at > 350 nm (Fig. 32), the majority of the 50 most abundant products from pH 4 experiments under air-saturated conditions were potential BrC chromophores composed of monomers and oligomers up to tetramers. However, as ESI-detected compounds in BB organic aerosols has been reported to be mainly molecules with n_c < 25 (Lin et al., 2018), there may be higher oligomers that were not detected in our reaction systems.

3.2 Effect of reactants concentration and molar ratios on the aqueous photo-oxidation of vanillin

To examine the influence of VL and nitrate concentration and their molar ratios on VL photo-oxidation, we also characterized the reaction products from lower [VL] (0.01 mM VL*; A104; Table S2), lower [VL] concentrations and an equal molar ratio of VL/nitrate (0.01 mM VL + 0.01 mM AN; A115; Table S2), and lower [VL] and 1:100 molar ratio of VL/nitrate (0.01 mM VL + 1 mM AN; A126; Table S2) at pH 4. The normalized abundance of products from low [VL] experiments (A104-A126; Table S2) were up to 1.4 times higher than that of high [VL] experiments (A5 and A7; Table S2). Nevertheless, the major products for both low and high [VL] experiments were functionalized monomers (Figs. 1c-d and S123a--c) such as $C_8H_6O_4$ (No. 7, Table S2) and $C_{10}H_{10}O_5$ (No. 4, Table S2). For both VL* and VL+AN, the contribution of < 200 m/z to the normalized abundance of products was higher at low [VL] than at high [VL], while the opposite was observed for > 300 m/z (Fig. S123d). This indicates that functionalization was favored at low [VL], as supported by the higher $\langle OS_c \rangle$, while oligomerization was the dominant pathway at high [VL], consistent with more oligomers or polymeric products reported from high phenols concentration (e.g., 0.1 to 3 mM) (Li et al., 2014; Slikboer et al., 2015; Ye et al., 2019). This is probably due to an increased concentration of phenoxy radicals (in resonance with a carbon-centered cyclohexadienyl radical) at high [VL], promoting radical-radical polymerization (Sun et al., 2010; Li et al., 2014). Moreover At low [VL], the contribution of < 200 m/z to the normalized abundance of products was higher for 1:1 than 1:100 VL/nitrate molar ratio, further suggesting the prevalence of functionalization for the former formation of more oxidized products. This may also be the reason why In addition, 1:1 VL/nitrate (A115; Table S2) had higher $\langle OS_c \rangle$ than 1:100 VL/nitrate (A126; Table S2) VL/nitrate, indicating the formation of more oxidized products, but had fewer N-containing compounds compared to the latter. A possible explanation is that at 1:1 VL/nitrate, VL may efficiently competes with NO_2^- for $^{\bullet}OH$ (from nitrate or nitrite photolysis, Reaction 4; Table 1) and indirectly reduces $^{\bullet}NO_2$. Similarly, hydroxylation has been suggested to be an more important pathway for 1:1 VL/nitrite than in 1:10 VL/nitrite (Pang et al., 2019a). This may also be the reason why 1:1 VL/nitrate (A15; Table S2) had higher $\langle OS_c \rangle$ than 1:100 (A16; Table S2) VL/nitrate but had fewer N-containing compounds compared to the latter. Moreover, the contribution of <200 m/z to the normalized abundance of products was higher for 1:1 than 1:100 VL/nitrate molar ratio, further suggesting the formation of more oxidized products. Fragmentation, which leads to the decomposition of previously formed oligomers and generation of small, oxygenated products such as organic acids (Huang et al., 2018), may also occur for the low [VL] experiments. However, its importance would likely be observed at longer irradiation times, similar to the high [VL] experiments.

3.3 Participation of ammonium in the aqueous photo-oxidation of vanillin

Imidazole and imidazole derivatives have been reported to be the major products of glyoxal and ammonium sulfate reactions at pH 4 (Galloway et al., 2009; Yu et al., 2011; Sedehi et al., 2013; Gen et al., 2018; Mabato et al., 2019). Here, we compared VL+AN and VL+SN at pH 4 in terms of reaction products and oxidative characteristics to confirm the participation of ammonium in the aqueous photo-oxidation of VL. In both experiments The normalized abundance of the products was

comparable ~~i~~In both experiments (A7 and A9~~13~~; Table ~~S~~2), with $C_{10}H_{10}O_5$ (No. 4, Table S2) as the most abundant product (Figs. 1d and S6a), but in VL+SN, there was a significant amount of a VL dimer ($C_{15}H_{12}O_8$; No. 8~~9~~, ~~Table S3~~Table S2). Moreover, the nitrogen-containing compounds were distinct. Aside from the potential imidazole derivative ($C_5H_5N_3O_2$; No. 5~~10~~, Table S2~~3~~), $C_8H_9NO_3$ (No. 2, Table S2) was also observed from VL+AN but only under N_2-saturated conditions (Fig. 1b), probably due to further oxidation by ~~secondary oxidants from~~ ^{3}VL*. The product analysis suggests the participation of ammonium in the aqueous-phase reactions. Ammonium salts are an important constituent of atmospheric aerosols particles (Jimenez et al., 2009), and reactions between dicarbonyls (e.g., glyoxal) and ammonia or primary amines have been demonstrated to form BrC (De Haan et al., 2009, 2011; Nozière et al., 2009; Shapiro et al., 2009; Lee et al., 2013; Powelson et al., 2014; Gen et al., 2018; Mabato et al., 2019). Relative to VL+AN, the products from VL+SN had higher O:C ratios (e.g., $C_7H_4N_2O_7$; No. 9~~11~~, Table S2~~3~~), OS_c, and $\langle OS_c \rangle$ values (Table ~~S~~2).

3.4 Oxidation of guaiacol by photosensitized reactions of vanillin and photolysis of nitrate

The oxidation of phenols by ^{3}C* has been mainly studied using non-phenolic aromatic carbonyls (Anastasio et al., 1996; Smith et al., 2014, 2015; Yu et al., 2014; Chen et al., 2020) and aromatic ketones (Canonica et al., 2000) as triplet precursors. Recently, ^{3}VL* have also been shown to oxidize syringol (Smith et al., 2016), a non-carbonyl phenol, although the reaction products remain unknown. In this section, we discussed the photo-oxidation of guaiacol (GUA), a lignocellulosic BB pollutant (Kroflič et al., 2015) that is also a non-carbonyl phenol, in the presence of VL (GUA+VL) or nitrate (GUA+AN). The dark experiments did not show any substantial loss of VL or GUA (Fig. S3ce). Due to its poor light absorption in the solar range, GUA is not an effective photosensitizer (Smith et al., 2014; Yu et al., 2014). Accordingly, the direct GUA photodegradation resulted in minimal decay, which plateaued after ~3 hours. However, in the presence of VL or nitrate, the GUA decay rate constant was ~~faster~~higher by 2.2 (GUA+VL) and 1.3~~2~~ (GUA+AN) times, respectively, than for direct GUA photodegradation. The enhancement of GUA decay rate constant in the presence of VL is statistically significant ($p < 0.05$), while that in the presence of AN is not ($p > 0.05$). This enhanced GUA decay rate constant may be due to the ~~following main reactions:~~ oxidation of GUA by ^{3}VL* ~~(or the secondary oxidants it generates upon reaction with O_2), oxidation by $^{\bullet}$OH produced from nitrate photolysis, or nitration by $^{\bullet}NO_2$ from nitrate photolysis~~. As mentioned earlier, ~~the~~ ^{3}VL* chemistry appears to be more important than that of nitrate photolysis even at 1:10 molar ratio of VL/nitrate on account of the much higher molar absorptivity of VL compared to that of nitrate (Fig. S1) and the high VL concentration (0.1 mM) used in this study. However, the apparent quantum efficiency of GUA photodegradation (φ_{GUA}) in the presence of nitrate ($1.3 \times 10^{-2} \pm 2.9 \times 10^{-3}$) is ~14 times larger than that in the presence of VL ($9.0 \times 10^{-4} \pm 4.0 \times 10^{-4}$), suggesting that nitrate-mediated photo-oxidation of GUA is more efficient than that by photosensitized reactions of VL (see Text S7 for more details). The decay of VL in GUA+VL (A1~~4~~8; Table ~~S~~2) was 3 times slower than that of VL* (A5; Table ~~S~~2), which may be due to competition between ground-state VL and GUA for reactions with ^{3}VL* ~~(or the secondary oxidants it generates upon reaction with O_2)~~ or increased conversion of ^{3}VL* back to the ground state through the oxidation of GUA (Anastasio et al., 1996; Smith et al., 2014). The corresponding absorbance changes for the GUA experiments (Fig. 3~~1~~ce) were consistent with the observed decay trends. The minimal absorbance changes

for the direct GUA photodegradation also plateaued after ~3 hours. Moreover, the difference between GUA photo-oxidation in the presence of VL or nitrate was more evident, with the former showing much higher absorbance enhancement. ~~Similarly,~~ Yang et al. (2021) also observed greater light absorption during nitrate-mediated photo-oxidation relative to direct GUA photodegradation.

For the direct GUA photodegradation, GUA+VL, and GUA+AN, the normalized abundance of products was calculated only for GUA+VL (2.2; Table ~~S~~2), as the GUA signal from the UHPLC-qToF-MS in the positive ion mode was weak, which may introduce large uncertainties during normalization. Nonetheless, the number of products detected from these experiments (178, 266, and 844 for the direct GUA photodegradation, GUA+AN, and GUA+VL, respectively) corroborates the kinetics and absorbance results. The major products (Fig. 4~~3~~a) from the direct photodegradation of GUA were $C_{14}H_{14}O_4$ (No. 1~~0~~9, ~~Table S3~~Table S2), a typical GUA dimer, and a trimer ($C_{21}H_{20}O_6$; No. 11~~20~~, ~~Table S3~~Table S2) which likely originated from photoinduced O-H bond-breaking (Berto et al., 2016). In general, higher absolute signals ~~areas~~ were~~as~~ noted for oligomers (e.g., $C_{14}H_{14}O_4$, No. 10 and $C_{21}H_{20}O_6$, No. 11, Table S2) and hydroxylated products (e.g., $C_7H_8O_4$) in both GUA+VL and GUA+AN, similar to those observed from GUA oxidation by triplets of 3,4-dimethoxybenzaldehyde (DMB; a non-phenolic aromatic carbonyl) or $^{\bullet}OH$ (from H_2O_2 photolysis) (Yu et al., 2014). In contrast to the GUA aqSOA reported by Yu et al. (2014), the photo-oxidation of GUA in this study yielded nitrated compounds (e.g., $C_9H_{14}N_2O_6$, $C_{11}H_{14}N_2O_9$) from GUA+AN and VL dimers (e.g., $C_{16}H_{12}O_6$) from GUA+VL. However, based on a recent work on the aqueous photo-oxidation of guaiacyl acetone (another aromatic phenolic carbonyl) by DMB triplets, the hydroxylation and dimerization of DMB can also contribute to aqSOA (Jiang et al., 2021). The contributions from DMB-participated reactions were only minor due to the low initial DMB concentration (0.005 mM). Relative to GUA+AN, higher signals for dimers such as $C_{14}H_{14}O_4$ (No. 10, Table S2) and $C_{16}H_{12}O_6$ were noted in GUA+VL, possibly due to both GUA and ground-state VL being available as oxidizable substrates for ^{3}VL* ~~and the secondary oxidants it can generate~~. Also, a potential GUA tetramer ($C_{28}H_{24}O_8$, No. 12~~21~~, Table S2~~3~~) was observed only in GUA+VL, consistent with higher oligomer formation from the triplets-mediated photo-oxidation of phenolics relative to $^{\bullet}OH$-assisted photo-oxidation (Yu et al., 2014). In general, the products from the direct GUA photodegradation, GUA+VL, and GUA+AN had similar OS_c values (-0.5 to 0.5) (Figs. 4~~3~~b ~~–~~d), falling into the criterion of BBOA and SV-OOA (Kroll et al., 2011). In this work, ~~efficient~~ GUA photo-oxidation was observed in the presence of VL or~~and~~ AN, forming aqSOA composed of oligomers, hydroxylated products, and nitrated compounds (for GUA+AN). The higher product signals from GUA+VL compared to GUA+AN is likely due to the availability of both GUA and ground-state VL as aqSOA precursors.

~~3.5 Photo-oxidation pathways of vanillin via direct photosensitization and in the presence of nitrate~~

~~The most probable pathways of direct photosensitized and nitrate-mediated photo-oxidation of VL were proposed (Fig. 4). In Scheme 1 (pH 4 and pH <4 under air-saturated conditions), ^{3}VL* and $^{\bullet}OH$ (from ^{3}VL* or nitrate photolysis) can initiate H-atom abstraction to generate phenoxy or ketyl radicals (Huang et al., 2018; Vione et al., 2019). At pH 4, ring-opening products~~

~~(Fig. S5) from fragmentation in both VL* and VL+AN may have reacted with VL or dissolved ammonia to generate $C_{10}H_{10}O_5$ (Pang et al., 2019b) and a potential imidazole derivative ($C_5H_5N_3O_2$), respectively. Moreover, nitrate photolysis products promoted functionalization and nitration (e.g., $C_{16}H_{10}N_2O_9$). At pH <4, the reactivity of ^{3}VL* increased as suggested by the abundance of oligomers (e.g., $C_{16}H_{14}O_6$) and increased normalized abundance of N-containing compound~~

~~In Scheme 2 (pH 4, IPA or NaBC, under air saturated conditions), additional radicals generated ($^{\bullet}HO_2$ and $CO_3^{\bullet-}$) likely promoted more reactions. An abundant dimer ($C_{16}H_{14}O_6$) and higher oligomers (e.g., tetramers, $C_{31}H_{22}O_{12}$) were identified in VL*+IPA, possibly due to $^{\bullet}HO_2$ initiated reactions, while a functionalized monomer ($C_7H_4O_4$) was abundant in VL*+NaBC. In general, nitrate enhanced both oligomerization and functionalization in VL+IPA or VL+NaBC. In VL+AN+IPA, $C_{15}H_{12}O_8$ likely originated from $C_{16}H_{14}O_6$ via demethylation and multiple hydroxylations. In VL+AN+NaBC, $C_8H_6O_4$ was possibly generated via H atom abstraction from OCH_3 by $^{\bullet}OH$, and further addition with O_2 is energy barrierless (Priya and Lakshmipathi, 2017; Sun et al., 2019), generating a hydroperoxide (OCH_2OOH) that readily decompose to form $OCH_2O^{\bullet}$ and $^{\bullet}OH$ (Yaremenko et al., 2016). OCH2O$^{\bullet}$ is finally transformed into OCHO with the elimination of HO_2 in the presence of O_2 (Sun et al., 2019). Moreover, the abundance of $C_{15}H_{12}O_8$ was higher in VL+AN+NaBC than in VL*+NaBC.~~

4 Conclusions and atmospheric implications

This study shows that the photo-oxidation of VL via its direct photosensitized reactions and in the presence of nitrate can generate aqSOA composed of oligomers, functionalized monomers, oxygenated ring-opening products, and nitrated compounds (for nitrate-mediated reactions). The characterization of products presented in this work complements earlier studies (e.g., Smith et al. 2014, 2015, 2016) that mainly discussed the kinetics and aqSOA yield of triplet-driven oxidation of phenols. Although nitrate did not substantially affect the VL decay rate~~s~~ constants, likely due to much higher molar absorptivity of VL than nitrate and high VL concentration used in this work, the presence of nitrate promoted functionalization and nitration, indicating the significance of nitrate photolysis in this aqSOA formation pathway. ~~While~~This work demonstrates that nitration, which is ~~can be~~ an important process for producing light-absorbing organics or BrC (Jacobson, 1999; Kahnt et al., 2013; Mohr et al., 2013; Laskin et al., 2015; Teich et al., 2017; Li et al., 2020), ~~its effect on~~can also affect the aqueous-phase processing of triplet-generating aromatics ~~has not yet been examined in detail~~. On a related note, a recent work (Ma et al., 2021) mimicking phenol oxidation by DMB (a non-phenolic aromatic carbonyl) triplets in more concentrated conditions in aerosol liquid water (ALW) showed that significantly higher AN concentration (0.5 M) increased the photodegradation rate constant for guaiacyl acetone (an aromatic phenolic carbonyl with high Henry's law constant, 1.2×10^6 M atm^{-1}; McFall et al., 2020) by > 20 times which was ascribed to $^{\bullet}OH$ formation from nitrate photolysis (Brezonik and Fulkerson-Brekken, 1998; Chu and Anastasio, 2003). The same study also estimated that reactions of phenols with high Henry's law constants (10^6 to 10^9 M atm^{-1}) can be important for SOA formation in ALW, with mechanisms mainly governed by ^{3}C* and $^1O_2$ (Ma et al., 2021). Likewise, Zhou et al. (2019) reported that the direct photodegradation of acetosyringone was faster by about 6 times in the presence of 2 M $NaClO_4$. However, the opposite was noted for the photodegradation of VL in sodium sulfate or sodium nitrate, which would

occur slower (~2 times slower in 0.5 M sodium sulfate and ~10 times slower in 0.124 M sodium nitrate) in ALW relative to dilute aqueous phase in clouds. These suggest that the nature of inorganic ions may have an essential role in the photodegradation of organic compounds in the aqueous phase (Loisel et al., 2021).

Furthermore, a potential imidazole derivative observed from the VL+AN (A7; Table S2) experiment suggests that ammonium may participate in aqSOA formation from the photo-oxidation of phenolic aromatic carbonyls. Also, the oligomers from these reaction systems may be rather recalcitrant to fragmentation based on their high abundance, even at the longest irradiation time used in this study. Nonetheless, the increasing concentration of small organic acids over time implies that fragmentation becomes important at extended irradiation times. Aromatic carbonyls and nitrophenols have been reported to be the most important classes of BrC in cloud water heavily affected by biomass burning in the North China Plain (Desyaterik et al., 2013). Correspondingly, the most abundant products from our reaction systems (pH 4, air-saturated solutions) are mainly potential BrC chromophores. These suggest that aqSOA generated in cloud/fog water from the oxidation of biomass burning aerosols via direct photosensitized reactions and nitrate photolysis products can impact aerosol optical properties and radiative forcing, particularly for areas where biomass burning is intensive.

Our results indicate that the photo-oxidation of VL is influenced by O_2secondary oxidants from VL triplets, pH, the presence of VOCs and inorganic anions, and reactants concentration and molar ratios. Compared to Under N_2-saturated conditions, the absence of O_2 likely hindered the secondary steps in VL decay (e.g., reaction of ketyl radical and O_2), regenerating VL as suggested by the minimal VL decaymore efficient VL photo-oxidation was observed under air-saturated conditions (O_2 is present), which can be attributed to the generation of secondary oxidants (e.g., $^1O_2$, $O_2^{\bullet-}$/$^{\bullet}HO_2$, $^{\bullet}OH$) from ^{3}VL*. Further enhancement of VL photo-oxidation under air-saturated conditions in the presence of nitrate indicates synergistic effects between secondary oxidants from VL triplets and nitrate photolysis products.In contrast, ^{3}VL*-initiated reactions proceeded rapidly under air-saturated conditions (O_2 is present) as indicated by higher VL decay rate constant and increased normalized abundance of products. For pH 4 experiments, the presence of both O_2 and nitrate resulted in the highest normalized abundance of products (including N-containing compounds) and $\langle OS_c \rangle$, which may be due to O_2 promoting VL nitration. Nevertheless, further work is necessary to assess the effect of O_2 on the reactive intermediates involved in ^{3}VL*-driven photo-oxidation and elucidate the mechanisms of VL photo-oxidation under air-saturated conditions. Additionally, the formation of oligomers from VL photo-oxidation was observed to be promoted at low pH (< 4) or in the presence of IPA/NaBC, which likely generated additional radicals such as $^{\bullet}HO_2$ and $CO_3^{\bullet-}$. As aerosols comprise more complex mixtures of organic and inorganic compounds, it is worthwhile to explore the impacts of other potential aerosol constituents on aqSOA formation and photo-oxidation studies. This can also be beneficial in understanding the interplay among different reaction mechanisms during photo-oxidation.Moreover, lLow VL concentration favored functionalization, while oligomerization prevailed at high VL concentration, consistent with past works (Li et al., 2014; Slikboer et al., 2015; Ye et al., 2019). Hydroxylation was observed to be important for equal molar ratios of VL and nitrate, likely due to VL competing with nitrite for $^{\bullet}OH$. The oxidation of guaiacol, a non-carbonyl phenol, by photosensitized reactions of vanillin was also shown to be moreless efficient than that by nitrate photolysis products based on its lower apparent quantum efficiency.

In this study, we investigated reactions of VL and nitrate at concentrations in cloud/fog water. The concentrations of VL and nitrate can be significantly higher in aqueous aerosol particles. As a major component of aerosols, the concentration of nitrate can be as high as sulfate (Huang et al., 2014). More studies should then explore the direct photosensitized oxidation and nitrate-mediated photo-oxidation of other biomass burning-derived phenolic aromatic carbonyls, particularly those with high molar absorption coefficients and can generate $^3C^*$. The influences of reaction conditions should also be investigated to better understand the oxidation pathways. As aerosols comprise more complex mixtures of organic and inorganic compounds, it is worthwhile to explore the impacts of other potential aerosol constituents on aqSOA formation and photo-oxidation studies. This can also be beneficial in understanding the interplay among different reaction mechanisms during photo-oxidation. Considering that biomass burning emissions are expected to increase continuously, further studies on these aqSOA formation pathways are strongly suggested.

Data availability.

The data used in this publication are available to the community and can be accessed by request to the corresponding author.

Author contributions.

BRGM designed and conducted the experiments; YL provided assistance in measurements and helped to analyze experimental data; YJ provided assistance in measurements; BRGM, YL, and CKC wrote the paper. All co-authors contributed to the discussion of the manuscript.

Competing interests.

The authors declare that they have no conflict of interest.

Acknowledgments.

This work was financially supported by the National Natural Science Foundation of China (41875142 and 42075100). Y.J.L acknowledges support from the Science and Technology Development Fund, Macau SAR (File no. 0019/2020/A1), the Multi-Year Research grant (No. MYRG2018-00006-FST) from the University of Macau. D.D.H. acknowledges support from the National Natural Science Foundation of China (21806108). X.L. acknowledges support from the Local Innovative and Research Teams Project of Guangdong Pearl River Talents Program (2019BT02Z546). T.N. acknowledges support from the Hong Kong Research Grants Council (21304919) and City University of Hong Kong (9610409). C.H.L. acknowledges support from the City University of Hong Kong (9610458 and 7005576).

References

Abida, O., Mielke, L. H., and Osthoff, H. D.: Observation of gas phase peroxynitrous and peroxynitric acid during the photolysis of nitrate in acidified frozen solutions, Chem. Phys. Lett., 511, 187–192, https://doi.org/10.1016/j.cplett.2011.06.055, 2011.

Anastasio, C., Faust, B. C., and Rao, C. J.: Aromatic carbonyl compounds as aqueous-phase photochemical sources of hydrogen peroxide in acidic sulfate aerosols, fogs, and clouds. 1. Non-phenolic methoxybenzaldehydes and methoxyacetophenones with reductants (phenols), Environ. Sci. Technol., 31, 218−232, https://doi.org/10.1021/es960359g, 1996.

Arakaki, T., Miyake, T., Hirakawa, T., and Sakugawa, H.: pH dependent photoformation of hydroxyl radical and absorbance of aqueous-phase N(III) (HNO_2 and NO_2^-), Environ. Sci. Technol., 33, 2561−2565, https://doi.org/10.1021/es980762i, 1999.

Bateman, A. P., Laskin, J., Laskin, A., and Nizkorodov, S. A.: Applications of high-resolution electrospray ionization mass spectrometry to measurements of average oxygen to carbon ratios in secondary organic aerosols, Environ. Sci. Technol., 46, 8315–8324, https://doi.org/10.1021/es3017254, 2012.

Benedict, K. B., McFall, A. S., and Anastasio, C.: Quantum yield of nitrite from the photolysis of aqueous nitrate above 300 nm, Environ. Sci. Technol., 51, 4387−4395, https://doi.org/10.1021/acs.est.6b06370, 2017.

~~Berke, A. E., Bhat, T. A., Myers, H., Gubbins, E. F., Nwankwo, A. A. O., Lu, K., Timpane, L., and Keller, C.: Effect of short-chain alcohols on the bulk-phase reaction between glyoxal and ammonium sulfate, Atmos. Environ., 198, 407−416, https://doi.org/10.1016/j.atmosenv.2018.11.015, 2019.~~

Berto, S., De Laurentiis, E., Tota, T., Chiavazza, E., Daniele, P.G., Minella, M., Isaia, M., Brigante, M., and Vione, D.: Properties of the humic-like material arising from the photo-transformation of L-tyrosine, Sci. Total Environ., 434–444, https://doi.org/10.1016/j.scitotenv.2015.12.047, 2016.

Bianco, A., Minella, M., De Laurentiis, E., Maurino, V., Minero, C., and Vione, D.: Photochemical generation of photoactive compounds with fulvic-like and humic-like fluorescence in aqueous solution, Chemosphere, 111, 529–536, https://doi.org/10.1016/j.chemosphere.2014.04.035, 2014.

Bianco, A., Deguillaume, L., Vaïtilingom, M., Nicol, E., Baray, J.-L., Chaumerliac, N., and Bridoux, M.: Chemical characterization of cloud water collected at Puy de Dôme by FT-ICR MS reveals the presence of SOA components, Environ. Sci. Technol., 52, 10275–10285, https://doi.org/10.1021/acsearthspacechem.9b00153, 2018.

Bianco, A., Passananti, M., Brigante, M., and Mailhot, G.: Photochemistry of the cloud aqueous phase: a review, Molecules, 25, 423, https://doi.org/10.3390/molecules25020423, 2020.

Birks, J.B.: Organic Molecular Photophysics, John Wiley & Sons, 1973.

Blando, J. D. and Turpin, B. J.: Secondary organic aerosol formation in cloud and fog droplets: a literature evaluation of plausibility, Atmos. Environ., 34, 1623−1632, https://doi.org/10.1016/S1352-2310(99)00392-1, 2000.

Bond, T. C., Streets, D. G., Yarber, K. F., Nelson, S. M., Woo, J-H., and Klimont, Z.: A technology-based global inventory of black and organic carbon emissions from combustion, J. Geophys. Res., 109, https://doi.org/10.1029/2003JD003697, 2004.

~~Bouillon, R.C. and Miller, W.L.: Photodegradation of dimethyl sulfide (DMS) in natural waters: laboratory assessment of the nitrate-photolysis-induced DMS oxidation, Environ. Sci. Technol., 39, 9471−9477, https://doi.org/10.1021/es048022z, 2005.~~

Brezonik, P. L. and Fulkerson-Brekken, J.: Nitrate-induced photolysis in natural waters: controls on concentrations of hydroxyl radical photo-intermediates by natural scavenging agents, Environ. Sci. Technol., 32, 3004−3010, mhttps://doi.org/10.1021/es9802908, 1998.

Canonica, S., Jans, U., Stemmler, K., and Hoigne, J.: Transformation kinetics of phenols in water: Photosensitization by dissolved natural organic material and aromatic ketones, Environ. Sci. Technol., 29, 1822–1831, https://doi.org/10.1021/es00007a020, 1995.

Canonica, S., Hellrung, B., and Wirz, J.: Oxidation of phenols by triplet aromatic ketones in aqueous solution, J. Phys. Chem, 104, 1226–1232, https://doi.org/10.1021/jp9930550, 2000.

~~Canonica, S., Kohn, T., Mac, M., Real, F.J., Wirz, J., and Von Gunten, U.: Photosensitizer method to determine rate constants for the reaction of carbonate radical with organic compounds, Environ. Sci. Technol., 39, 9182−9188, https://doi.org/10.1021/es051236b, 2005.~~

~~Carey, F. A.: Organic Chemistry, 4th Ed., McGraw-Hill, USA, 2000.~~

Chang, J. L. and Thompson, J. E.: Characterization of colored products formed during irradiation of aqueous solutions containing H_2O_2 and phenolic compounds, Atmos. Environ., 44, 541−551, https://doi.org/10.1016/j.atmosenv.2009.10.042, 2010.

Chen, Y., Li, N., Li, X., Tao, Y., Luo, S., Zhao, Z., Ma, S., Huang, H., Chen, Y., Ye, Z., and Ge, X.: Secondary organic aerosol formation from $^{3}C^{*}$-initiated oxidation of 4-ethylguaiacol in atmospheric aqueous-phase, Sci. Total Environ., 723. 137953, https://doi.org/10.1016/j.scitotenv.2020.137953, 2020.

Chu, L. and Anastasio, C.: Quantum yields of hydroxyl radical and nitrogen dioxide from the photolysis of nitrate on ice, J. Phys. Chem. A, 107, 9594−9602, https://doi.org/10.1021/jp0349132, 2003.

Collett, J. L. Jr., Hoag, K. J., Sherman, D. E., Bator, A., and Richards, L. W.: Spatial and temporal variations in San Joaquin Valley fog chemistry, Atmos. Environ., 33, 129−140, https://doi.org/10.1016/S1352-2310(98)00136-8, 1998.

~~Collett, J. L. Jr., Hoag, K. J., Rao, X., and Pandis, S. N.: Internal acid buffering in San Joaquin Valley fog drops and its influence on aerosol processing, Atmos. Environ., 33, 4833–4847, https://doi.org/10.1016/S1352-2310(99)00221-6, 1999.~~

~~De Gouw, J. and Jimenez, J. L.: Organic aerosols in the Earth's atmosphere, Environ. Sci. Technol., 43, 7614–7618, https://doi.org/10.1021/es9006004, 2009.~~

De Haan, D. O., Corrigan, A. L., Tolbert, M. A., Jimenez, J. L., Wood, S. E., and Turley, J. J.: Secondary organic aerosol formation by self-reactions of methylglyoxal and glyoxal in evaporating droplets, Environ. Sci. Technol., 43, 8184−8190, https://doi.org/10.1021/es902152t, 2009.

De Haan, D. O., Hawkins, L. N., Kononenko, J. A., Turley, J. J., Corrigan, A. L., Tolbert, M. A., and Jimenez, J. L.: Formation of nitrogen-containing oligomers by methylglyoxal and amines in simulated evaporating cloud droplets, Environ. Sci. Technol., 45, 984−991, ttps://doi.org/10.1021/es102933x, 2011.

De Haan, D.O., Pajunoja, A., Hawkins, L. N., Welsh, H.G., Jimenez, N. G., De Loera, A., Zauscher, M., Andretta, A. D., Joyce, B. W., De Haan, A. C., Riva, M., Cui, T., Surratt, J. D., Cazaunau, M., Formenti, P., Gratien, A., Pangui, E., and Doussin, J-F.: Methylamine's effects on methylglyoxal-containing aerosol: chemical, physical, and optical changes, ACS Earth Space Chem., 3, 1706–1716, https://doi.org/10.1021/acsearthspacechem.9b00103, 2019.

De Laurentiis, E., Socorro, J., Vione, D., Quivet, E., Brigante, M., Mailhot, G., Wortham, H., and Gligorovski, S.: Phototransformation of 4-phenoxyphenol sensitised by 4-carboxybenzophenone: Evidence of new photochemical pathways in the bulk aqueous phase and on the surface of aerosol deliquescent particles, Atmos. Environ., 81, 569–578, https://doi.org/10.1016/j.atmosenv.2013.09.036, 2013a.

De Laurentiis, E., Sur, B., Pazzi, M., Maurino, V., Minero, C., Mailhot, G., Brigante, M., and Vione, D.: Phenol transformation and dimerisation, photosensitised by the triplet state of 1-nitronaphthalene: A possible pathway to humic-like substances (HULIS) in atmospheric waters, Atmos. Environ., 70, 318–327, https://doi.org/10.1016/j.atmosenv.2013.01.014, 2013b.

Desyaterik, Y., Sun, Y., Shen, X., Lee, T., Wang, X., Wang, T., and Collett, J. L. Jr.: Speciation of "brown" carbon in cloud water impacted by agricultural biomass burning in eastern China, J. Geophys. Res. Atmos., 118, 7389–7399, https://doi.org/10.1002/jgrd.50561, 2013.

Du, Y., Fu, Q. S., Li, Y., and Su, Y.: Photodecomposition of 4-chlorophenol by reactive oxygen species in UV/air system, J. Hazard. Mater., 186, 491–496, https://doi.org/10.1016/j.jhazmat.2010.11.023, 2011.

Dzengel, J., Theurich, J., and Bahnemann, D. W.: Formation of nitroaromatic compounds in advanced oxidation processes: photolysis versus photocatalysis, Environ. Sci. Technol., 33, 294–300, https://doi.org/10.1021/es980358j, 1999.

Ervens, B., Turpin, B. J., and Weber, R. J.: Secondary organic aerosol formation in cloud droplets and aqueous particles (aqSOA): a review of laboratory, field and model studies, Atmos. Chem. Phys., 11, 11069−11102, https://doi.org/10.5194/acp-11-11069-2011, 2011.

Fischer, M. and Warneck, P.: Photodecomposition of nitrite and undissociated nitrous acid in aqueous solution, J. Phys. Chem., 100, 18749−18756, https://doi.org/10.1021/jp961692+, 1996.

Fleming, L. T., Lin, P., Laskin, A., Laskin, J., Weltman, R., Edwards, R. D., Arora, N. K., Yadav, A., Meinardi, S., Blake, D. R., Pillarisetti, A., Smith, K. R., and Nizkorodov, S. A.: Molecular composition of particulate matter emissions from dung and brushwood burning household cookstoves in Haryana, India, Atmos. Chem. Phys., 18, 2461–2480, https://doi.org/10.5194/acp-18-2461-2018, 2018.

Foote, C.S.: Definition of type I and type II photosensitized oxidation, Photochem. Photobiol., 54, 659, https://doi.org/10.1111/j.1751-1097.1991.tb02071.x, 1991.

Galloway, M. M., Chhabra, P. S., Chan, A. W. H., Surratt, J. D., Flagan, R. C., Seinfeld, J. H., and Keutsch, F. N.: Glyoxal uptake on ammonium sulphate seed aerosol: reaction products and reversibility of uptake under dark and irradiated conditions, Atmos. Chem. Phys., 9, 3331−3345, https://doi.org/10.5194/acp-9-3331-2009, 2009.

Gelencsér, A., Hoffer, A., Kiss, G., Tombácz, E., Kurdi, R., and Bencze, L.: In-situ formation of light-absorbing organic matter in cloud water, J. Atmos. Chem., 45, 25–33, https://doi.org/10.1023/A:1024060428172, 2003.

Gen, M., Huang, D. D., and Chan, C. K., Reactive uptake of glyoxal by ammonium-containing salt particles as a function of relative humidity, Environ. Sci. Technol., 52, 6903−6911, https://doi.org/10.1021/acs.est.8b00606, 2018.

Gen, M., Zhang, R., Huang, D. D., Li, Y., and Chan, C. K.: Heterogeneous SO_2 oxidation in sulfate formation by photolysis of particulate nitrate, Environ. Sci. Technol. Lett., 6, 86–91, https://doi.org/10.1021/acs.estlett.8b00681, 2019a.

Gen, M., Zhang, R., Huang, D. D., Li, Y., and Chan, C. K.: Heterogeneous oxidation of SO_2 in sulfate production during nitrate photolysis at 300 nm: Effect of pH, relative humidity, irradiation intensity, and the presence of organic compounds, Environ. Sci. Technol., 53, 8757–8766, https://doi.org/10.1021/acs.est.9b01623, 2019b.

George, C., Ammann, M., D'Anna, B., Donaldson, D.J., and Nizkorodov, S.A.: Heterogeneous photochemistry in the atmosphere, Chem. Rev., 115, 4218–4258, https://doi.org/10.1021/cr500648z, 2015.

George, C., Brüggemann, M., Hayeck, N., Tinel, L., and Donaldson, D. J.: Interfacial photochemistry: physical chemistry of gas-liquid interfaces, in: Developments in Physical & Theoretical Chemistry, edited by: Faust, J. A. and House, J. E., Elsevier, 435−457, https://doi.org/10.1016/B978-0-12-813641-6.00014-5, 2018.

Gilardoni, S., Massoli, P., Paglione, M., Giulianelli, L., Carbone, C., Rinaldi, M., Decesari, S., Sandrini, S., Costabile, F., Gobbi, G.P., Pietrogrande, M.C., Visentin, M., Scotto, F., Fuzzi, S., and Facchini, M.C.: Direct observation of aqueous secondary organic aerosol from biomass-burning emissions, PNAS., 113, 10013–10018, https://doi.org/10.1073/pnas.1602212113, 2016.

Giulianelli, L., Gilardoni, S., Tarozzi, L., Rinaldi, M., Decesari, S., Carbone, C., Facchini, M. C., and Fuzzi, S.: Fog occurrence and chemical composition in the Po valley over the last twenty years, Atmos. Environ., 98, 394–401, https://doi.org/10.1016/j.atmosenv.2014.08.080, 2014.

Gold, M. H., Kutsuki, H., and Morgan, M. A.: Oxidative degradation of lignin by photochemical and chemical radical generating systems, Photochem. Photobiol., 38, 647–651, https://doi.org/10.1111/j.1751-1097.1983.tb03595.x, 1983.

Goldstein, S. and Czapski, G.: Kinetics of nitric oxide autoxidation in aqueous solution in the absence and presence of various reductants. The nature of the oxidizing intermediates, J. Am. Chem. Soc., 117, 12078–12084, https://doi.org/10.1021/ja00154a007, 1995a.

Goldstein, S. and Czapski, G.: The reaction of •NO with $O_2^{\bullet-}$ and $^{\bullet}HO_2$: a pulse radiolysis study, Free Radical Biol. Med., 19, 505–510, https://doi.org/10.1016/0891-5849(95)00034-U, 1995b.

Goldstein, S., Czapski, G., Lind, J., and Merényi, G.: Mechanism of decomposition of peroxynitric Ion (O_2NOO^-): Evidence for the formation of $O_2^{\bullet-}$ and $^{\bullet}NO_2$ radicals, Inorg. Chem., 37, 3943−3947, https://doi.org/10.1021/ic9800511, 1998.

Goldstein, S., Lind, J., and Merényi, G.: Chemistry of peroxynitrites as compared to peroxynitrates, Chem. Rev., 10, 2457−2470, https://doi.org/10.1021/cr0307087, 2005.

Grosjean, D.: Reactions of o-cresol and nitrocresol with nitrogen oxides (NO_x) in sunlight and with ozone–nitrogen dioxide mixtures in the dark, Environ. Sci. Technol., 19, 968–974, https://doi.org/10.1021/es00140a014, 1985.

Herrmann, H.: On the photolysis of simple anions and neutral molecules as sources of O^-/OH, SO_x^- and Cl in aqueous solution, Phys. Chem. Chem. Phys., 9, 3935-3964, https://doi.org/10.1039/B618565G, 2007.

Herrmann, H., Hoffmann, D., Schaefer, T., Bräuer, P., and Tilgner, A.: Tropospheric aqueous-phase free-radical chemistry: Radical sources, spectra, reaction kinetics and prediction tools, Chem Phys Chem., 11, 3796−3822, https://doi.org/10.1002/cphc.201000533, 2010.

Hippelein, M.: Background concentrations of individual and total volatile organic compounds in residential indoor air of Schleswig-Holstein, Germany, J. Environ. Monit., 6, 745–752, https://doi.org/10.1039/b401139m, 2004.

Hoffer, A., Kiss, G., Blazsó, M., and Gelencsér, A.: Chemical characterization of humic-like substances (HULIS) formed from a lignin-type precursor in model cloud water, Geophys. Res. Lett., 31, https://doi.org/10.1029/2003GL018962, 2004.

Hoffmann, E.H., Tilgner, A., Wolke, R., Böge, O., Walter, A., and Herrmann, H.: Oxidation of substituted aromatic hydrocarbons in the tropospheric aqueous phase: kinetic mechanism development and modelling, Phys. Chem. Chem. Phys., 20, 10960–10977, https://doi.org/10.1039/C7CP08576A, 2018.

Holčapek, M., Jirásko, R., and Lísa, M.: Basic rules for the interpretation of atmospheric pressure ionization mass spectra of small molecules, J. Chromatogr. A, 1217, 3908–3921, https://doi.org/10.1016/j.chroma.2010.02.049, 2010.

Huang, D. D., Zhang, Q., Cheung, H. H. Y., Yu, L., Zhou, S., Anastasio, C., Smith, J. D., and Chan, C. K.: Formation and evolution of aqSOA from aqueous-phase reactions of phenolic carbonyls: comparison between ammonium sulfate and ammonium nitrate solutions, Environ. Sci. Technol., 52, 9215–9224, https://doi.org/10.1021/acs.est.8b03441, 2018.

Huang, J. P. and Mabury, S. A.: The role of carbonate radical in limiting the persistence of sulfur-containing chemicals in sunlit natural waters, Chemosphere, 41, 1775−1782, https://doi.org/10.1016/S0045-6535(00)00042-4, 2000.

Huang, R.-J., Zhang, Y., Bozzetti, C., Ho, K.-F., Cao, J.-J., Han, Y., Daellenbach, K. R., Slowik, J. G., Platt, S. M., Canonaco, F., Zotter, P., Wolf, R., Pieber, S. M., Bruns, E. A., Crippa, M., Ciarelli, G., Piazzalunga, A., Schwikowski, M., Abbaszade,

G., Schnelle-Kreis, J., Zimmermann, R., An, Z., Szidat, S., Baltensperger, U., El Haddad, I., and Prévôt, A. S. H.: High secondary aerosol contribution to particulate pollution during haze events in China, Nature, 514, 218–222, https://doi.org/10.1038/nature13774, 2014.

Huang, X. H. H., Ip, H. S. S., and Yu, J. Z.: Secondary organic aerosol formation from ethylene in the urban atmosphere of Hong Kong: A multiphase chemical modeling study, J. Geophys. Res., 116, D03206, https://doi.org/10.1029/2010JD014121, 2011.

Jacobson, M. Z.: Isolating nitrated and aromatic aerosols and nitrated aromatic gases as sources of ultraviolet light absorption, J. Geophys. Res., 104, 3527–3542, https://doi.org/10.1029/1998JD100054, 1999.

Jiang, W., Misovich, M. V., Hettiyadura, A. P. S., Laskin, A., McFall, A. S., Anastasio, C., and Zhang, Q.: Photosensitized reactions of a phenolic carbonyl from wood combustion in the aqueous phase—chemical evolution and light absorption properties of aqSOA, Environ. Sci. Technol., 55, 5199–5211, https://doi.org/10.1021/acs.est.0c07581, 2021.

Jimenez, J. L., Canagaratna, M. R., Donahue, N. M., Prevot, A.S.H., Zhang, Q., Kroll, J. H., DeCarlo, P. F., Allan, J. D., Coe, H., Ng, N. L., Aiken, A.C., Docherty, K.S., Ulbrich, I. M., Grieshop, A. P., Robinson, A. L., Duplissy, J., Smith, J. D., Wilson, K. R., Lanz, V.A., Hueglin, C., Sun, Y. L., Tian, J., Laaksonen, A., Raatikainen, T., Rautiainen, J., Vaattovaara, P., Ehn, M., Kulmala, M., Tomlinson, J. M., Collins, D. R., Cubison, M. J., Dunlea, E., J., Huffman, J. A., Onasch, T. B., Alfarra, M. R., Williams, P. I., Bower, K., Kondo, Y., Schneider, J., Drewnick, F., Borrman, S., Weimer, S., Demerjian, K., Salcedo, D., Cottrell, L., Griffin, R., Takami, A., Miyoshi, T., Hatakeyama, S., Shimono, A., Sun, J. Y., Zhang, Y. M., Dzepina, K., Kimmel, J. R., Sueper, D., Jayne, J. T., Herndon, S. C., Trimborn, A. M., Williams, L. R., Wood, E. C., Middlebrook, A. M., Kolb, C. E., Baltensperger, U., and Worsnop, D. R.: Evolution of organic aerosols in the atmosphere, Science, 326, 1525–1529, https://doi.org/10.1126/science.1180353, 2009.

~~Jung, H., Chadha, T. S., Kim, D., Biswas, P., and Jun, Y.-S.: Photochemically assisted fast abiotic oxidation of manganese and formation of δ-MnO_2 nanosheets in nitrate solution, Chem. Commun., 53, 4445–4448, https://doi.org/10.1039/C7CC00754J, 2017.~~

Kahnt, A., Behrouzi, S., Vermeylen, R., Shalamzari, M. S., Vercauteren, J., Roekens, E., Claeys, M., and Maenhaut, W.: One-year study of nitro-organic compounds and their relation to wood burning in PM_{10} aerosol from a rural site in Belgium, Atmos. Environ., 81, 561−568, https://doi.org/10.1016/j.atmosenv.2013.09.041, 2013.

~~Kanakidou, M., Seinfeld, J. H., Pandis, S. N., Barnes, I., Dentener, F. J., Facchini, M. C., Van Dingenen, R., Ervens, B., Nenes, A., Nielsen, C. J., Swietlicki, E., Putaud, J. P., Balkanski, Y., Fuzzi, S., Horth, J., Moortgat, G. K., Winterhalter, R., Myhre, C. E. L., Tsigaridis, K., Vignati, E., Stephanou, E. G., and Wilson, J.: Organic aerosol and global climate modelling: a review, Atmos. Chem. Phys., 5, 1053–1123, https://doi.org/10.5194/acp-5-1053-2005, 2005.~~

Kaur, R. and Anastasio, C.: First measurements of organic triplet excited states in atmospheric waters, Environ. Sci. Technol., 52, 5218–5226., https://doi.org/10.1021/acs.est.7b06699, 2018.

Kaur, R., Labins, J. R., Helbock, S. S., Jiang, W., Bein, K. J., Zhang, Q., and Anastasio, C.: Photooxidants from brown carbon and other chromophores in illuminated particle extracts, Atmos. Chem. Phys., 19, 6579–6594, https://doi.org/10.5194/acp-19-6579-2019, 2019.

Kebarle, P. A.: A brief overview of the mechanisms involved in electrospray mass spectrometry, J. Mass Spectrom., 35, 804−817, https://doi.org/10.1002/9783527628728.ch1, 2000.

Kim, D.-h., Lee, J., Ryu, J., Kim, K., and Choi, W.: Arsenite oxidation initiated by the UV photolysis of nitrite and nitrate, Environ. Sci. Technol., 48, 4030−4037, https://doi.org/10.1021/es500001q, 2014.

Kitanovski, Z., Čusak, A., Grgić, I., and Claeys, M.: Chemical characterization of the main products formed through aqueous-phase photonitration of guaiacol, Atmos. Meas. Tech., 7, 2457–2470, https://doi.org/10.5194/amt-7-2457-2014, 2014.

Klodt, A.L., Romonosky, D.E., Lin, P., Laskin, J., Laskin, A., and Nizkorodov, S.A.: Aqueous photochemistry of secondary organic aerosol of α-pinene and α-humulene in the presence of hydrogen peroxide or inorganic salts, ACS Earth Space Chem., 3, 12, 2736–2746, https://doi.org/10.1021/acsearthspacechem.9b00222, 2019.

Kourtchev, I., Fuller, S. J., Giorio, C., Healy, R. M., Wilson, E., O'Connor, I., Wenger, J. C., McLeod, M., Aalto, J., Ruuskanen, T. M., Maenhaut, W., Jones, R., Venables, D. S., Sodeau, J. R., Kulmala, M., and Kalberer, M.: Molecular composition of biogenic secondary organic aerosols using ultrahigh-resolution mass spectrometry: comparing laboratory and field studies, Atmos. Chem. Phys., 14, 2155−2167, https://doi.org/10.5194/acp-14-2155-2014, 2014.

Kroflič, A., Grilc, M., and Grgić, I.: Unraveling pathways of guaiacol nitration in atmospheric waters: nitrite, a source of reactive nitronium ion in the atmosphere, Environ. Sci. Technol., 49, 9150–9158, https://doi.org/10.1021/acs.est.5b01811, 2015.

Kroflič, A., Anders, J., Drventić, I., Mettke, P., Böge, O., Mutzel, A., Kleffmann, J., and Herrmann, H.: Guaiacol nitration in a simulated atmospheric aerosol with an emphasis on atmospheric nitrophenol formation mechanisms, ACS Earth Space Chem., https://doi.org/10.1021/acsearthspacechem.1c00014, 2021.

Kroll, J. H., Donahue, N. M., Jimenez, J. L., Kessler, S. H., Canagaratna, M. R., Wilson, K. R., Altieri, K. E., Mazzoleni, L. R., Wozniak, A. S., Bluhm, H., Mysak, E. R., Smith, J. D., Kolb, C. E., and Worsnop, D. R.: Carbon oxidation state as a metric for describing the chemistry of atmospheric organic aerosol, Nat. Chem., 3, 133–139, https://doi.org/10.1038/nchem.948, 2011.

Kruve, A., Kaupmees, K., Liigand, J., and Leito, I.: Negative electrospray ionization via deprotonation: predicting the ionization efficiency, Anal. Chem., 86, 4822–4830, https://doi.org/10.1021/ac404066v, 2014.

~~Lammel, G., Perner, D., and Warneck, P.: Decomposition of pernitric acid in aqueous solution, J. Phys. Chem., 94, 6141−6144, https://doi.org/10.1021/j100378a091, 1990.~~

Laskin, A., Laskin, J., and Nizkorodov, S.A.: Chemistry of atmospheric brown carbon, Chem. Rev., 115, 4335–4382, https://doi.org/10.1021/cr5006167, 2015.

Lathioor, E. C., Leigh, W. J., and St. Pierre, M. J.: Geometrical effects on intramolecular quenching of aromatic ketone (π,π*) triplets by remote phenolic hydrogen abstraction, J. Am. Chem. Soc., 121, 11984–11992, https://pubs.acs.org/doi/abs/10.1021/ja991207z, 1999.

LeClair, J. P., Collett, J. L., and Mazzolen, L. R.: Fragmentation analysis of water-soluble atmospheric organic matter using ultrahigh-resolution FT-ICR mass spectrometry, Environ. Sci. Technol., 46, 4312–4322, https://doi.org/10.1021/es203509b, 2012.

Lee, A. K. Y., Herckes, P., Leaitch, W. R., Macdonald, A. M., and Abbatt, J. P. D.: Aqueous OH oxidation of ambient organic aerosol and cloud water organics: Formation of highly oxidized products, Geophys. Res. Lett., 38, L11805, https://doi.org/10.1029/2011GL047439, 2011.

Lee, A. K. Y., Zhao, R., Li, R., Liggio, J., Li, S.-M., and Abbatt, J. P. D.: Formation of light absorbing organo-nitrogen species from evaporation of droplets containing glyoxal and ammonium sulfate, Environ. Sci. Technol., 47, 12819−12826, https://doi.org/10.1021/es402687w, 2013.

Lee, H. J., Aiona, P. K., Laskin, A., Laskin, J., and Nizkorodov, S. A.: Effect of solar radiation on the optical properties and molecular composition of laboratory proxies of atmospheric brown carbon, Environ. Sci. Technol., 48, 10217–10226, https://doi.org/10.1021/es502515r, 2014.

Lee, P. C. C. and Rodgers, M. A. J.: Laser flash photokinetic studies of Rose Bengal sensitized photodynamic interactions of nucleotides and DNA, Photochem. Photobiol., 45, 79–86, https://doi.org/10.1111/j.1751-1097.1987.tb08407.x, 1987.

Leito, I., Herodes, K., Huopolainen, M., Virro, K., Künnapas, A., Kruve, A., and Tanner, R.: Towards the electrospray ionization mass spectrometry ionization efficiency scale of organic compounds, Rapid Commun. Mass Sp., 22, 379–384, https://doi.org/10.1002/rcm.3371, 2008.

~~Lewis, A. C., Hopkins, J. R., Carslaw, D. C., Hamilton, J. F., Nelson, B. S., Stewart, G., Dernie, J., Passant, N., and Murrells, T.: An increasing role for solvent emissions and implications for future measurements of volatile organic compounds, Philos. Trans. R. Soc., 378, https://doi.org/10.1098/rsta.2019.0328, 2020.~~

Li, F., Tang, S., Tsona, N. T., and Du, L.: Kinetics and mechanism of OH-induced α-terpineol oxidation in the atmospheric aqueous phase, Atmos. Environ., 237, 117650, https://doi.org/10.1016/j.atmosenv.2020.117650, 2020.

Li, P., Li, X., Yang, C., Wang, X., Chen, J., and Collett, J. L. Jr.: Fog water chemistry in Shanghai, Atmos. Environ., 45, 4034−4041, https://doi.org/10.1016/j.atmosenv.2011.04.036, 2011.

Li, Y. J., Huang, D. D., Cheung, H. Y., Lee, A. K. Y., and Chan, C. K.: Aqueous-phase photochemical oxidation and direct photolysis of vanillin - a model compound of methoxy phenols from biomass burning, Atmos. Chem. Phys., 14, 2871−2885, https://doi.org/10.5194/acp-14-2871-2014, 2014.

Liang, Z., Zhang, R., Gen, M., Chu, Y., and Chan, C. K.: Nitrate photolysis in mixed sucrose–nitrate–sulfate particles at different relative humidities, J. Phys. Chem. A, 125, 3739–3747, https://doi.org/10.1021/acs.jpca.1c00669, 2021.

Liigand, P., Kaupmees, K., Haav, K., Liigand, J., Leito, I., Girod, M., Antoine, R., and Kruve, A.: Think negative: finding the best electrospray ionization/MS mode for your analyte, Anal. Chem., 89, 5665–5668, https://doi.org/10.1021/acs.analchem.7, 2017.

Lim, Y. B., Tan, Y., Perri, M. J., Seitzinger, S. P., and Turpin, B. J.: Aqueous chemistry and its role in secondary organic aerosol (SOA) formation, Atmos. Chem. Phys., 10, 10521−10539, https://doi.org/10.5194/acp-10-10521-2010, 2010.

Lin, P., Fleming, L. T., Nizkorodov, S. A., Laskin, J., and Laskin, A.: Comprehensive molecular characterization of atmospheric brown carbon by high resolution mass spectrometry with electrospray and atmospheric pressure photoionization, Anal. Chem., 90, 12493–12502, https://doi.org/10.1021/acs.analchem.8b02177, 2018.

Lin, P., Yu, J. Z., Engling, G., and Kalberer, M.: Organosulfates in humic-like substance fraction isolated from aerosols at seven locations in East Asia: a study by ultra-high-resolution mass spectrometry, Environ. Sci. Technol., 46, 13118–13127, https://doi.org/10.1021/es303570v, 2012.

~~Lin, P., Fleming, L. T., Nizkorodov, S. A., Laskin, J., and Laskin, A.: Comprehensive molecular characterization of atmospheric brown carbon by high resolution mass spectrometry with electrospray and atmospheric pressure photoionization, Anal. Chem., 90, 12493–12502, https://doi.org/10.1021/acs.analchem.8b02177, 2018.~~

Liu, C., Liu, J., Liu, Y., Chen, T., and He, H.: Secondary organic aerosol formation from the OH-initiated oxidation of guaiacol under different experimental conditions, Atmos. Environ., 207, 30–37, https://doi.org/10.1016/j.atmosenv.2019.03.021, 2019.

Lobodin, V. V., Marshall, A. G., and Hsu, C. S.: Compositional space boundaries for organic compounds, Anal. Chem., 84, 3410–3416, https://doi.org/10.1021/ac300244f, 2012.

Loisel, G., Mekic, M., Liu, S., Song, W., Jiang, B., Wang, Y., Deng, H., and Gligorovski, S.: Ionic strength effect on the formation of organonitrate compounds through photochemical degradation of vanillin in liquid water of aerosols, Atmos. Environ., 246, 118140, https://doi.org/10.1016/j.atmosenv.2020.118140, 2021.

Ma, L., Guzman, C., Niedek, C., Tran, T., Zhang, Q., and Anastasio, C.: Kinetics and mass yields of aqueous secondary organic aerosol from highly substituted phenols reacting with a triplet excited state, Environ. Sci. Technol., 55, 5772–5781, https://doi.org/10.1021/acs.est.1c00575, 2021.

Mabato, B. R. G., Gen, M., Chu, Y., and Chan, C. K.: Reactive uptake of glyoxal by methylaminium-containing salts as a function of relative humidity, ACS Earth Space Chem., 3, 150–157, https://doi.org/10.1021/acsearthspacechem.8b00154, 2019.

Machado, F. and Boule, P.: Photonitration and photonitrosation of phenolic derivatives induced in aqueous solution by excitation of nitrite and nitrate ions, J. Photochem. Photobiol. A: Chem., 86, 73–80, https://doi.org/10.1016/1010-6030(94)03946-R, 1995.

Mack, J. and Bolton, J.R.: Photochemistry of nitrite and nitrate in aqueous solution: a review, J. Photochem. Photobiol. Chem., 128, 1–13, https://doi.org/10.1016/S1010-6030(99)00155-0, 1999.

Mazzoleni, L. R., Saranjampour, P., Dalbec, M. M., Samburova, V., Hallar, A. G., Zielinska, B., Lowenthal, D. H., and Kohl, S.: Identification of water-soluble organic carbon in non-urban aerosols using ultrahigh-resolution FT-ICR mass spectrometry: organic anions, Environ. Chem., 9, 285−297, https://doi.org/10.1071/EN11167, 2012.

McFall, A. S., Johnson, A. W., and Anastasio, C.: Air–water partitioning of biomass-burning phenols and the effects of temperature and salinity, Environ. Sci. Technol., 54, 3823–3830, https://doi.org/10.1021/acs.est.9b06443, 2020.

McNally, A. M., Moody, E. C., and McNeill, K.: Kinetics and mechanism of the sensitized photodegradation of lignin model compounds, Photochem. Photobiol. Sci., 4, 268−274, https://doi.org/10.1039/B416956E, 2005.

Minella, M., Romeo, F., Vione, D., Maurino, V., and Minero, C.: Low to negligible photoactivity of lake-water matter in the size range from 0.1 to 5 µm, Chemosphere, 83, 1480–1485, https://doi.org/10.1016/j.chemosphere.2011.02.093, 2011.

Minero, C., Bono, F., Rubertelli, F., Pavino, D., Maurino, V., Pelizzetti, E., and Vione, D.: On the effect of pH in aromatic photonitration upon nitrate photolysis, Chemosphere, 66, 650−656, https://doi.org/10.1016/j.chemosphere.2006.07.082, 2007.

Mohr, C., Lopez-Hilfiker, F. D., Zotter, P., Prévôt, A. S. H., Xu, L., Ng, N. L., Herndon, S. C., Williams, L. R., Franklin, J. P., Zahniser, M. S., Worsnop, D. R., Knighton, W. B., Aiken, A. C., Gorkowski, K. J., Dubey, M. K., Allan, J. D., and Thornton, J. A.: Contribution of nitrated phenols to wood burning brown carbon light absorption in Detling, United Kingdom during winter time, Environ. Sci. Technol., 47, 6316–6324, https://doi.org/10.1021/es400683v, 2013.

Munger, J. W., Jacob, D. J., Waldman, J. M., and Hoffmann, M. R.: Fogwater chemistry in an urban atmosphere, J. Geophys. Res. Oceans, 88, 5109–5121, https://doi.org/10.1029/JC088iC09p05109, 1983.

~~Neta, P., Huie, R. E., and Ross, A.: Rate constants for reactions of inorganic radicals in aqueous solution, J. Phys. Chem. Ref. Data, 17, 1027–1284, https://doi.org/10.1063/1.555808, 1988.~~

Neumann, M. G., De Groote, R. A. M. C., and Machado, A. E. H.: Flash photolysis of lignin: Part 1. Deaerated solutions of dioxane-lignin, Polym. Photochem., 7, 401–407, https://doi.org/10.1016/0144-2880(86)90007-2, 1986a.

Neumann, M. G., De Groote, R. A. M. C., and Machado, A. E. H.: Flash photolysis of lignin: II. Oxidative photodegradation of dioxane-lignin, Polym. Photochem., 7, 461–468, https://doi.org/10.1016/0144-2880(86)90015-1, 1986b.

Ning, C., Gao, Y., Zhang, H., Yu, H., Wang, L., Geng, N., Cao, R., and Chen, J.: Molecular characterization of dissolved organic matters in winter atmospheric fine particulate matters ($PM_{2.5}$) from a coastal city of northeast China, Sci. Total Environ., 689, 312–321, https://doi.org/10.1016/j.scitotenv.2019.06.418, 2019.

Nolte, C. G., Schauer, J. J., Cass, G. R., and Simoneit, B. R. T.: Highly polar organic compounds present in wood smoke and in the ambient atmosphere, Environ. Sci. Technol., 35, https://doi.org/10.1021/es001420r, 1912−1919, 2001.

Nozière, B., Dziedzic, P., and Córdova, A.: Products and kinetics of the liquid-phase reaction of glyoxal catalyzed by ammonium ions (NH_4^+), J. Phys. Chem. A, 113, 231−237, https://doi.org/10.1021/jp8078293, 2009.

Olofsson, M., Ek Olausson, B., Ljungström, E., and Langer, S.: Flux of organic compounds from grass measured by relaxed eddy accumulation technique, J. Environ. Monit., 5, 963–970, https://doi.org/10.1039/B303329E, 2003.
Onori, G. and Santucci, A.: Dynamical and structural properties of water/alcohol mixtures, J. Mol. Liq., 69, 161–181, https://doi.org/10.1016/S0167-7322(96)90012-4, 1996.

Pang, H., Zhang, Q., Lu, X. H., Li, K. , Chen, H., Chen, J. , Yang, X., Ma, Y., Ma, J., and Huang, C.: Nitrite-mediated photooxidation of vanillin in the atmospheric aqueous phase, Environ. Sci. Technol., 53, 14253−14263, https://doi.org/10.1021/acs.est.9b03649, 2019a.

Pang, H., Zhang, Q., Wang, H., Cai, D., Ma, Y., Li, L., Li, K., Lu, X., Chen, H., Yang, X., and Chen, J.: Photochemical aging of guaiacol by Fe(III)-oxalate complexes in atmospheric aqueous phase, Environ. Sci. Technol., 53, 127−136, https://doi.org/10.1021/acs.est.8b04507, 2019b.

Perry, R. H., Cooks, R. G., and Noll, R. J.: Orbitrap mass spectrometry: instrumentation, ion motion and applications, Mass Spectrom. Rev., 27, 661–699, https://doi.org/10.1002/mas.20186, 2008.

Powelson, M. H., Espelien, B. M., Hawkins, L. N., Galloway, M. M., and De Haan, D. O.: Brown carbon formation by aqueous-phase carbonyl compound reactions with amines and ammonium sulfate, Environ. Sci. Technol., 48, 985−993, https://doi.org/10.1021/es4038325, 2014.

Pöschl, U.: Atmospheric aerosols: composition, transformation, climate, and health effects, Angew. Chem. Int., 44, 7520–7540, https://doi.org/10.1002/anie.200501122, 2005.
Priya, A. M. and Lakshmipathi, S.: DFT study on abstraction reaction mechanism of oh radical with 2-methoxyphenol, J. Phys. Org. Chem., 30, https://doi.org/10.1002/poc.3713, 2017.

Pye, H., Nenes, A., Alexander, B., Ault, A. P., Barth, M. C., Clegg, S. L., Collett, J. L. Jr., Fahey, K. M., Hennigan, C. J., Herrmann, H., Kanakidou, M., Kelly, J. T., Ku, I. T., McNeill, V. F., Riemer, N., Schaefer, T., Shi, G., Tilgner, A., Walker, J. T., Wang, T., Weber, R., Xing, J., Zaveri, R. A., and Zuend, A.: The acidity of atmospheric particles and clouds, Atmos. Chem. Phys., 20, 4809–4888, https://doi.org/10.5194/acp-20-4809-2020, 2020.

Qi, L., Chen, M., Stefenelli, G., Pospisilova, V., Tong, Y., Bertrand, A., Hueglin, C., Ge, X., Baltensperger, U., Prévôt, A. S. H., and Slowik, J.G.: Organic aerosol source apportionment in Zurich using an extractive electrospray ionization time-of-flight mass spectrometer (EESI-TOF-MS) — Part 2: Biomass burning influences in winter, Atmos. Chem. Phys., 19, 8037–8062, https://doi.org/10.5194/acp-19-8037-2019, 2019.

Rizzo, L.V., Artaxo, P., Karl, T., Guenther, A.B., and Greenberg, J.: Aerosol properties, in-canopy gradients, turbulent fluxes and VOC concentrations at a pristine forest site in Amazonia, Atmos. Environ., 44, 503-511, https://doi.org/10.1016/j.atmosenv.2009.11.002, 2010.

Rogge, W. F., Hildemann, L. M., Mazurek, M. A., Cass, G. R., and Simoneit, B. R. T.: Sources of fine organic aerosol. 9. Pine, oak, and synthetic log combustion in residential fireplaces, Environ. Sci. Technol., 32, 13−22, https://doi.org/10.1021/es960930b, 1998.

Romonosky, D. E., Li, Y., Shiraiwa, M., Laskin, A., Laskin, J., and Nizkorodov, S. A.: Aqueous photochemistry of secondary organic aerosol of α-Pinene and α-Humulene oxidized with ozone, hydroxyl radical, and nitrate radical, J. Phys. Chem. A, 121, 1298–1309, https://doi.org/10.1021/acs.jpca.6b10900, 2017.

Scharko, N. K., Berke, A. E., and Raff, J. D.: Release of nitrous acid and nitrogen dioxide from nitrate photolysis in acidic aqueous solutions, Environ. Sci. Technol., 48, 20, 11991–1200, https://doi.org/10.1021/es503088x, 2014.

Schauer, J. J., Kleeman, M. J., Cass, G. R., and Simoneit, B. R. T.: Measurement of emissions from air pollution sources. 3. C_1−C_{29} organic compounds from fireplace combustion of wood, Environ. Sci. Technol., 35, 1716−1728, https://doi.org/10.1021/es001331e, 2001.

Schmidt, A-C., Herzschuh, R., Matysik, F-M., and Engewald, W.: Investigation of the ionisation and fragmentation behaviour of different nitroaromatic compounds occurring as polar metabolites of explosives using electrospray ionisation tandem mass spectrometry, Rapid Commun. Mass Sp., 20, 2293–2302, https://doi.org/10.1002/rcm.2591, 2006.

Sedehi, N., Takano, H., Blasic, V. A., Sullivan, K. A., and De Haan, D. O.: Temperature- and pH-dependent aqueous-phase kinetics of the reactions of glyoxal and methylglyoxal with atmospheric amines and ammonium sulfate, Atmos. Environ., 77, 656−663, https://doi.org/10.1016/j.atmosenv.2013.05.070, 2013.

Shapiro, E. L., Szprengiel, J., Sareen, N., Jen, C. N., Giordano, M. R., and McNeill, V. F.: Light-absorbing secondary organic material formed by glyoxal in aqueous aerosol mimics, Atmos. Chem. Phys., 9, 2289−2300, https://doi.org/10.5194/acp-9-2289-2009, 2009.

Siegmann, K. and Sattler, K. D.: Formation mechanism for polycyclic aromatic hydrocarbons in methane flames, J. Chem. Phys., 112, 698–709, https://doi.org/10.1063/1.480648, 2000.

Slikboer, S., Grandy, L., Blair, S. L., Nizkorodov, S. A., Smith, R. W., and Al-Abadleh, H. A.: Formation of light absorbing soluble secondary organics and insoluble polymeric particles from the dark reaction of catechol and guaiacol with Fe(III), Environ. Sci. Technol., 49, 7793–7801, https://doi.org/10.1021/acs.est.5b01032, 2015.

Smith, J. D., Sio, V., Yu, L., Zhang, Q., and Anastasio, C.: Secondary organic aerosol production from aqueous reactions of atmospheric phenols with an organic triplet excited state, Environ. Sci. Technol., 48, 1049–1057, https://doi.org/10.1021/es4045715, 2014.

Smith, J. D., Kinney, H., and Anastasio, C.: Aqueous benzene-diols react with an organic triplet excited state and hydroxyl radical to form secondary organic aerosol, Phys. Chem. Chem. Phys., 17, 10227–10237, https://doi.org/10.1039/C4CP06095D, 2015.

Smith, J. D., Kinney, H., and Anastasio, C.: Phenolic carbonyls undergo rapid aqueous photodegradation to form low-volatility, light-absorbing products, Atmos. Environ., 126, 36−44, https://doi.org/10.1016/j.atmosenv.2015.11.035, 2016.

~~Straub, D. J.: Radiation fog chemical composition and its temporal trend over an eight year period, Atmos. Environ., 148, 49–61, https://doi.org/10.1016/j.atmosenv.2016.10.031, 2017.~~

~~Straub, D. J., Hutchings, J. W., and Herckes, P.: Measurements of fog composition at a rural site, Atmos. Environ., 47, 195–205., https://doi.org/10.1016/j.atmosenv.2011.11.014, 2012.~~

Song, J., Li, M., Jiang, B., Wei, S., Fan, X., and Peng, P.: Molecular characterization of water-soluble humic like substances in smoke particles emitted from combustion of biomass materials and coal using ultrahigh-resolution electrospray ionization Fourier transform ion cyclotron resonance mass spectrometry, Environ. Sci. Technol., 52, 2575–2585, https://doi.org/10.1021/acs.est.7b06126, 2018.

~~Sturzbecher Höhne, M., Nauser, T., Kissner, R., and Koppenol, W. H.: Photon initiated homolysis of peroxynitrous acid, Inorg. Chem., 48, 7307−7312, https://doi.org/10.1021/ic900614e, 2009.~~

~~Sun, Y., Xu, F., Li, X., Zhang, Q., and Gu, Y.: Mechanisms and kinetic studies of OH-initiated atmospheric oxidation of methoxyphenols in the presence of O2 and NOx, Phys. Chem. Chem. Phys., 21, 21856−21866, https://doi.org/10.1039/C9CP03246K, 2019.~~

Sun, Y. L., Zhang, Q., Anastasio, C., and Sun, J.: Insights into secondary organic aerosol formed via aqueous-phase reactions of phenolic compounds based on high resolution mass spectrometry, Atmos. Chem. Phys., 10, 4809−4822, https://doi.org/10.5194/acp-10-4809-2010, 2010.

Teich, M., van Pinxteren, D., Wang, M., Kecorius, S., Wang, Z., Müller, T., Močnik, G., and Herrmann, H.: Contributions of nitrated aromatic compounds to the light absorption of water-soluble and particulate brown carbon in different atmospheric environments in Germany and China, Atmos. Chem. Phys., 17, 1653–1672, https://doi.org/10.5194/acp-17-1653-2017, 2017.

~~Tinel, L., George, C., Brüggemann, M., Hayeck, N., Tinel, L.,and Donaldson, D. J.: Interfacial photochemistry: physical chemistry of gas-liquid interfaces, in: Developments in Physical & Theoretical Chemistry, edited by: Faust, J. A. and House, J. E., Elsevier, 435−457, https://doi.org/10.1016/B978-0-12-813641-6.00014-5, 2018.~~

Tratnyek, P. G. and Hoigne, J.: Oxidation of substituted phenols in the environment: a QSAR analysis of rate constants for reaction with singlet oxygen, Environ. Sci. Technol., 25, 1596−1604, https://doi.org/10.1021/es00021a011, 1991.

Turro, N., Ramamurthy, V., and Scaiano, J.C.: Modern Molecular Photochemistry, University Science Book, 2010.

Vione, D., Maurino, V., Minero, C., and Pelizzetti, E.: Phenol photonitration upon UV irradiation of nitrite in aqueous solution I: effects of oxygen and 2-propanol, Chemosphere, 45, 893–902, https://doi.org/10.1016/S0045-6535(01)00035-2, 2001.

Vione, D., Maurino, V., Minero, C., and Pelizzetti, E.: Reactions induced in natural waters by irradiation of nitrate and nitrite ions, in: The Handbook of Environmental Chemistry Vol. 2M - Environmental Photochemistry Part II, Springer, Berlin, Heidelberg, Germany, 221−253, https://doi.org/10.1007/b138185, 2005.

Vione, D., Maurino, V., Minero, C., Pelizzetti, E., Harrison, M. A. J., Olariu, R., and Arsene, C.: Photochemical reactions in the tropospheric aqueous phase and on particulate matter, Chem. Soc. Rev., 35, 441−453, https://doi.org/10.1039/B510796M, 2006.

Vione, D., Khanra, S., Cucu-Man, S., Maddigapu, P. R., Das, R., Arsene, C., Olariu, R-I., Maurino, V., and Minero, C.: Inhibition vs. enhancement of the nitrate-induced phototransformation of organic substrates by the •OH scavengers bicarbonate and carbonate, Water Res., 43, 4718–4728, https://doi.org/10.1016/j.watres.2009.07.032, 2009.

Vione, D., Albinet, A., Barsotti, F., Mekic, M., Jiang, B., Minero, C., Brigante, M., and Gligorovski, S.: Formation of substances with humic-like fluorescence properties, upon photoinduced oligomerization of typical phenolic compounds emitted by biomass burning, Atmos. Environ., 206, 197−207, https://doi.org/10.1016/j.atmosenv.2019.03.005, 2019.

Volkamer, R., Ziemann, P. J., Molina, and M. J.: Secondary organic aerosol formation from acetylene (C_2H_2): seed effect on SOA yields due to organic photochemistry in the aerosol aqueous phase, Atmos. Chem. Phys., 9, 1907−1928, https://doi.org/10.5194/acp-9-1907-2009, 2009.

Wang, X., Dalton, E. Z., Payne, Z. C., Perrier, S., Riva, M., Raff, J. D., and George, C.: Superoxide and nitrous acid production from nitrate photolysis is enhanced by dissolved aliphatic organic matter, Environ. Sci. Technol. Lett., 8, 53−58, https://doi.org/10.1021/acs.estlett.0c00806, 2021.

Warneck, P. and Wurzinger, C.: Product quantum yields for the 305-nm photodecomposition of nitrate in aqueous solution, J. Phys. Chem., 92, 6278−6283, https://doi.org/10.1021/j100333a022, 1988.

Wang, K., Huang, R-J., Brüggemann, M., Zhang, Y., Yang, L., Ni, H., Guo, J., Wang, M., Han, J., Bilde, M., Glasius, M., and Hoffmann, T.: Urban organic aerosol composition in eastern China differs from north to south: molecular insight from a liquid chromatography–mass spectrometry (Orbitrap) study, Atmos. Chem. Phys., 21, 9089–9104, https://doi.org/10.5194/acp-21-9089-2021, 2021.

Wang, X., Hayeck, N., Brüggemann, M., Yao, L., Chen, H., Zhang, C., Emmelin, C., Chen, J., George, C., and Wang, L.: Chemical characterization of organic aerosols in Shanghai: A study by ultrahigh-performance liquid chromatography coupled with orbitrap mass spectrometry, J. Geophys. Res. Atmos., 122, 11703–11722, https://doi.org/10.1002/2017JD026930, 2017.

Williams, D. H. and Fleming, I.: Spectroscopic methods in organic chemistry, 6th Ed., McGraw-Hill Education, London, 2008.

Wojnárovits, L., Tóth, T., and Takács, E.: Rate constants of carbonate radical anion reactions with molecules of environmental interest in aqueous solution: a review, Sci. Total Environ., 717, 137219, https://doi.org/10.1016/j.scitotenv.2020.137219, 2020.

Xie, Q., Su, S., Chen, S., Xu, Y., Cao, D., Chen, J., Ren, L., Yue, S., Zhao, W., Sun, Y., Wang, Z., Tong, H., Su, H., Cheng, Y., Kawamura, K., Jiang, G., Liu, C-Q., and Fu, P.: Molecular characterization of firework-related urban aerosols using Fourier transform ion cyclotron resonance mass spectrometry, Atmos. Chem. Phys., 20, 6803–6820, 10.5194/acp-2019-1180, https://doi.org/10.5194/acp-20-6803-2020, 2020.

Yang, J., Au, W. C., Law, H., Lam, C. H., and Nah, T.: Formation and evolution of brown carbon during aqueous-phase nitrate-mediated photooxidation of guaiacol and 5-nitroguaiacol, Atmos. Environ., 254, 118401, https://doi.org/10.1016/j.atmosenv.2020.118140, 2021.

Yaremenko, I. A., Vil', V. A., Demchuk, D. V., and Terent'ev, A. O.: Rearrangements of organic peroxides and related processes, Beilstein J. Org. Chem., 12., 1647–1748, https://doi.org/10.3762/bjoc.12.162, 2016.

Yaws, C. L.: Handbook of vapor pressure: Volume 3: Organic compounds C_8 to C_{28}, Gulf Professional Publishing, USA, 1994.

Ye, Z., Qu, Z., Ma, S., Luo, S., Chen, Y., Chen, H., Chen, Y., Zhao, Z., Chen, M., and Ge, X.: A comprehensive investigation of aqueous-phase photochemical oxidation of 4-ethylphenol, Sci. Total Environ., 685, 976–985, https://doi.org/10.1016/j.scitotenv.2019.06.276, 2019.

Yu, G., Bayer, A. R., Galloway, M. M., Korshavn, K. J., Fry, C. G., and Keutsch, F. N.: Glyoxal in aqueous ammonium sulfate solutions: products, kinetics and hydration effects, Environ. Sci. Technol., 45, 6336−6342, https://doi.org/10.1021/es200989n, 2011.

Yu, L., Smith, J., Laskin, A., Anastasio, C., Laskin, J., and Zhang, Q.: Chemical characterization of SOA formed from aqueous-phase reactions of phenols with the triplet excited state of carbonyl and hydroxyl radical, Atmos. Chem. Phys., 14, 13801−13816, https://doi.org/10.5194/acp-14-13801-2014, 2014.

Zhang, Q. and Anastasio, C.: Conversion of fogwater and aerosol organic nitrogen to ammonium, nitrate, and NO_x during exposure to simulated sunlight and ozone, Environ. Sci. Technol., 37, 3522–3530, https://doi.org/10.1021/es034114x, 2003.

Zhang, R., Gen, M., Fu, T-M., and Chan, C. K.: Production of formate via oxidation of glyoxal promoted by particulate nitrate photolysis, Environ. Sci. Technol., 55, 5711–5720, https://doi.org/10.1021/acs.est.0c08199, 2021.

Zhao, R., Lee, A. K. Y., Huang, L., Li, X., Yang, F., and Abbatt, J. P. D.: Photochemical processing of aqueous atmospheric brown carbon, Atmos. Chem. Phys., 15, 6087–6100, https://doi.org/10.5194/acp-15-6087-2015, 2015.

Zhao, Y., Hallar, A.G., and Mazzoleni, L.R.: Atmospheric organic matter in clouds: exact masses and molecular formula identification using ultrahigh-resolution FT-ICR mass spectrometry, Atmos. Chem. Phys. 13, 12343–12362, https://doi.org/10.5194/acp-13-12343-2013, 2013.

Zhou, W., Mekic, M., Liu, J., Loisel, G., Jin, B., Vione, D., and Gligorovski, S.: Ionic strength effects on the photochemical degradation of acetosyringone in atmospheric deliquescent aerosol particles, Atmos. Environ., 198, 83–88, https://doi.org/10.1016/j.atmosenv.2018.10.047, 2019.

Zielinski, T., Bolzacchini, E., Cataldi, M., Ferrero, L., Graßl, S., Hansen, G., Mateos, D., Mazzola, M., Neuber, R., Pakszys, P., Posyniak, M., Ritter, C., Severi, M., Sobolewski, P., Traversi, R., and Velasco-Merino, C.: Study of chemical and optical properties of biomass burning aerosols during long-range transport events toward the Arctic in summer 2017, Atmosphere, 11, 84, https://doi.org/10.3390/atmos11010084, 2020.

~~Ziemann, P. J. and Atkinson, R.: Kinetics, products, and mechanisms of secondary organic aerosol formation, Chem. Soc. Rev., 41, 6582–6605, https://doi.org/10.1039/C2CS35122F, 2012.~~

Table 1. List of reactions involving reactive species relevant to this study.

No.	Reactions	References
1	$NO_3^- + h\nu \rightarrow {}^\bullet NO_2 + O^-$; $\phi = 0.01$	Vione et al., 2006; ~~Scharko et al., 2014~~Benedict et al., 2017
2	$O^- + H_3O^+ \leftrightarrow {}^\bullet OH + H_2O$	
3	$NO_3^- + h\nu \rightarrow NO_2^- + O(^3P)$; $\phi = 0.~~0~~011$	
4	$NO_2^- + {}^\bullet OH \rightarrow {}^\bullet NO_2 + OH^-$ ($k = 1.0 \times 10^{10}$ M^{-1} s^{-1})	Mack and Bolton, 1999; Pang et al., 2019a
5	$O_2^{\bullet-} + NO_2^- + 2H^+ \rightarrow {}^\bullet NO_2 + H_2O_2$	Vione et al., 2001; Pang et al., 2019a
6	$NO_2^- + h\nu \rightarrow {}^\bullet NO + O^-$; $\phi_{OH,300} = 6.7$ (± 0.9)%	Fischer and Warneck, 1996; Mack and Bolton, 1999; Pang et al., 2019a
7	${}^\bullet NO + O_2 \leftrightarrow {}^\bullet ONOO$	Goldstein and Czapski, 1995~~a~~; Pang et al., 2019a
8	${}^\bullet ONOO + {}^\bullet NO \rightarrow ONOONO$	
9	$ONOONO \rightarrow 2{}^\bullet NO_2$	
~~10~~	~~NO_3^- + $h\nu$ → $^\bullet NO_2$ + OH (reactions 1 & 2) → $HOONO$ ⇌ $^\bullet NO$ + $^\bullet HO_2$ (pK_a = 6.8)~~	~~Goldstein et al., 2005; Vione et al., 2005; Sturzbecher-Höhne et al., 2009; Abida et al., 2011; Wang et al., 2021~~
~~11~~	~~$^\bullet HO_2 \rightleftharpoons H^+ + O_2^{\bullet-}$ (pK_a = 4.8); $O_2^{\bullet-}$ + NO_2 → $OONO_2^-$ → O_2 + NO_3^- + H^+ → $HONO$ + O_2 (pK_a = 3.2)~~	~~mmel et al., 1990; Goldstein et al., 1998; Wang et al., 21~~
~~12~~	~~NO_2^- + $HOONO_2$ ⇌ $OONO_2^-$ + H^+; $O_2^{\bullet-}$ + NO ⇌ $OONO^-$ (pK_a = 5.9) → NO_3^-~~	~~Goldstein and Czapski, 1995b; Wang et al., 2021~~
~~13~~	~~$HNO_2 + h\nu \rightarrow {}^\bullet NO + OH$; $\phi_{OH,300}$ = 36.2(±4.7)%~~	~~Fischer and Warneck, 1996; Kim et al., 2014; Pang et al., 2019a~~
~~14~~	~~$HOONO \rightarrow {}^\bullet NO_2 + {}^\bullet OH$ (k = 0.35 ± 0.03 s^{-1})~~	~~Goldstein et al., 2005; Pang et al., 2019a~~
1~~5~~	$HNO_2 + {}^\bullet OH \rightarrow {}^\bullet NO_2 + H_2O$ ($k = 2.6 \times 10^9$ M^{-1} s^{-1})	Kim et al., 2014; Pang et al., 2019a
~~16~~	~~$(CH_3)_2CHOH^- + {}^\bullet OH \rightarrow (CH_3)_2COH^\bullet + H_2O$~~	~~Warneck and Wurzinger, 1988; Pang et al., 2019a~~
~~17~~	~~$(CH_3)_2COH^\bullet + O_2 \rightarrow (CH_3)_2CO + {}^\bullet HO_2$~~	
~~18~~	~~$^\bullet OH + HCO_3^- \rightarrow CO_3^{\bullet-} + H_2O$ ($k = 8.5 \times 10^6$ M^{-1} s^{-1})~~	~~Wojnárovits et al., 2020~~
~~19~~	~~$^\bullet OH + CO_3^{2-} \rightarrow CO_3^{\bullet-} + OH^-$ ($k = 3.9 \times 10^8$ M^{-1} s^{-1})~~	
~~20~~	~~$^3C^* + HCO_3^- \rightarrow CO_3^{\bullet-} + H^+ + C^\bullet$ ($k = 10^6$–10^7 M^{-1} s^{-1}; $^3C^*$: triplet aromatic ketones)~~	~~Canonica et al., 2005~~
~~21~~	~~$^3C^* + CO_3^{2-} \rightarrow CO_3^{\bullet-} + C^\bullet$ ($k = 10^6$–10^7 M^{-1} s^{-1}; $^3C^*$: triplet aromatic ketones)~~	

Table 2. Reaction conditions, initial VL (and GUA) decay rate constants, normalized abundance of products, and average carbon oxidation state (<OS_c>) in each experiment. Except where noted, the reaction systems consisted of VL (0.1 mM); GUA (0.1 mM), AN (1 mM); sodium nitrate (SN) (1 mM) under air-saturated conditions after 6 h of simulated sunlight irradiation. Analyses were performed using UHPLC-qToF-MS equipped with an ESI source and operated in the positive ion mode.

Exp no.	pH	Reaction conditions	Initial VL (and GUA) decay rate constants (min^{-1})[b]	Ratio of 50 most abundant products to total products[c]	Normalized abundance of products[d]	Normalized abundance of N-containing compounds[d]	$\langle OS_c \rangle$[e] (OS_c of VL: -0.25)
A1	2.5	VL*	$2.0 \times 10^{-2} \pm 5.8 \times 10^{-5}$	0.59	1.7 ± 0.16	N/A	-0.05
A2		VL+AN	$1.7 \times 10^{-2} \pm 7.3 \times 10^{-4}$	0.63	1.4 ± 0.19	5.3×10^{-2}	-0.04
A3	3	VL*	$1.5 \times 10^{-2} \pm 4.2 \times 10^{-4}$	0.53	1.9 ± 0.33	N/A	-0.04
A4		VL+AN	$1.5 \times 10^{-2} \pm 2.3 \times 10^{-4}$	0.56	1.9 ± 0.30	3.6×10^{-2}	-0.05
A5	4	VL*	$1.2 \times 10^{-2} \pm 5.9 \times 10^{-4}$	0.58	0.26 ± 0.42	N/A	-0.16
A6		VL* (N_2-saturated)	$3.2 \times 10^{-3} \pm 1.1 \times 10^{-3}$	0.96	4.7×10^{-2} ± 0.0027	N/A	-0.24
A7		VL+AN	$1.2 \times 10^{-2} \pm 8.8 \times 10^{-4}$	0.53	0.37 ± 0.38	1.7×10^{-2}	-0.13
A8		VL+AN (N_2-saturated)	$1.9 \times 10^{-3} \pm 9.2 \times 10^{-5}$	0.89	0.12 ± 0.0095	6.3×10^{-3}	-0.21
A9		VL+SN	N/A	0.51	0.42 ± 0.33	1.7×10^{-2}	-0.07
A10		VL* (0.01 mM)[a]	N/A	0.90	0.37 ± 0.018	N/A	-0.07
A11		VL (0.01 mM) + AN (0.01 mM)	N/A	0.77	0.40 ± 0.074	8.6×10^{-3}	0.12
A12		VL (0.01 mM) + AN	N/A	0.42	0.45 ± 0.025	1.2×10^{-2}	-0.06
A13		GUA only	$6.2 \times 10^{-3} \pm 2.5 \times 10^{-4}$	0.77	N/A	N/A	-0.28
A14		GUA+VL	GUA: $1.4 \times 10^{-2} \pm 4.0 \times 10^{-4}$ VL: $4.3 \times 10^{-3} \pm 2.2 \times 10^{-4}$	0.60	2.2 ± 0.47	N/A	-0.27
A15		GUA+AN	$8.0 \times 10^{-3} \pm 2.9 \times 10^{-3}$	0.77	N/A	N/A	-0.26

[a]Irradiation time for VL* (0.01 mM, A10) was 3 h. [b]The data fitting was performed in the initial linear region. Each value is the average of results from triplicate experiments. Errors represent one standard deviation. Kinetic measurements were not performed for experiments marked with N/A. [c]Ratio of the normalized abundance of the 50 most abundant products to that of total products, except for direct GUA photodegradation, GUA+VL, and GUA+AN (A13–15) whose ratios are based on the absolute signals of products. [d]The normalized abundance of products was calculated using Eq. 2. The samples for experiments without nitrate (marked with N/A) were not analyzed for N-containing compounds. For the GUA experiments, the normalized abundance of products was calculated only for GUA+VL as the GUA signal from the UHPLC-qToF-MS in the positive ion mode was weak, which may introduce large uncertainties during normalization. [e]$\langle OS_c \rangle$ of the 50 most abundant products.

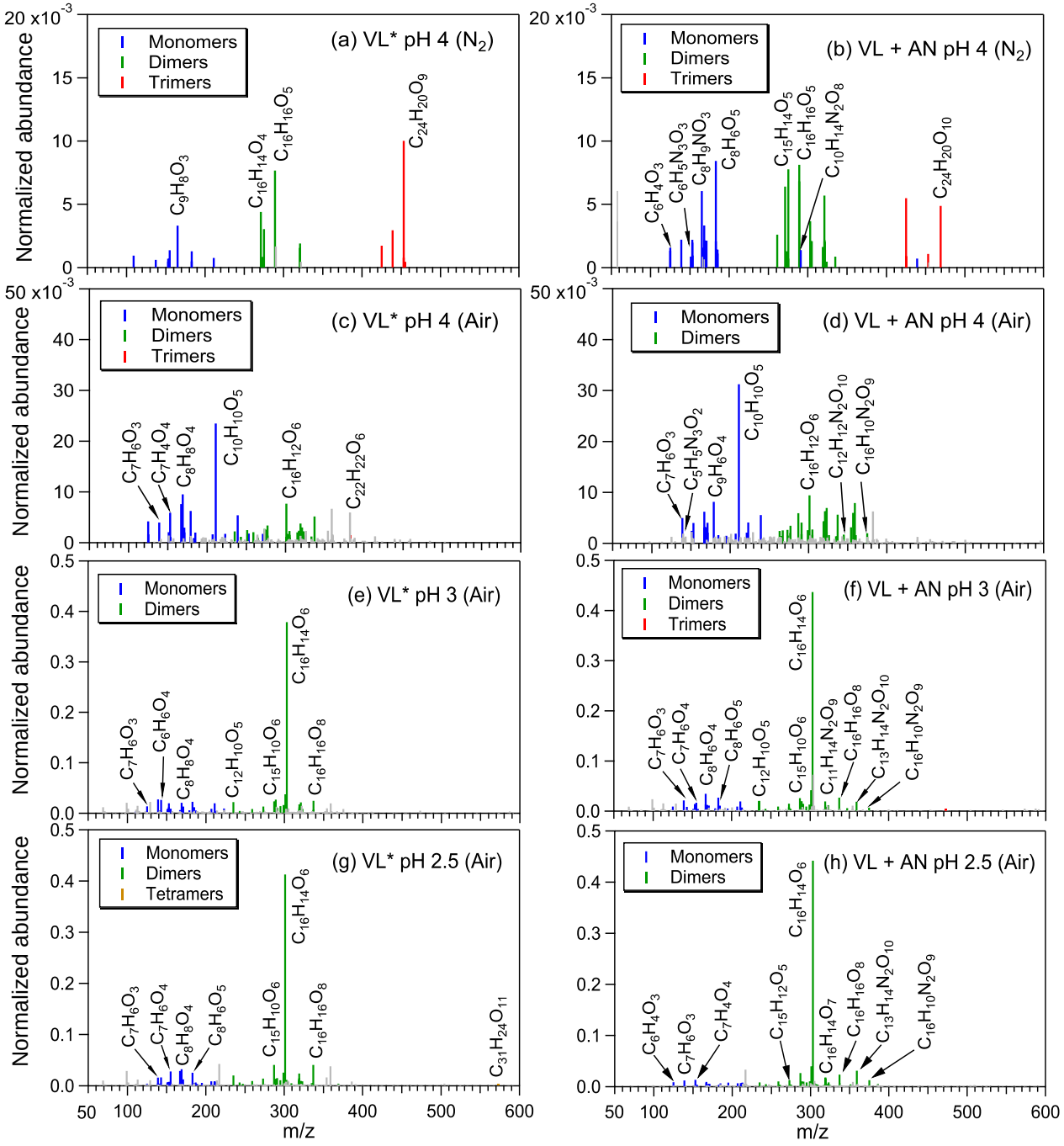

Figure 1. Reconstructed mass spectra of assigned peaks from (a) VL* pH 4 (N_2-saturated; A6), (b) VL+AN pH 4 (N_2-saturated; A8), (c) VL* pH 4 (air-saturated; A5), (d) VL+AN pH 4 (air-saturated; A7), (e) VL* pH 3 (air-saturated; A3), (f) VL+AN pH 3 (air-saturated; A4), (g) VL* pH 2.5 (air-saturated; A1), and (h) VL+AN pH 2.5 (air-saturated; A2) after 6 h of simulated

sunlight irradiation. The normalized abundance of products was calculated from the ratio of the peak area of the product to that of VL (Eq. 2). The 50 most abundant products contributed more than half of the total normalized abundance of products, and they were identified as monomers (blue), dimers (green), trimers (red), and tetramers (orange). Grey peaks denote peaks with low abundance or unassigned formula. Examples of high-intensity peaks were labeled with the corresponding neutral formulas. Note the different scales on the y-axes.

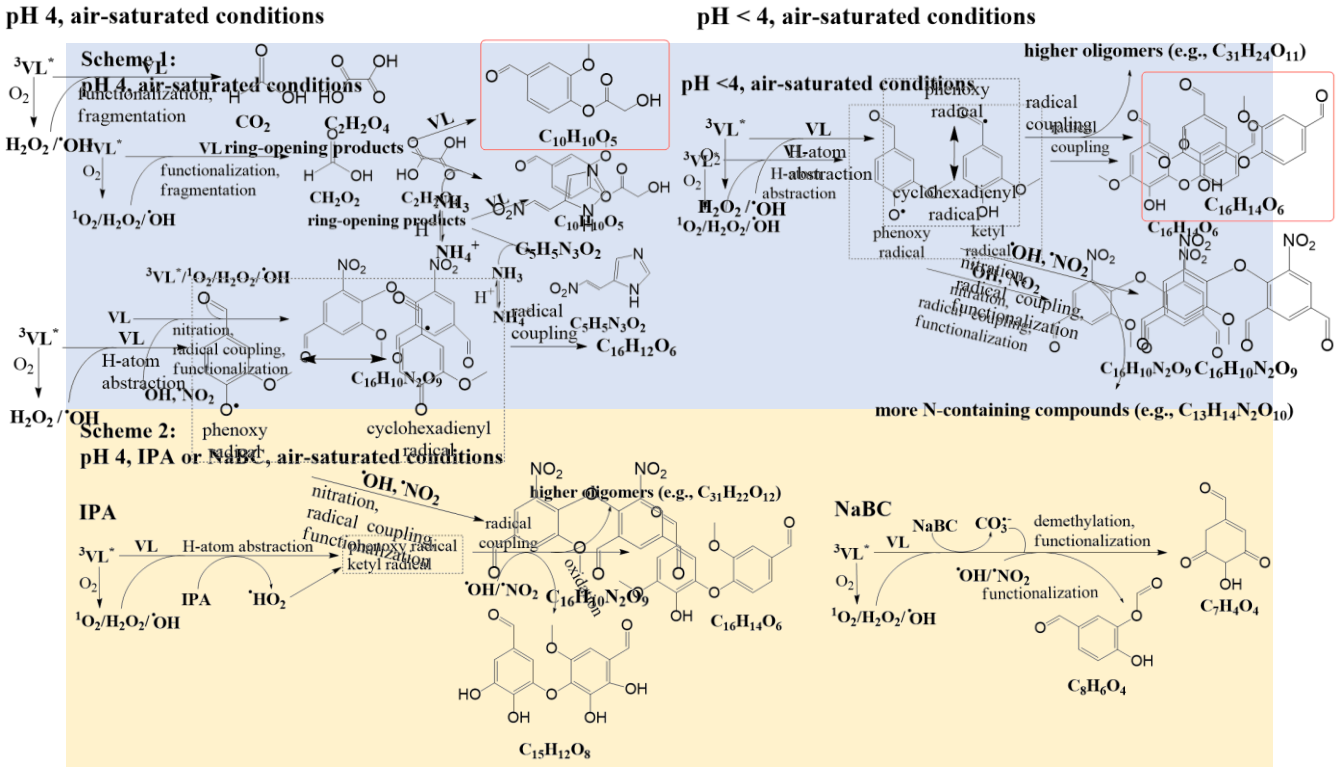

Figure 2. Potential aqSOA formation pathways via direct photosensitized oxidation of VL and nitrate-mediated VL photo-oxidation at pH 4 and pH < 4 under air-saturated conditions. Product structures were proposed based on the molecular formulas, DBE values, and MS/MS fragmentation patterns. The molecular formulas presented were the major products detected using UHPLC-qToF-MS in positive ESI mode. The highlighted structures are the most abundant product for each condition.

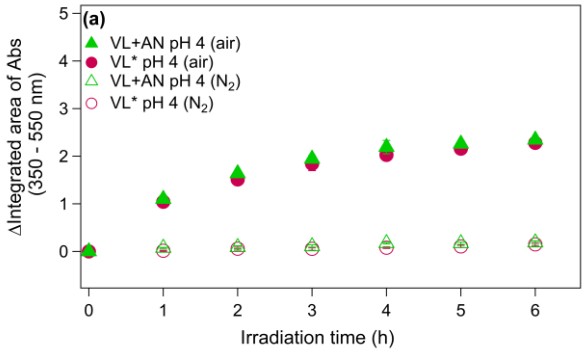
(a)
VL+AN pH 4 (air)
VL* pH 4 (air)
VL+AN pH 4 (N2)
VL* pH 4 (N2)
ΔIntegrated area of Abs (350 - 550 nm)
Irradiation time (h)

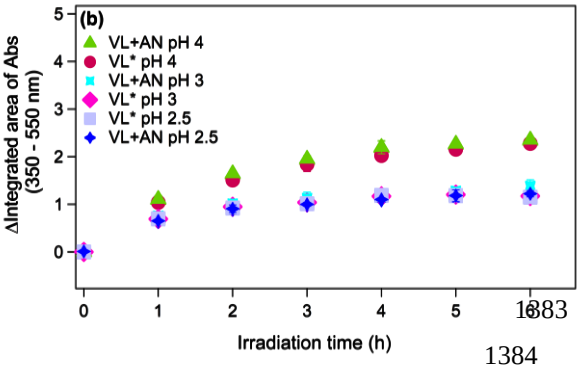
(b)
VL+AN pH 4
VL* pH 4
VL+AN pH 3
VL* pH 3
VL* pH 2.5
VL+AN pH 2.5
ΔIntegrated area of Abs (350 - 550 nm)
Irradiation time (h)

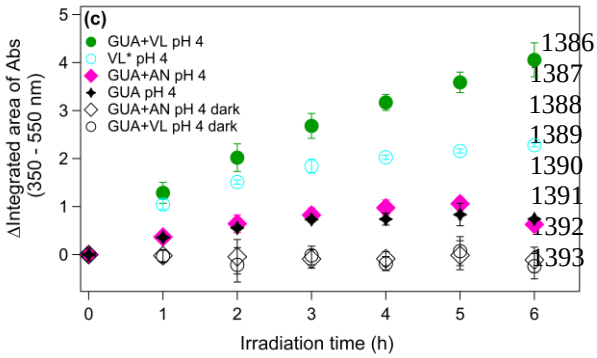
(c)
GUA+VL pH 4
VL* pH 4
GUA+AN pH 4
GUA pH 4
GUA+AN pH 4 dark
GUA+VL pH 4 dark
ΔIntegrated area of Abs (350 - 550 nm)
Irradiation time (h)

Figure 32. (a~~–c~~d) Increase in light absorption under different experimental conditions for direct photosensitized oxidation of VL (VL*) and nitrate-mediated VL photo-oxidation (VL+AN): (a) ~~Effect of secondary oxidants from VL triplets on~~ VL* and VL+AN at pH 4 under N_2- (A6, A8) and air-saturated (A5, A7) conditions. (b) Effect of pH on VL* and VL+AN at pH 2.5 (A1, A2), 3 (A3, A4), and 4 (A5, A7) under air-saturated conditions. ~~(c) Effect of VOCs and inorganic anions: IPA (A9) and NaBC (A10) on VL* at pH 4 under air-saturated conditions. (d) Effect of VOCs and inorganic anions: IPA (A11) and NaBC (A12) on VL+AN at pH 4 under air-saturated conditions.~~ (ce) Increase in light absorption during direct GUA photodegradation (A137) and photo-oxidation of GUA in the presence of VL (GUA+VL; A148) or nitrate (GUA+AN; A159) at pH 4 under air-saturated conditions after 6 h of simulated sunlight irradiation. Error bars represent one~~1~~ standard deviation; most error bars are smaller than the markers.

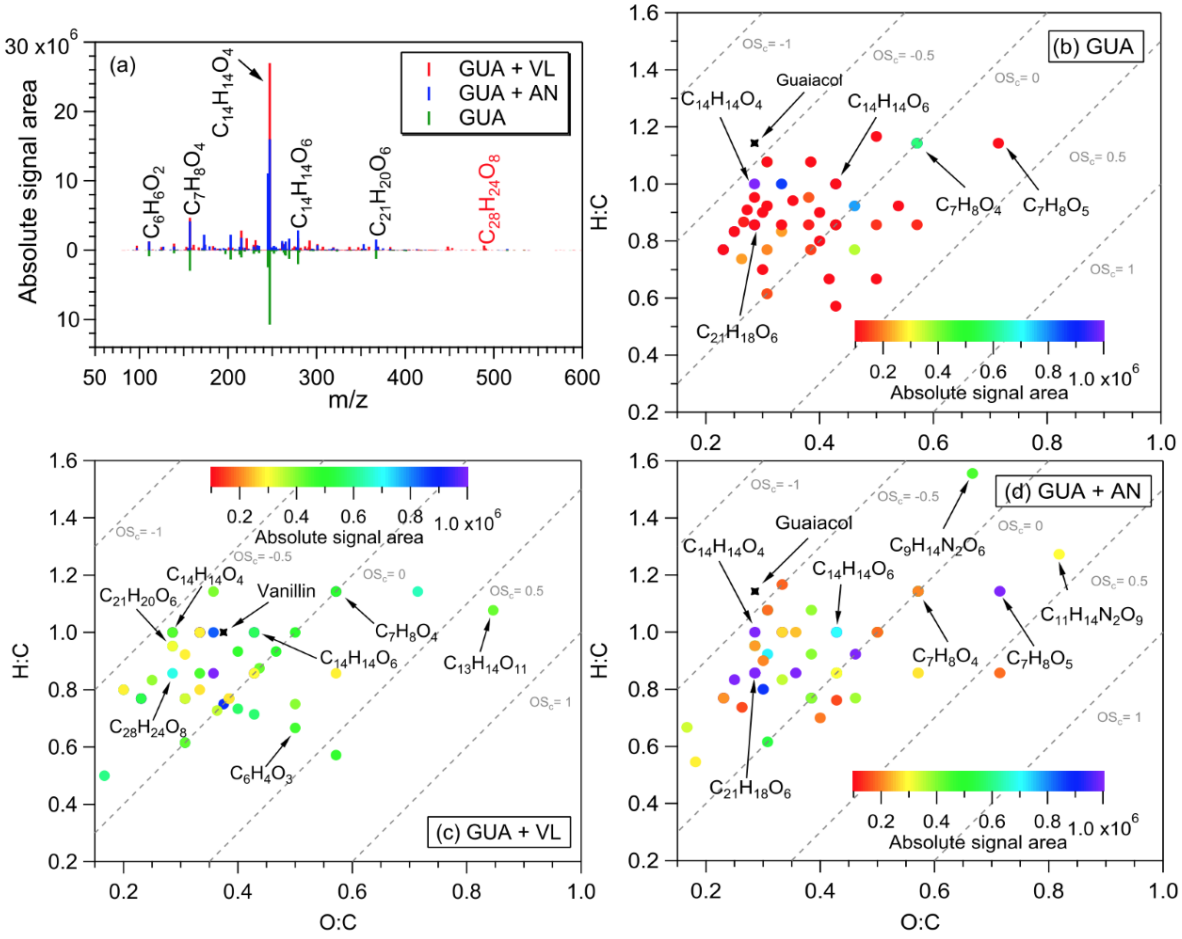

Figure 43. (a) Reconstructed mass spectra of assigned peaks from the direct GUA photodegradation (A137) and photo-oxidation of GUA in the presence of VL (GUA+VL; A148) or nitrate (GUA+AN; A159) at pH 4 under air-saturated

conditions after 6 h of simulated sunlight irradiation. The y-axis is the absolute signal area of the products. Examples of high-intensity peaks were labeled with the corresponding neutral formulas. (b-d) van Krevelen diagrams of the 50 most abundant products from the (b) direct photodegradation of GUA (A137), (c) GUA+VL (A148), and (d) GUA+AN (A159) at pH 4 under air-saturated conditions after 6 h of simulated sunlight irradiation. The color bar denotes the absolute signal area. The grey dashed lines indicate the carbon oxidation state values (e.g., OS_c =-1, 0, and 1).

Figure 4. Potential photo-oxidation pathways of VL via direct photosensitized reactions and in the presence of nitrate to illustrate the effects of secondary oxidants from VL triplets, pH, and the presence of VOCs (IPA) and inorganic anions (NaBC). Product structures were proposed based on the molecular formulas, DBE values, and MS/MS fragmentation patterns. The molecular formulas presented were the most abundant products or products with a significant increase in normalized abun

Supplementary material

Aqueous SOA formation from the photo-oxidation of vanillin: Direct photosensitized reactions and nitrate-mediated reactions

Beatrix Rosette Go Mabato[1], Yan Lyu[1], Yan Ji[1], Yong Jie Li[2], Dan Dan Huang[3], Xue Li[4], Theodora Nah[1], Chun Ho Lam[1], and Chak K. Chan[1]*

[1]School of Energy and Environment, City University of Hong Kong, Hong Kong, China

[2]Department of Civil and Environmental Engineering, and Centre for Regional Ocean, Faculty of Science and Technology, University of Macau, Macau, China

[3]Shanghai Academy of Environmental Sciences, Shanghai 200233, China

[4]Institute of Mass Spectrometry and Atmospheric Environment, Jinan University No. 601 Huangpu Avenue West, Guangzhou 510632, China

Correspondence to: Chak K. Chan (Chak.K.Chan@cityu.edu.hk)

Text S1. Materials.

Initial solutions of 0.1 mM vanillin (VL, Acros Organics, 99%, pure), 0.1 mM guaiacol (GUA, Sigma Aldrich, ≥ 98.0%), 1 mM ammonium nitrate (AN, Acros Organics, 99+%, for analysis), and 1 mM sodium nitrate (SN, Sigma-Aldrich, ≥ 99.5%)~~, 1 mM of 2-propanol (IPA, Optima LC/MS grade), and 1 mM of sodium bicarbonate (NaBC, Fisher BioReagents, 99.7-100.3%)~~ were prepared in Milli-Q water. The pH values of the samples were adjusted using sulfuric acid (H_2SO_4; Acros Organics, ACS reagent, 95% solution in water).

Text S2. UV-Vis spectrophotometric analyses.

The absorbance changes for all samples were characterized using a UV-Vis spectrophotometer (UV-3600, Shimadzu Corp., Japan). The absorbance values from 200 to 700 nm were recorded instantly after sample collection, and measurements were done in triplicate. Absorbance enhancements were calculated as the change in the integrated area of absorbance from 350 to 550 nm. The increase of light absorption at this wavelength range, where VL and GUA did not initially absorb light, suggests the formation of light-absorbing compounds (Zhou et al., 2019).

Text S3. UHPLC-PDA analyses.

An ultra-high performance liquid chromatography system (UHPLC, Waters Acquity H-Class, Waters, Milford, USA) coupled to a photodiode array (PDA) detector (Waters, Milford, USA) was used for the quantification of VL and GUA concentrations. The drawn solutions were first filtered through a 0.2 μm Chromafil ®Xtra PTFE filter (Macherey-Nagel GmbH & Co. KG, Germany). Briefly, the separation of products was performed using an Acquity HSS T3 column

(1.8 μm, 2.1 mm × 100 mm; Waters Corp.). The column oven was held at 30 ºC, and the autosampler was cooled at 4 ºC. The injection volume was set to 5 μL. The binary mobile phase consisted of A (water) and B (acetonitrile). The gradient elution was performed at a flow rate of 0.2 mL/min: 0–1 min, 10% eluent B; 1–25 min, linear increase to 90% eluent B; 25–29.9 min, hold 90% eluent B; 29.9–30 min, decrease to 10% eluent B; 30–35 min, re-equilibrate at 10% eluent B for 5 min. Standard solutions of VL and GUA ranging from 10 to 130 μM were analyzed along with samples and blanks using the channels with UV absorption at 300 and 274 nm, respectively. The calibration curves for VL and GUA standard solutions are shown in Figure S2.

Text S4. IC analyses of small organic acids.

The small organic acids were analyzed using an ion chromatography system (IC, Dionex ICS-1100, Sunnyvale, CA) equipped with a Dionex AS-DV autosampler (Sunnyvale, CA). The separation was achieved using an IonPac^{TM} AS15 column (4 × 250 mm) with an AG15 guard column (4 × 50 mm). The isocratic gradient was applied at a flow rate of 1.2 mL/min with 38 mM sodium hydroxide (NaOH) as the eluent. The total run time was set at 20 min. The standard solutions (1–50 μM) of formic, succinic, and oxalic acid were analyzed three times along with the samples and water blank. Formic, succinic, and oxalic acid had retention times of 3.6 min, 8.3 min, and 11.9 min, respectively.

Text S5. UHPLC-qToF-MS analyses.

The characterization of reaction products was performed using a UHPLC system (ExionLC^{TM} AD, ABSciex, Concord, Canada) coupled to a quadrupole time-of-flight mass spectrometer (qToF-MS) (TripleTOF 6600+, ABSciex). The settings (e.g., column, mobile phase, gradient, oven temperature) in the UHPLC system were the same as those used in UHPLC-PDA

(Text S3). The mass spectrometer was equipped with an electrospray ionization (ESI) source and operated in the positive ion mode (the negative ion mode signals were too low for our analyses) at a resolving power (full width at half-maximum (fwhm) at m/z 300) of 30000 in MS and 30000 in MS/MS (high-resolution mode). Information-dependent acquisition (IDA) scanning was adapted for product identification. The acquisition using IDA consisted of a ToF-MS scan and information-dependent trigger events. The ToF-MS scan had an accumulation time of 250 ms and covered a mass range of m/z 30–700 with a declustering potential (DP) of 40 and collision energy (CE) of 10 eV. The accumulation time for the IDA experiment was 100 ms, and the MS/MS scan range was set from m/z 30–700 in high-resolution mode. The IDA criteria were as follows: 5 most intense ions (number of IDA experiments) with an intensity threshold above 50 cps, isotope exclusion was switched off, and dynamic background subtraction was switched on. The automated calibration device system (CDS) was set to perform an external calibration every four samples. The ESI source conditions were as follows: temperature, 500 °C; curtain gas (CUR), 25 psi; ion source gas 1 at 50 psi; ion source gas 2 at 50 psi; and ion-spray voltage floating (ISVF) at 4.5 kV.

All parameters in the liquid chromatography system and mass spectrometer were controlled using Analyst TF Software 1.8 (ABSciex). The high-resolution LC-MS data were processed with PeakView and Analyst in the SCIEX OS software 1.5 (ABSciex). Peaks from the blank sample were subtracted from the sample signals. In addition to a minimum signal-to-noise ratio of 30, a peak was determined as a product if the difference in peak area between the samples before and after irradiation is $\geq$ 10 times. The formula assignments were carried out using the MIDAS molecular formula calculator (http://magnet.fsu.edu/~midas/) with the following constraints: $C \leq 35$, $H \leq 70$, $N \leq 5$, $O \leq 20$, $Na \leq 1$, and the mass error was initially set as 10 ppm. The nitrogen atom was removed in the constraints for the experiments without AN or SN. The detected adducts

in ESI positive ion mode have several types (e.g., $[M+H]^+$, $[M+Na]^+$), and their formation can be influenced by the sample matrix (Erngren et al., 2019). For simplification purposes, we mainly considered $[M+H]^+$ adducts for formula assignments, except for specific experiments with AN or SN in which $[M+NH_4]^+$ adducts and $[M+Na]^+$ adducts were observed. The final assigned formulas were constrained by a mass error mostly < 5 ppm, which is a requirement for product identification using positive ion mode (Roemmelt et al., 2015). The double bond equivalent (DBE) values and carbon oxidation state (OS_c) of the neutral formulas were calculated using the following equations (Koch and Dittmar, 2006):

$$DBE = C - H/2 + N/2 + 1 \quad \text{(Eq. S1)}$$

$$OS_c = 2 \times O/C - H/C \quad \text{(Eq. S2)}$$

where C, H, O, and N correspond to the number of carbon, hydrogen, oxygen, and nitrogen atoms in the neutral formula, respectively. Based on the identified products, the average oxygen to carbon (O:C) ratios, <O:C>: $(< O:C >= \sum_i(\text{abundance}_i)O_i / \sum_i(\text{abundance}_i)C_i)$ and average hydrogen to carbon (H:C) ratios, <H:C>: $(< H:C >= \sum_i(\text{abundance}_i)H_i / \sum_i(\text{abundance}_i)C_i)$ after the reactions were further estimated using the signal-weighted method (Bateman et al., 2012). The average OS_c ($<OS_c>$) was calculated as follows:

$$<OS_c> = 2 \times <O:C> - <H:C> \quad \text{(Eq. S3)}$$

Based on the typical MS/MS fragmentation behavior for individual functional groups (Table S1) and DBE values, examples of structures for products identified from VL (and GUA) photo-oxidation experiments were proposed (Table S2~~3~~).

Text S6. Photon flux measurements.

In this work, 2-nitrobenzaldehyde (2NB), a chemical actinometer, was used to determine the photon flux in the aqueous photoreactor. ~~We first measured the relative intensity of light passing through the empty reactor, then the reactor containing 50 μM 2NB using a high-sensitivity spectrophotometer (Brolight Technology Co. Ltd, Hangzhou, China) equipped with an optical fiber (Brolight). Then, the average relative intensity absorbed by 2NB solution as a function of wavelength was calculated.~~ Briefly, the photolysis of 50 μM 2NB in the reactor was monitored by determining its concentration every 5 min for a total of 35 min, during which 2NB was almost completely decayed. The concentration of 2NB was measured using UHPLC-PDA, and the settings (e.g., column, mobile phase, gradient, oven temperature) were the same as those for VL decay analysis (Text S3). The channel with UV absorption at 254 nm was used for the quantification of 2NB. The concentration of 2NB in the reactor followed exponential decay, and its decay rate constant was determined using the following equation:

$$ln\left(\frac{[2\mathrm{NB}]_t}{[2\mathrm{NB}]_0}\right) = -j(2\mathrm{NB}) \times t \qquad \text{(Eq. S4)}$$

where $[2\mathrm{NB}]_t$ and $[2\mathrm{NB}]_0$ are the 2NB concentrations at time t and 0, respectively. The calculated 2NB decay rate constant, j(2NB), was 0.0026 s^{-1}. The following equation can also be used to calculate j(2NB):

$$j(2\mathrm{NB}) = 2.303 \times (10^3\ \mathrm{cm^3\ L^{-1}} \times\ 1\ \mathrm{mol/N_A\ mlc}) \times \sum\left(I_\lambda^{'} \times \Delta\lambda \times \varepsilon_{2\mathrm{NB},\lambda} \times \Phi_{2\mathrm{NB}}\right) \qquad \text{(Eq. S5)}$$

where N_A is Avogadro's number, I'_λ is the actinic flux (photons cm^{-2} s^{-1} nm^{-1}), $\Delta\lambda$ is the wavelength interval between actinic flux data points (nm), and $\varepsilon_{2NB,\lambda}$ and $\Phi_{2NB,\lambda}$ are the base-10 molar absorptivity (M^{-1} cm^{-1}) and quantum yield (molecule $photon^{-1}$) for 2NB, respectively. Values of $\varepsilon_{2NB,\lambda}$ (in water) at each wavelength under 298 K and a wavelength-independent Φ_{2NB} value of 0.41 were adapted from Galbavy et al. (2010). Similar to Smith et al. (2014, 2016), we measured the spectral shape of the photon output of our illumination system (i.e., the relative flux at each wavelength) using a high-sensitivity spectrophotometer (Brolight Technology Co. Ltd, Hangzhou, China). Using a scaling factor (SF), this measured relative photon output, $I_\lambda^{relative}$, is related to I'_λ as follows:

$$I'_\lambda = I_\lambda^{relative} \times SF \quad \text{(Eq. S6)}$$

Substitution of Eq. S6 into Eq. S5 and rearrangement yields:

$$SF = \frac{j(2NB)}{2.303 \times (10^3\ cm^3\ L^{-1} \times 1\ mol/N_A\ mlc) \times \sum(I_\lambda^{relative} \times \Delta\lambda \times \varepsilon_{2NB,\lambda} \times \Phi_{2NB})} \quad \text{(Eq. S7)}$$

and substitution of Eq. S6 into Eq. S7 yields:

$$I'_\lambda = I_\lambda^{relative} \frac{j(2NB)}{2.303 \times (10^3\ cm^3\ L^{-1} \times 1\ mol/N_A\ mlc) \times \sum(I_\lambda^{relative} \times \Delta\lambda \times \varepsilon_{2NB,\lambda} \times \Phi_{2NB})} \quad \text{(Eq. S8)}$$

Finally, I'_λ was estimated through Eq. S8~~5~~. The estimated photon flux in the aqueous reactor is shown in Figure S1~~2~~.

The actinic flux during a haze event over Beijing (40° N, 116° E) on January 12, 2013, at 12:00 pm (GMT+8) (Che et al., 2014) estimated using the National Center for Atmospheric Research Tropospheric Ultraviolet-Visible (TUV) Radiation Model

(http://cprm.acom.ucar.edu/Models/TUV/Interactive_TUV/) is also shown in Figure S2. The parameters used for the Quick TUV calculator were: Overhead Ozone Column: 300 du; Surface Albedo: 0.1; Ground Elevation: 0 km asl; Measured Altitude: 0 km asl; Clouds optical depth: 0, base: 4, top: 5; Aerosols optical depth: 2.5, single scattering albedo: 0.9, Angstrom exponent: 1; Sunlight direct beam, diffuse down, diffuse up: 1; 4 streams transfer model. For clear days, the actinic flux was estimated over Beijing (at the same date and time) using the default parameters.

Text S7. Estimation of the apparent quantum efficiency of guaiacol photodegradation.

The apparent quantum efficiency of GUA photodegradation (φ_{GUA}) in the presence of either VL or nitrate during simulated sunlight illumination can be defined as (Anastasio et al., 1996; Smith et al., 2014, 2016):

$$\Phi_{GUA} = \frac{\text{mol GUA destroyed}}{\text{mol photons absorbed}} \quad \text{(Eq. S9)}$$

Φ_{GUA} was calculated using the measured rate of GUA decay and rate of light absorption by either VL or nitrate through the following equation:

$$\Phi_{GUA} = \frac{\text{rate of GUA decay}}{\text{rate of light absorption by VL or nitrate}} = \frac{k'_{GUA} \times [GUA]}{\sum[\left(1-10^{-\varepsilon_\lambda [C] l}\right) \times I'_\lambda]} \quad \text{(Eq. S10)}$$

where k'_{GUA} is the pseudo-first-order rate constant for GUA decay, [GUA] is the concentration of GUA (M), ε_λ is the base-10 molar absorptivity (M^{-1} cm^{-1}) of VL or nitrate at wavelength λ, [C] is the concentration of VL or nitrate (M), l is the pathlength of the illumination cell (cm), and I'_λ is the volume-averaged photon flux (mol-photons L^{-1} s^{-1} nm^{-1}) determined from 2NB actinometry:

$$j(2NB) = 2.303 \times \Phi_{2NB} \times l \times \Sigma_{300\,nm}^{350\,nm} (\varepsilon_{2NB,\lambda} \times I'_\lambda \times \Delta\lambda) \quad \text{(Eq. S11)}$$

Table S1. Typical fragmentation behavior observed in MS/MS spectra for individual functional groups from Holčapek et al. (2010).

Functional group	**Fragment ions**	**MS/MS loss**
Nitro (RNO_2)	$[M+H-OH]^{+\bullet}$	-OH
	$[M+H-H_2O]^+$	$-H_2O$
	$[M+H-NO]^{+\bullet}$	-NO
	$[M+H-NO_2]^{+\bullet}$	$-NO_2$
Nitroso (RNO)	$[M+H-NO]^+$	-NO
Carboxylic acid (ROOH)	$[M+H-H_2O]^+$	$-H_2O$
	$[M+H-CO_2]^+$	$-CO_2$
	$[M+H-H_2O-CO]^+$	$-H_2O-CO$
Phenol (ROH)	$[M+H-H_2O]^+$	$-H_2O$
	$[M+H-CO]^+$	-CO
Methoxy ($ROCH_3$)	$[M+H-CH_3]^{+\bullet}$	$-CH_3$
	$[M+H-CH_3O]^{+\bullet}$	$-CH_3O$
	$[M+H-CH_3OH]^+$	$-CH_3OH$
	$[M+H-HCOH]^+$	-HCOH
Ester (R^1COOR^2)	$[M+H-R^2OH]^+$	$-R^2OH$
	$[M+H-R^2OH-CO]^+$	$-R^2OH-CO$
Amine	$[M+H-NH_3]^+$	$-NH_3$
Aldehyde (RCHO)	$[M+H-CO]^+$	-CO

Table S2. Reaction conditions, initial VL (and GUA) decay rates, normalized abundance of products, and average carbon oxidation state (<OS_c>) in each experiment. Except where noted, the reaction systems consisted of VL (0.1 mM); GUA (0.1 mM), AN (1 mM); sodium nitrate (SN) (1 mM); VOC (IPA) (1 mM) or inorganic anions (NaBC) (1 mM) under air-saturated conditions after 6 h of simulated sunlight irradiation. Analyses were performed using UHPLC-qToF-MS equipped with an ESI source and operated in the positive ion mode.

Exp no.	pH	Reaction conditions	Initial VL (and GUA) decay rates (min^{-1})[b]	Ratio of 50 most abundant products to total products[c]	Normalized abundance of products[d]	Normalized abundance of N-containing compounds[d]	<OS_c>[e]
A1	2.5	VL*	2.8×10^{-3}	0.59	1.7	-	-0.05
A2		VL+AN	2.5×10^{-3}	0.63	1.4	5.3×10^{-2}	-0.04
A3	3	VL*	2.1×10^{-3}	0.53	1.9	--	-0.04
A4		VL+AN	2.1×10^{-3}	0.56	1.9	3.6×10^{-2}	-0.05
A5	4	VL*	1.9×10^{-3}	0.58	0.26	--	-0.16
A6		VL* (N_2-saturated)	4.6×10^{-4}	0.96	4.7×10^{-2}	--	-0.24
A7		VL+AN	1.9×10^{-3}	0.53	0.37	1.7×10^{-2}	-0.13
A8		VL+AN (N_2-saturated)	2.9×10^{-4}	0.89	0.12	6.3×10^{-3}	-0.21
A13		VL+SN	--	0.51	0.42	1.7×10^{-2}	-0.07
A14		VL* (0.01 mM)[a]	--	0.90	0.37	--	-0.07

A15		VL (0.01 mM) + AN (0.01 mM)	–	0.77	0.40	8.6×10^{-3}	0.12
A16		VL (0.01 mM) + AN	–	0.42	0.45	1.2×10^{-2}	0.06
A17		GUA only	9.0×10^{-4}	0.77	–	–	0.28
A18		GUA+VL	GUA: 2.0×10^{-3} VL: 6.2×10^{-4}	0.60	2.2	–	0.27
A19		GUA+AN	1.1×10^{-3}	0.77	–	–	0.26

[a]Irradiation time for VL* (0.01 mM, A14) was 3 h. [b]The data fitting was performed in the initial linear region. [c]Ratio of the normalized abundance of the 50 most abundant products to that of total products, except for direct GUA photodegradation (A17), GUA+VL (A18), and GUA+AN (A19) whose ratios are based on the absolute signal area of products. [d]The normalized abundance of products was calculated using Eq. 2. [e]$\langle OS_c \rangle$ of the 50 most abundant products.

Table S23. Examples of proposed molecular structures for products identified from vanillin (and guaiacol) photo-oxidation experiments in this study.

No.	Formula	DBE	Proposed structure	MS/MS fragment ions		
1	$C_8H_8O_3$ (VL; the aqSOA precursor)	5	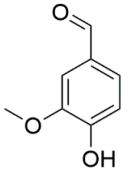	-CO-CH_3OH	-CO	-CO-CH_3OH-CO
2	$C_8H_9NO_3$	5	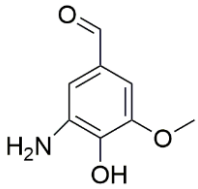	-CO-CH_3	-NH_3	
3	$C_{16}H_{10}N_2O_9$	13	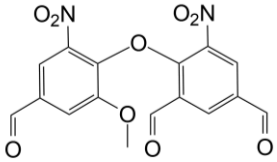	-NO_2		
4	$C_{10}H_{10}O_5$	6	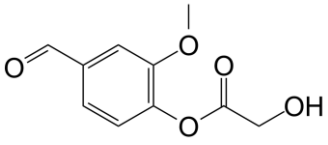	-CH_3OH	-CH_3OH-CO	
4	$C_{10}H_{10}O_5$	6		-CH_3OH	-CH_3OH-CO	

5	$C_5H_5N_3O_2$	5	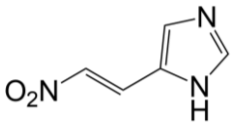	-NH		
6~~5~~	$C_{16}H_{14}O_6$	10	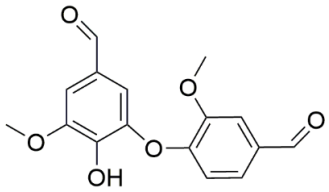	-CO-CH_3OH-CO	-CO-CH_3OH-CO-CH_3OH	-CO-CH_3OH-CO-CO
7	$C_8H_6O_4$	6	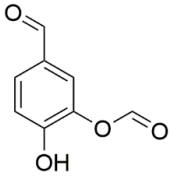	-CO	-CO-CO	
8	$C_{15}H_{12}O_8$	10	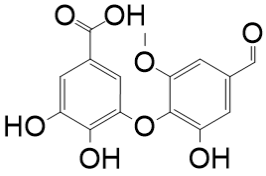	-COOH		
9	$C_7H_4N_2O_7$	7	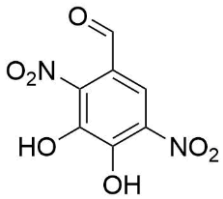			
10	$C_{14}H_{14}O_4$	8	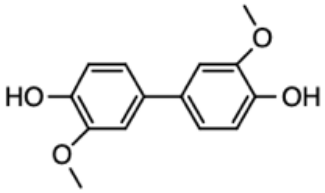			
11~~6~~	$C_{21}H_{20}O_6$~~$C_7H_4O_4$~~	12 ~~6~~	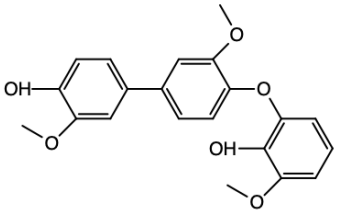	~~-CO~~	~~-CO-CO~~	

127	$C_{28}H_{24}O_8C_{15}H_{12}O_8$	1710	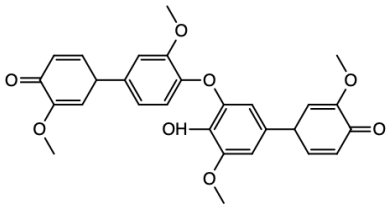	-CO	$-CH_3$	
138	$C_7H_4O_4C_8H_6O_4$	6 6	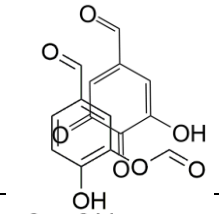	-CO-CO	-CO-CO-CO-CO	
149	$C_8H_8O_4C_{15}H_{12}O_8$	510	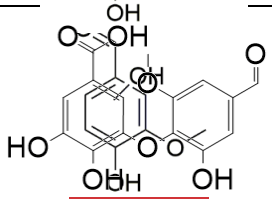	-CO-CH_3OH-COOH	-CO	$-H_2O$
10	$C_5H_5N_3O_2$	5	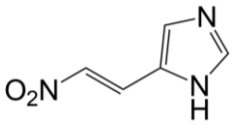	-NH		
11	$C_7H_4N_2O_7$	7	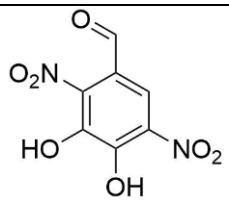			
12	$C_{15}H_{14}O_8$	9	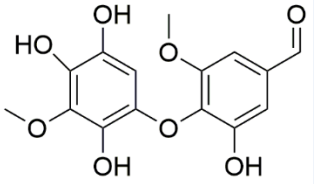	-CO-CH_3OH-CO-CO	-CO-CH_3OH-CO-H_2O	-CO-CH_3OH-CO
13	$C_8H_8O_4$	5	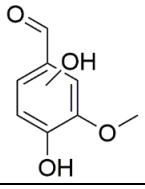	-CO-CH_3OH	-CO	$-H_2O$
14	$C_8H_8O_5$	5		-CO-CH_3OH	$-CO_2$	-CH_3OH

~~15~~	~~$C_{23}H_{18}O_9$~~	~~15~~	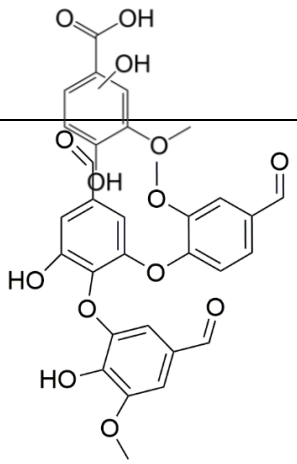			
~~19~~	~~$C_{14}H_{14}O_4$~~	~~8~~	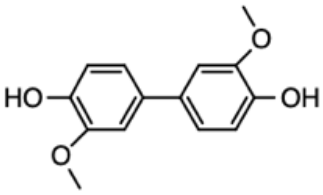			
~~20~~	~~$C_{21}H_{20}O_6$~~	~~12~~	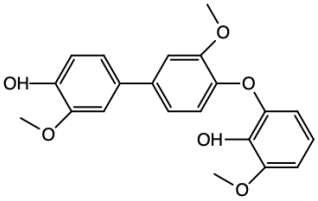			
~~21~~	~~$C_{28}H_{24}O_8$~~	~~17~~	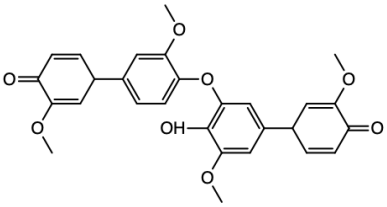			

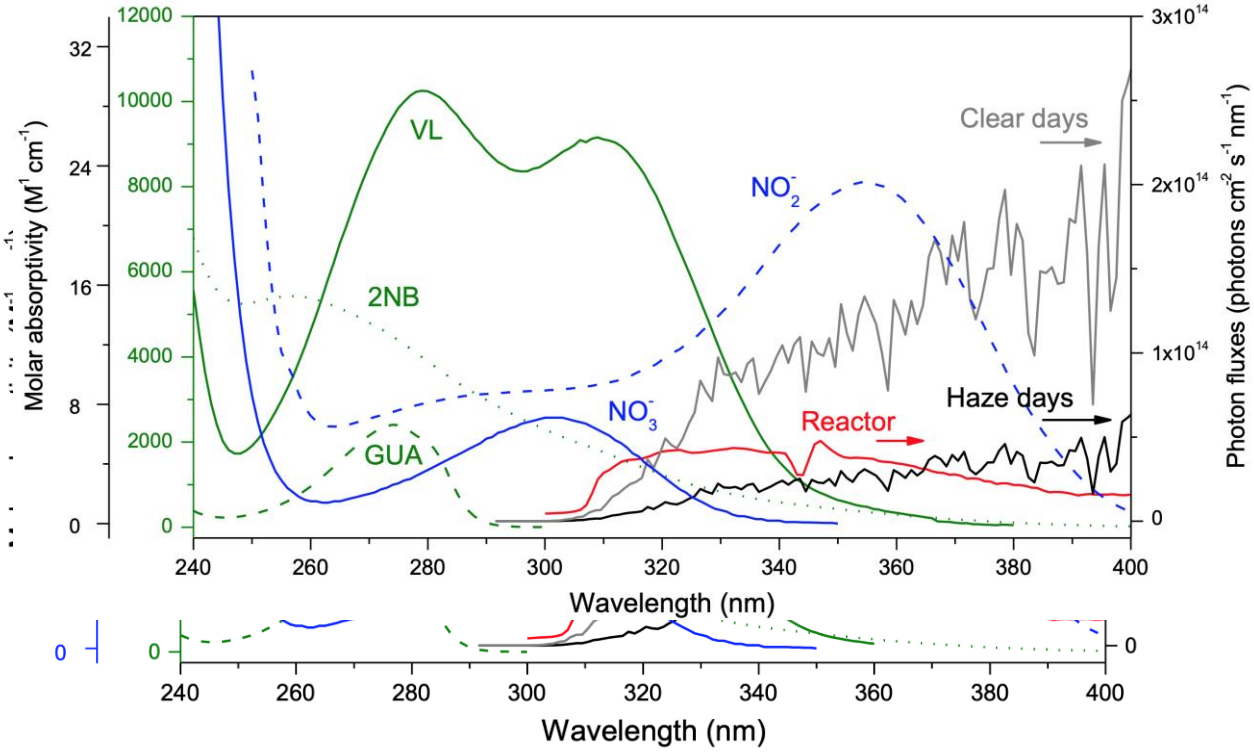

Figure S1. The base-10 molar absorptivities (ε, M^{-1} cm^{-1}) of vanillin (VL, green solid line), 2-nitrobenzaldehyde (2NB, green dotted line), guaiacol (GUA, green dashed line), NO_2^- (blue dashed line), NO_3^- (blue solid line), and photon flux in the aqueous reactor (red line) during typical haze days (black line) or clear days (grey line) in Beijing, China. The ε values for 2NB and NO_2^- were adapted from Galbavy et al. (2010) and Chu and Anastasio (2007), respectively.

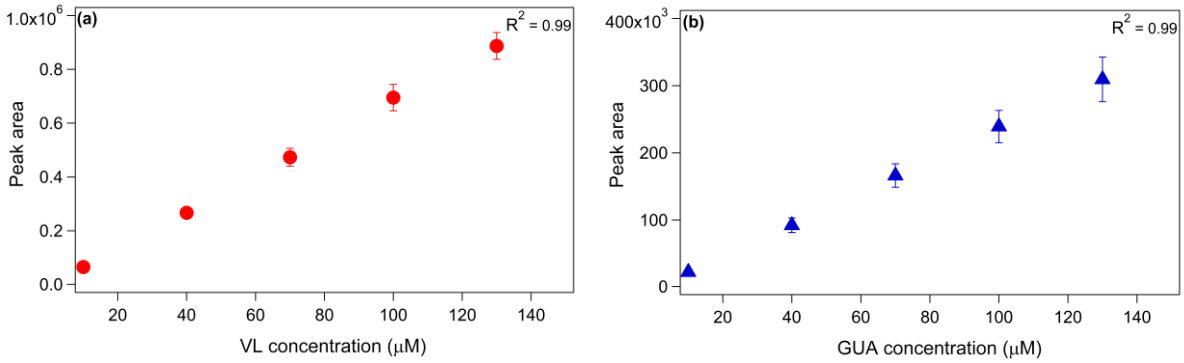

Figure S2. Calibration curves for (a) VL and (b) GUA standard solutions (10–130 μM). Error bars represent one standard deviation.

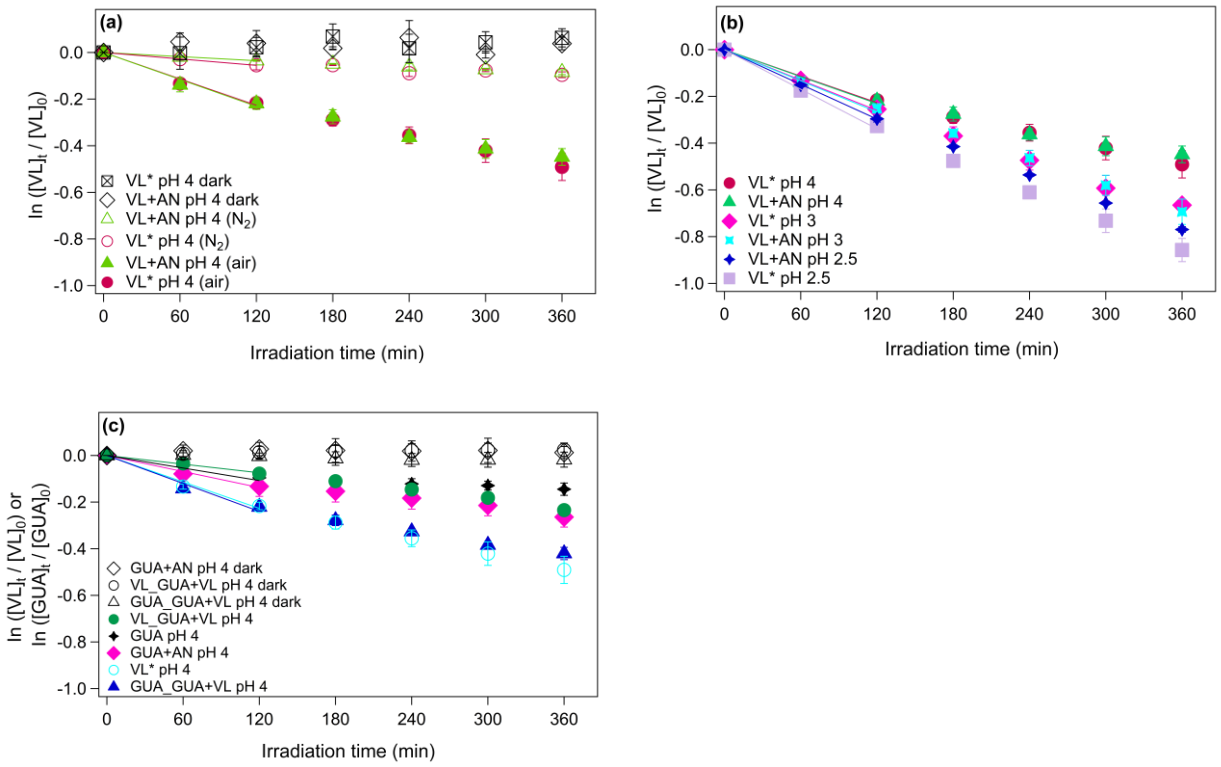

Figure S3. (a–~~c~~d) The decay of VL under different experimental conditions for direct photosensitized oxidation of VL (VL*) and nitrate-mediated VL photo-oxidation (VL+AN): (a) ~~Effect of secondary oxidants from VL triplets on~~ VL* and VL+AN at pH 4 under N_2- (A6, A8) and air-saturated (A5, A7) conditions. (b) Effect of pH on VL* and VL+AN at pH 2.5 (A1, A2), 3 (A3, A4), and 4 (A5, A7) under air-saturated conditions. ~~(c) Effect of the presence of VOCs and inorganic anions: IPA (A9) and NaBC (A10) on VL* at pH 4 under air-saturated conditions. (d) Effect of the presence of VOCs and inorganic anions: IPA (A11) and NaBC (A12) on VL+AN at pH 4 under air-saturated conditions.~~ (ce) The decay of VL (and GUA) during direct GUA photodegradation (A13~~7~~) and photo-oxidation of GUA in the presence of VL (GUA+VL; A14~~8~~) or nitrate (GUA+AN; A15~~9~~) at pH 4 under air-saturated conditions after 6 h of simulated sunlight irradiation. Error bars represent one~~1~~ standard deviation; most error bars are smaller than the markers.

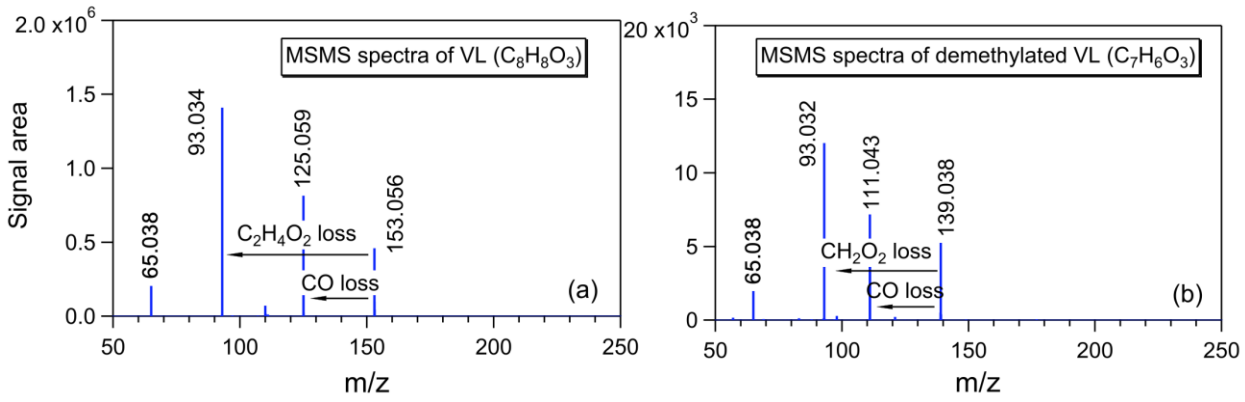

312

313 **Figure S4.** MS/MS spectra of (a) VL and (b) demethylated VL. The arrows indicate possible
314 fragmentation pathways of VL and demethylated VL.

315

316

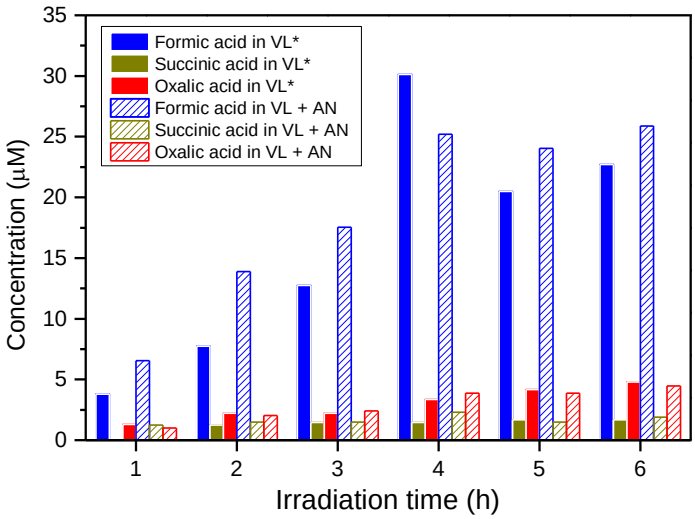

317

318 **Figure S5**. The concentration of formic, oxalic, and succinic acid at different reaction times for
319 VL* (A5) and VL+AN (A7) at pH 4 under air-saturated conditions.

320

321

322

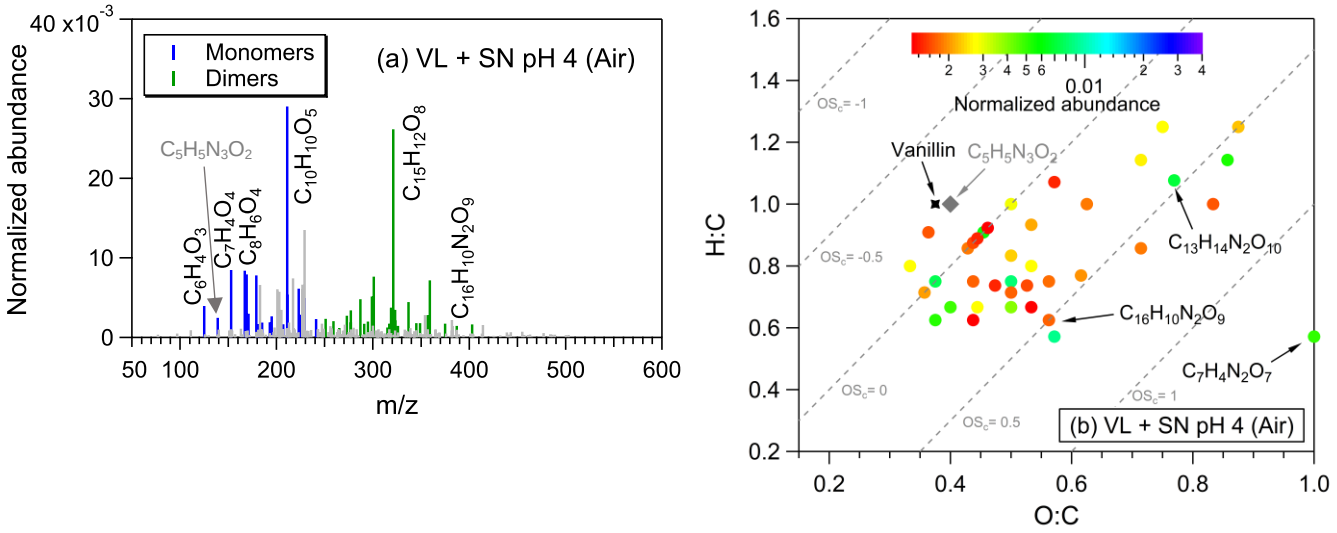

Figure S6. (a) Reconstructed mass spectra of assigned peaks and (b) van Krevelen diagram of the 50 most abundant products from VL+SN (A~~913~~) at pH 4 under air-saturated conditions after 6 h of simulated sunlight irradiation. The normalized abundance of products was calculated from the ratio of the peak area of the product to that of VL (Eq. 2). The 50 most abundant products contributed more than half of the total normalized abundance of products, and they were identified as monomers (blue) and dimers (green). Grey peaks denote peaks with low abundance or unassigned formula. Examples of high-intensity peaks were labeled with the corresponding neutral formulas. The color bar denotes the normalized abundance of products. The grey dashed lines indicate the carbon oxidation state values (e.g., OS_c = -1, 0, and 1). The grey arrows show where the potential imidazole derivative ($C_5H_5N_3O_2$) from VL+AN was observed.

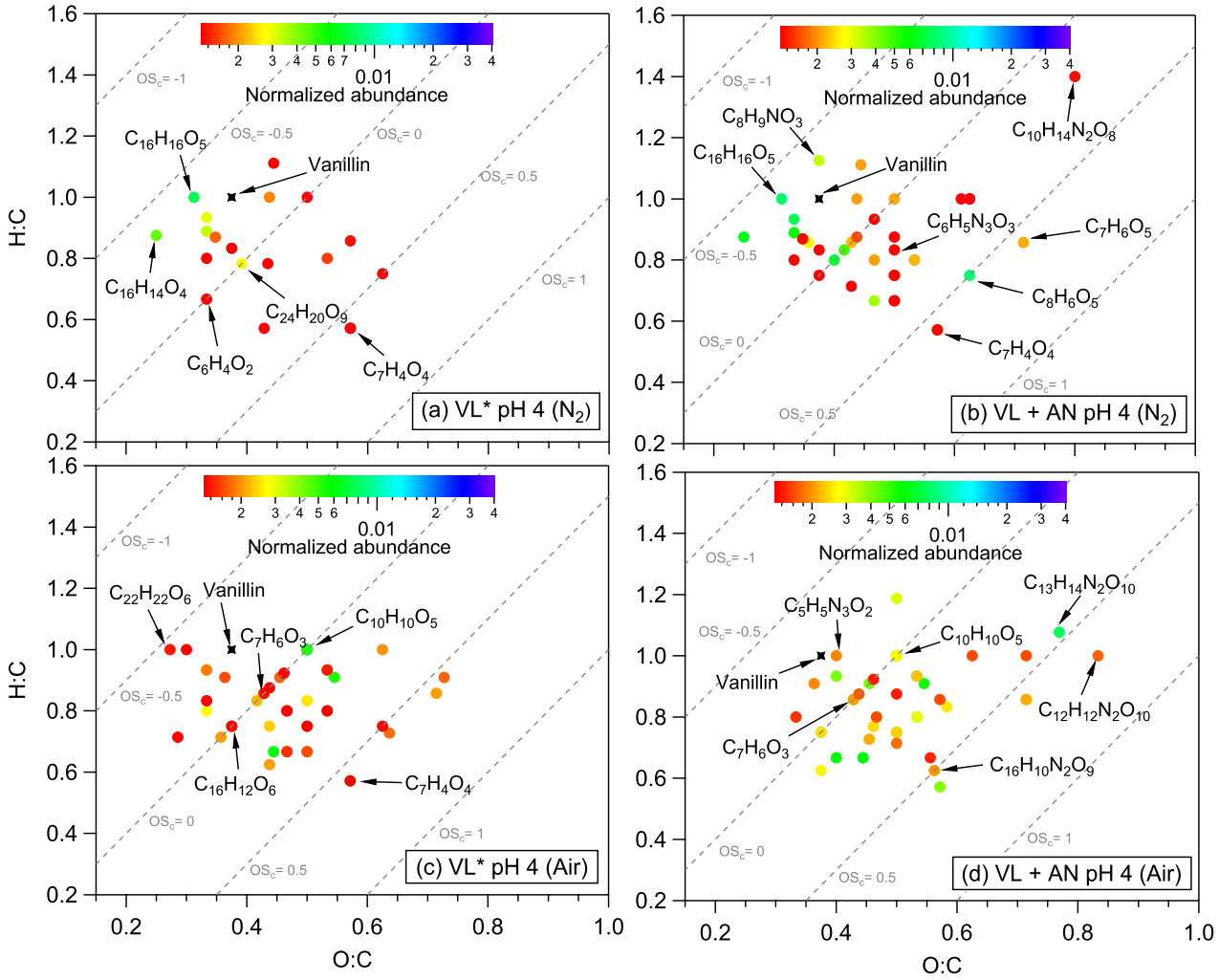

365

366 **Figure S7.** van Krevelen diagrams of the 50 most abundant products from (a) VL* (N_2-saturated;
367 A6), (b) VL+AN (N_2-saturated; A8), (c) VL* (air-saturated; A5), and (d) VL+AN (air-saturated;
368 A7) at pH 4 after 6 h of simulated sunlight irradiation. The color bar denotes the normalized
369 abundance of products. The grey dashed lines indicate the carbon oxidation state values (e.g., OS_c
370 = -1, 0, and 1).

371

372

373

374

375

376

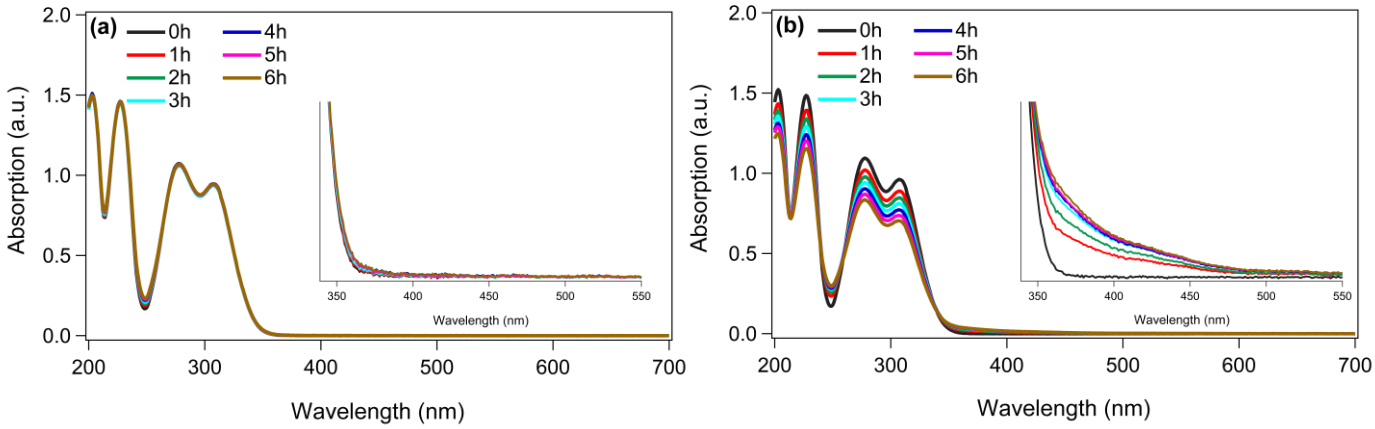

Figure S8. UV–Vis absorption spectra of VL* (A6, A5; pH 4) under (a) N_2- and (b) air-saturated conditions at different time intervals. The insets show the absorbance enhancement from 350 to 550 nm.

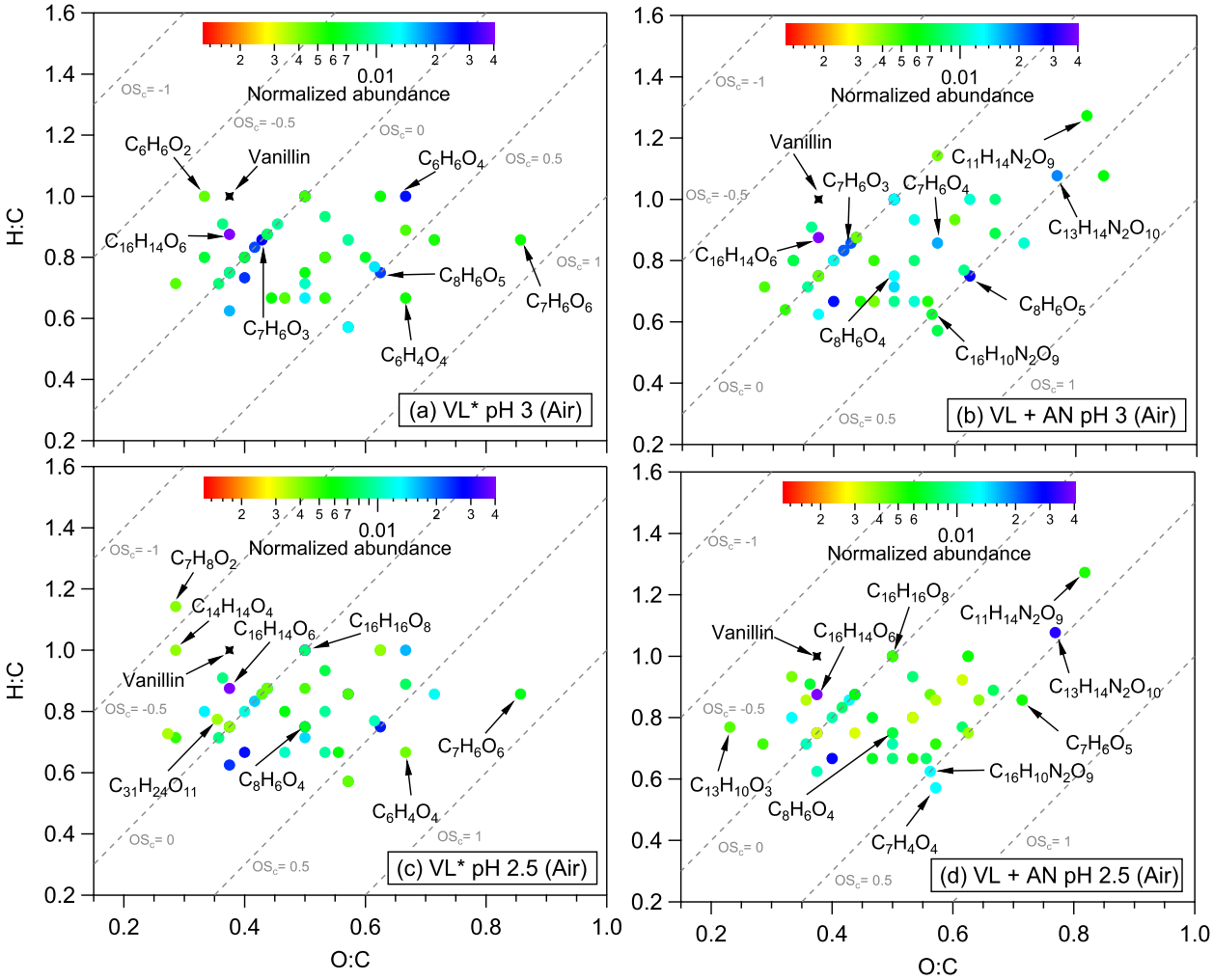

Figure S9. van Krevelen diagrams of the 50 most abundant products from (a) VL* pH 3 (A3), (b) VL+AN pH 3 (A4), (c) VL* pH 2.5 (A1), and (d) VL+AN pH 2.5 (A2) under air-saturated conditions after 6 h of simulated sunlight irradiation. The color bar denotes the normalized abundance of products. The grey dashed lines indicate the carbon oxidation state values (e.g., OS_c =-1, 0, and 1).

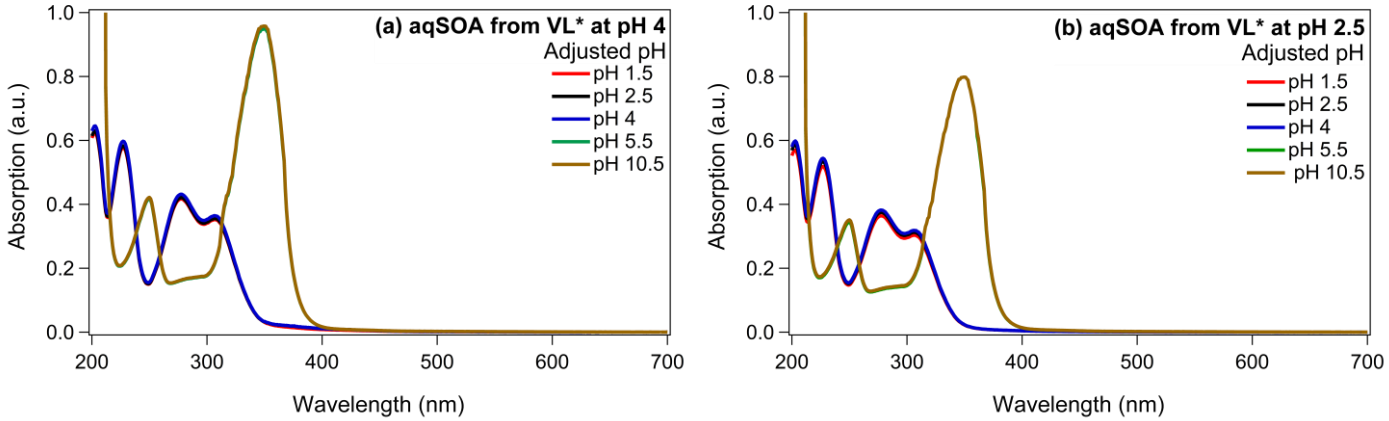

Figure S10. UV–Vis absorption spectra of VL*-derived aqSOA formed at (a) pH 4 and (b) pH 2.5 over a range of pH conditions from 1.5 to 10.5.

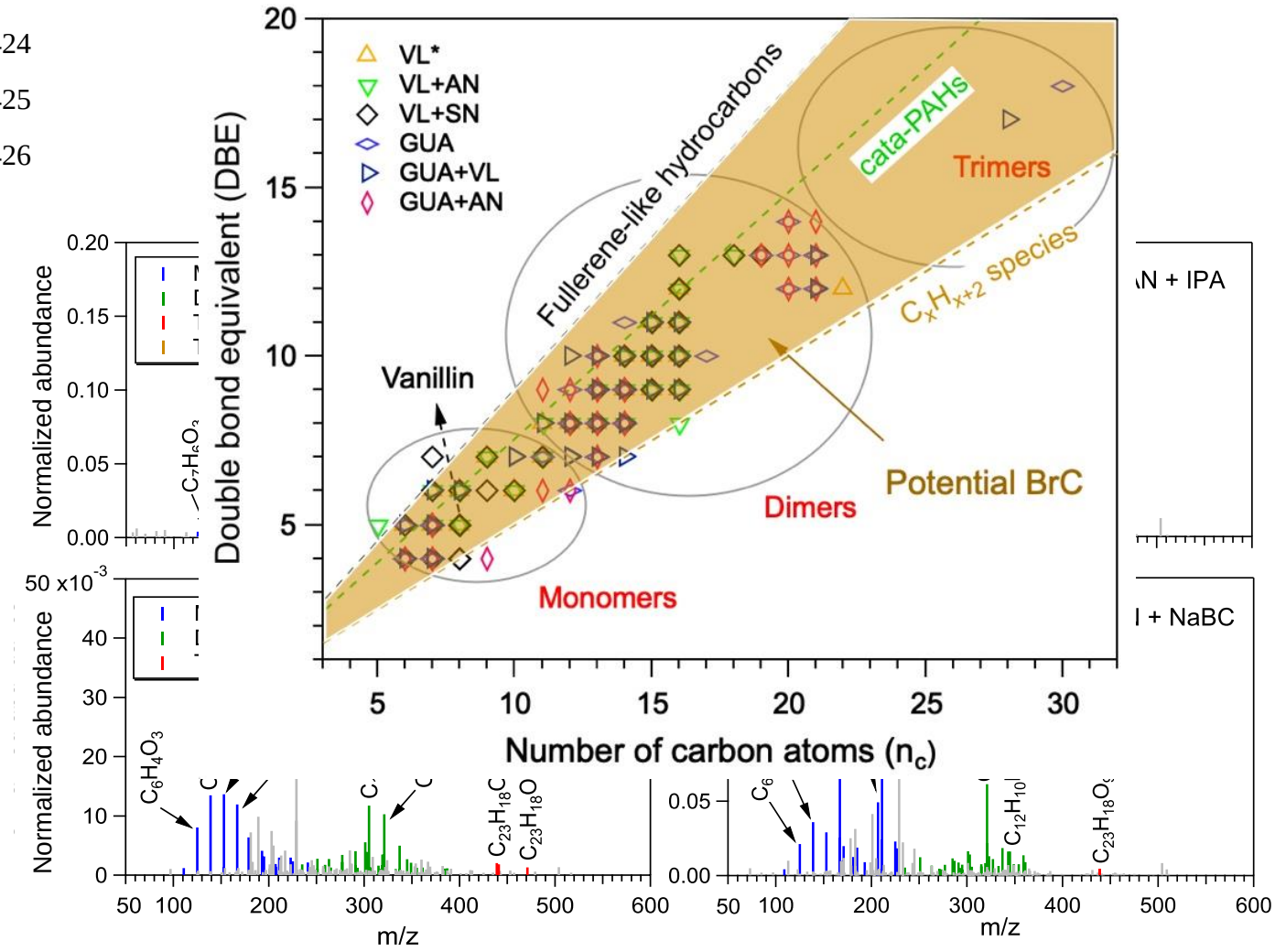

Figure S10. Reconstructed mass spectra of assigned peaks from (a) VL*+IPA (A9), (b) VL+AN+IPA (A11), (c) VL*+NaBC (A10), and (d) VL+AN+NaBC (A12) at pH 4 under air-saturated conditions after 6 h of simulated sunlight irradiation. The normalized abundance of products was calculated from the ratio of the peak area of the product to that of VL (Eq. 2). The 50 most abundant products contributed more than half of the total normalized abundance of products, and they were identified as monomers (blue), dimers (green), trimers (red), and tetramers (orange). Grey peaks denote peaks with low abundance or unassigned formula. Examples of high-intensity peaks were labeled with the corresponding neutral formulas. Note the different scales on the y-axes.

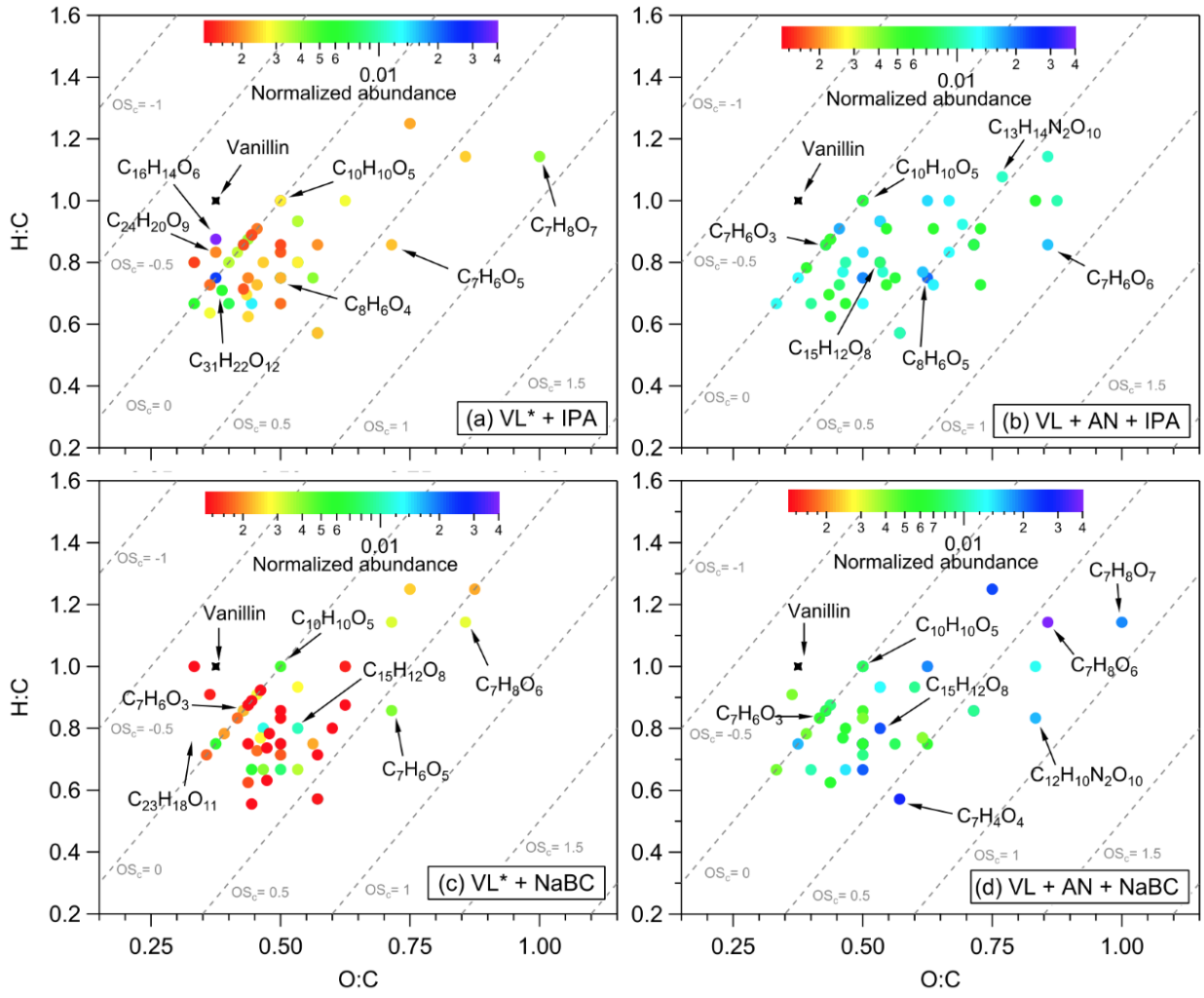

~~**Figure S11.** van Krevelen diagrams of the 50 most abundant products from (a) VL*+IPA (A9), (b) VL+AN+IPA (A11), (c) VL*+NaBC (A10), and (d) VL+AN+NaBC (A12) at pH 4 under air-saturated conditions after 6 h of simulated sunlight irradiation. The color bar denotes the normalized abundance of products. The grey dashed lines indicate the carbon oxidation state values (e.g., OS_c = -1, 0, and 1).~~

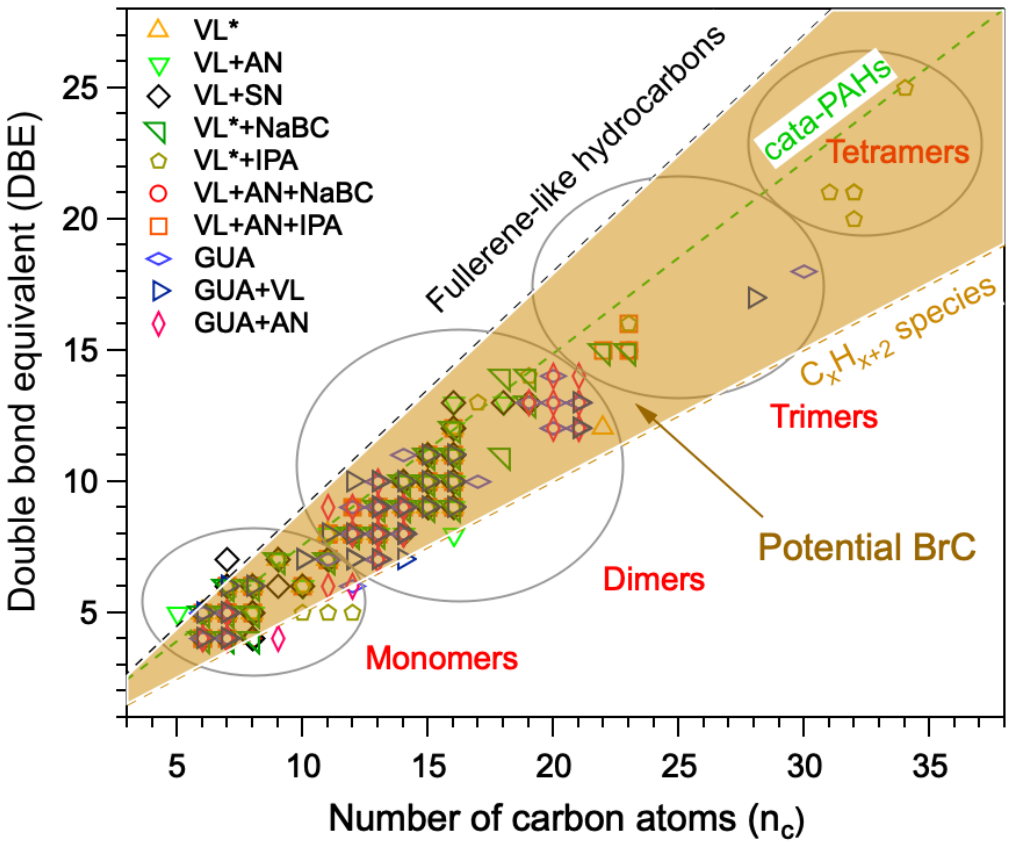

Figure S11~~2~~. The plot of the double bond equivalent (DBE) values vs. number of carbon atoms (n_c) (Lin et al., 2018) for the 50 most abundant products from pH 4 experiments under air-saturated conditions. Dashed lines indicate DBE reference values of fullerene-like hydrocarbons (Lobodin et al, 2012) (black dashed line), cata-cond~~s~~ensed polycyclic aromatic hydrocarbons (PAHs) (Siegmann and Sattler, 2000) (green dashed line), and linear conjugated polyenes (general formula C_xH_{x+2}) (brown dashed line). Data points within the shaded area are potential BrC chromophores.

Light grey circles show the classification of the data points as monomers, dimers, trimers, or tetramers.

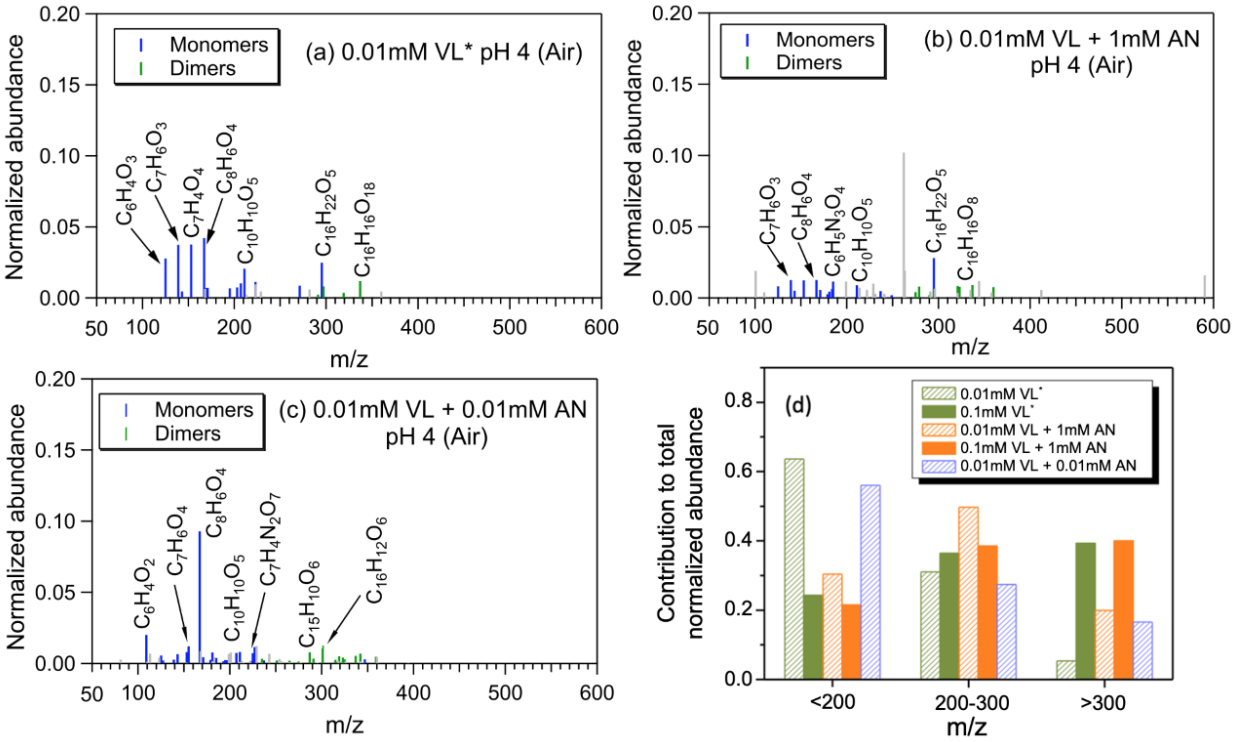

Figure S1~~2~~3. Reconstructed mass spectra of assigned peaks from (a) 0.01 mM VL* (A1~~0~~4), (b) 0.01 mM VL + 1 mM AN (A1~~1~~6), and (c) 0.01 mM VL + 0.01 mM AN (A1~~2~~5) at pH 4 under air-saturated conditions after 6 h of simulated sunlight irradiation. The normalized abundance of products was calculated from the ratio of the peak area of the product to that of VL (Eq. 2). The 50 most abundant products contributed more than half of the total normalized abundance of products, and they were identified as monomers (blue) and dimers (green). Grey peaks denote peaks with low abundance or unassigned formula. Examples of high-intensity peaks were labeled with the corresponding neutral formulas. (d) Contributions of different m/z ranges to the normalized abundance of products from experiments with low [VL] = 0.01 mM (A1~~0~~4–A1~~2~~6) and high [VL] = 0.1 mM (A5 and A7) at pH 4 under air-saturated conditions after 6 h of simulated sunlight irradiation.

References

Anastasio, C., Faust, B. C., and Rao, C. J.: Aromatic carbonyl compounds as aqueous-phase photochemical sources of hydrogen peroxide in acidic sulfate aerosols, fogs, and clouds. 1. Non-phenolic methoxybenzaldehydes and methoxyacetophenones with reductants (phenols), Environ. Sci. Technol., 31, 218−232, https://doi.org/10.1021/es960359g, 1996.

Bateman, A. P., Laskin, J., Laskin, A., and Nizkorodov, S. A.: Applications of high-resolution electrospray ionization mass spectrometry to measurements of average oxygen to carbon ratios in secondary organic aerosols, Environ. Sci. Technol., 46, 8315–8324, https://doi.org/10.1021/es3017254, 2012.

Che, H., Xia, X., Zhu, J., Li, Z., Dubovik, O., Holben, B., Goloub, P., Chen, H., Estelles, V., Cuevas-Agulló, E., Blarel, L., Wang, H., Zhao, H., Zhang, X., Wang, Y., Sun, J., Tao, R., Zhang, X., and Shi, G.: Column aerosol optical properties and aerosol radiative forcing during a serious haze-fog month over North China Plain in 2013 based on ground-based sunphotometer measurements, Atmos. Chem. Phys., 14, 2125–2138, https://doi.org/10.5194/acp-14-2125-2014, 2014.

Chu, L. and Anastasio, C.: Temperature and wavelength dependence of nitrite photolysis in frozen and aqueous solutions, Environ. Sci. Technol., 41, 3626–3632, ttps://doi.org/10.1021/es062731q, 2007.

Erngren, I., Haglöf, J., Engskog, M. K. R., Nestor, M., Hedeland, M., Arvidsson, T., and Pettersson, C.: Adduct formation in electrospray ionisation-mass spectrometry with hydrophilic interaction liquid chromatography is strongly affected by the inorganic ion concentration of the samples, J. Chromatogr. A, 1600, 174–182, https://doi.org/10.1016/j.chroma.2019.04.049, 2019.

Galbavy, E. S., Ram, K., and Anastasio, C.: 2-Nitrobenzaldehyde as a chemical actinometer for solution and ice photochemistry, J. Photochem. Photobiol. A, 209, 186–192, https://doi.org/10.1016/j.jphotochem.2009.11.013, 2010.

Holčapek, M., Jirásko, R., and Lísa, M.: Basic rules for the interpretation of atmospheric pressure ionization mass spectra of small molecules, J. Chromatogr. A, 1217, 3908–3921, https://doi.org/10.1016/j.chroma.2010.02.049, 2010.

Koch, B. P. and Dittmar, T.: From mass to structure: an aromaticity index for high-resolution mass data of natural organic matter, Rapid Commun. Mass Spectrom., 20, 926–932, https://doi.org/10.1002/rcm.7433, 2006.

Lin, P., Fleming, L. T., Nizkorodov, S. A., Laskin, J., and Laskin, A.: Comprehensive molecular characterization of atmospheric brown carbon by high resolution mass spectrometry with electrospray and atmospheric pressure photoionization, Anal. Chem., 90, 12493–12502, https://doi.org/10.1021/acs.analchem.8b02177, 2018.

Lobodin, V. V., Marshall, A. G., and Hsu, C. S.: Compositional space boundaries for organic compounds, Anal. Chem., 84, 3410–3416, https://doi.org/10.1021/ac300244f, 2012.

Roemmelt, A. T., Steuer, A. E., and Kraemer, T.: Liquid chromatography, in combination with aquadrupole time-of-flight instrument, with sequential window acquisition of all theoretical fragment-ion spectra acquisition: validated quantification of 39 antidepressants in whole blood as part of a simultaneous screening and quantification procedure, Anal. Chem., 87, 9294–9301, https://doi.org/10.1021/acs.analchem.5b02031, 2015.

Siegmann, K. and Sattler, K. D.: Formation mechanism for polycyclic aromatic hydrocarbons in methane flames, J. Chem. Phys., 112, 698–709, https://doi.org/10.1063/1.480648, 2000.

Smith, J. D., Sio, V., Yu, L., Zhang, Q., and Anastasio, C.: Secondary organic aerosol production from aqueous reactions of 973 atmospheric phenols with an organic triplet excited state, Environ. Sci. Technol., 48, 1049–1057, https://doi.org/10.1021/es4045715, 2014.

Smith, J. D., Kinney, H., and Anastasio, C.: Phenolic carbonyls undergo rapid aqueous photodegradation to form low-volatility, light-absorbing products, Atmos. Environ., 126, 36−44, https://doi.org/10.1016/j.atmosenv.2015.11.035, 2016.

Zhou, W., Mekic, M., Liu, J., Loisel, G., Jin, B., Vione, D., and Gligorovski, S.: Ionic strength effects on the photochemical degradation of acetosyringone in atmospheric deliquescent aerosol particles, Atmos. Environ., 198, 83–88, https://doi.org/10.1016/j.atmosenv.2018.10.047, 2019.